UNIVERSITÀ DEGLI STUDI DI PADOVA

Dipartimento di Medicina Animale, Produzioni e Salute

Corso di Laurea magistrale a ciclo unico in
MEDICINA VETERINARIA

Evaluation of corneal biomechanical behavior using uniaxial tensile test applied on fresh and cultured ex vivo models in healthy, injured and helium plasma treated populations

Relatore:
Prof.ssa Anna Perazzi
Correlatori:
Prof.ssa Chiara Giulia Fontanella
Dott.ssa Simona Neri

Laureanda:
Morgana Kozlovic
Matricola n.
1165182

ANNO ACCADEMICO 2021-2022

INDEX

SUMMARY

Corneal ulcers, which can be caused by dangerous microorganisms (bacteria, fungi, amoebae, and viruses), ocular trauma or chemical exposure, constitute a medical issue of major concern. They may be simple or complicated, and in the worst instance, even collagenolytic. Collagen, the primary component of the stroma, is destroyed by collagenase enzymes in these complex ulcers.
Techniques for treating wounds that effectively eradicate invasive microorganism while simultaneously reducing ulceration and inflammation and promoting wound healing are urgently needed. In our study, we suggested using helium plasma, a cold atmospheric-pressure plasma (CAP), as an effective treatment to improve the healing of corneal ulcers.

We divided 71 porcine corneas into 12 populations after collecting them, taking into consideration the following conditions: healthy or experimentally injured, fresh after enucleation or cultured for seven days, and treated with helium plasma for two or four minutes.
All the populations underwent a uniaxial tensile test to evaluate stress-strain and relaxation curves. We confirmed the viscoelastic behavior of healthy, fresh corneas (control group) by comparing the results to those published in the literature. Additionally, we observed that the lesion induction and the culture medium decrease the stiffness and increase the tissue's ability to relax in the immediate and short-term periods whereas the helium plasma, particularly the 4 minutes treatment, increase the tissue's stiffness and decrease its ability to relax. Additionally, we found that the treatment applied to healthy corneas has a negative effect on stiffness. This was an unexpected finding that requires further investigations.

Helium plasma treatment, which is already used to treat human skin ulcers, shows the potential to be used to treat different corneal disorders in both dogs and cats. This therapy looks to be effective and promising for veterinary ophthalmology also

considering the data provided in the literature. Due to its simplicity, cheap cost, rapidity, and good outcomes, cold atmospheric pressure plasma has the potential to be a successful therapy for corneal ulcers in domestic animals. If this is the case, it may ultimately be often employed as a synergic treatment.

RIASSUNTO

Le ulcere corneali possono essere causate da microrganismi patogeni (batteri, funghi, amebe o virus) oppure da traumi oculari o da esposizione diretta a sostanze chimiche. Le ulcere rappresentano un problema medico di grande interesse e possono essere semplici o complicate, e nel peggiore dei casi possono diventare collagenolitiche. In questo ultimo caso il collagene, il principale componente dello stroma corneale, viene degradato da enzimi collagenasi che possono essere prodotti dai batteri patogeni o possono derivare dal film lacrimale e dai neutrofili residenti nel limbo.
In campo oftalmologico è urgente e necessario lo sviluppo di tecniche in grado di eliminare i microrganismi patogeni dalla lesione e allo stesso tempo di ridurne i fenomeni infiammatori e ulcerativi agevolando la guarigione delle ferite. Nel nostro studio è stato proposto l'utilizzo del plasma di elio come trattamento per facilitare i meccanismi di guarigione delle lesioni.

Sono stati selezionati e raccolti 71 campioni di cornee suine, i quali sono stati successivamente suddivisi in 12 popolazioni prendendo in considerazione diverse condizioni: campioni sani o lesionati, freschi o in coltura per sette giorni ed infine trattati con il plasma per due o quattro minuti.
Tutte le popolazioni sono state sottoposte a test di tensione uniassiale per poterne valutare le curve di tensione-deformazione e di rilassamento. Abbiamo confermato la viscoelasticità delle cornee sane confrontando i risultati ottenuti con quelli della letteratura. Inoltre, abbiamo osservato come le cornee lesionate e quelle in coltura presentino una diminuita rigidità e un aumento della capacità di rilassamento. L'effetto del trattamento al plasma, al contrario, ha determinato un aumento della rigidità del tessuto e una diminuita tendenza al rilassamento. Infine, abbiamo riscontrato che il trattamento al plasma applicato alle cornee fresche sane ha un effetto negativo sulla rigidità del materiale. Quest'ultimo è stato un risultato inaspettato che richiederà in futuro ulteriori approfondimenti.

Il trattamento con il plasma di elio, il quale viene già ampiamente utilizzato in medicina umana per il trattamento delle ulcere cutanee, ha il potenziale di diventare una terapia efficace e promettente in oftalmologia veterinaria per il trattamento delle patologie corneali del cane e del gatto. Grazie alla sua semplicità, economicità, rapidità ed efficacia, potrà essere utilizzato come trattamento sinergico nella gestione delle ulcere corneali.

1. THE EYE

1.1 ANATOMY OF THE EYE

The eye is the organ designated for the visual function. A bone orbit and moveable eyelids serve to insulate the globe from external harm. The aqueous humor, vitreous, and lens, which are dioptric components, make up the majority of the eye's volume. The arrangement of these structures forms the anterior chamber, the posterior chamber and the vitreous chamber. The anterior chamber is located between the cornea and the iris and contains the aqueous humor; the posterior chamber stays between the iris and the lens and contains also aqueous humor; the vitreous chamber is set between the lens and the retina and contains the vitreous (Zachary, 2017).

The globe surrounding is formed by three concentric layers (tunics), from the outer to the inner:

- Fibrous tunic
- Vascular tunic (uvea)
- Inner tunic (retina)

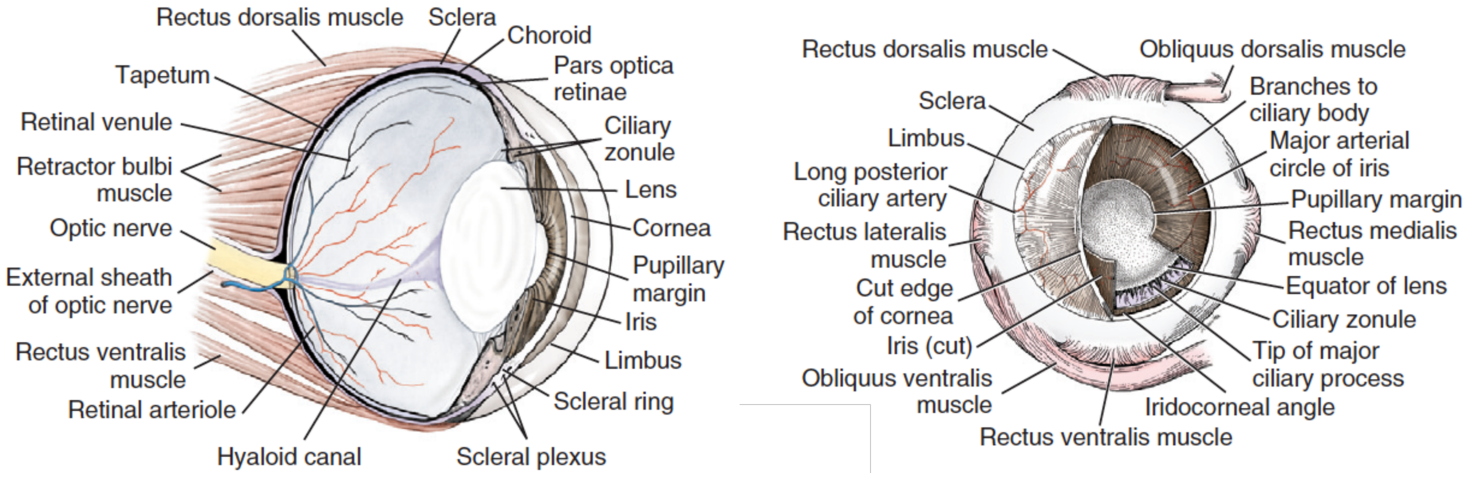

Figure 1-2. Bulbus oculi (Evans & de Lahunta, 2012)

THE FIBROUS TUNIC

The fibrous tunic is composed by a posterior opaque part, the sclera, and an anterior transparent part, the cornea. The sclera covers three-quarters of the eye's surface, while the cornea covers the rest. The junction of the sclera and the cornea is called limbus corneae (Zachary, 2017).

The **sclera** is composed by collagen and elastic fibers that are densely packed and run parallel to the surface: such tissue composition allows this layer to provide structural support in response to the high intraocular pressure and to the tension created by the insertion of the extraocular muscles. Between the fibers and the fibrocytes there is the extracellular matrix, which contains proteoglycans and glycoproteins. The scleral annulus, which is formed by a bulge of collagen and elastic fibers at the level of the limbus corneae, contains the scleral venous plexus, which provides portion of the aqueous humor's outflow. The anterior part of the sclera is covered by the conjunctive tunic. Whereas the axons of the retinal ganglion cells exit the globe there is a fenestrated area termed lamina cribrosa that allows the passage of the optic nerve (Zachary, 2017).

The **cornea** is composed of four layers: the corneal epithelium and its basement membrane, the corneal stroma, the Descemet's membrane and the corneal endothelium.

The epithelium is made up of stratified non-keratinizing cells that are covered with a mixture of mucus, water and lipids called the tear film. In dogs and cats, the epithelium is 5 to 7 layers thick while in larger animals it is 8 to 15 layers thick; it undergoes complete renewal every 5 to 7 days. Since keratinization or pigmentation are absent, the corneal epithelium is different from that of the conjunctiva or the skin (Zachary, 2017).

In terms of optics, the tear film is crucial for removing small surface defects. Conjunctival goblet cells create the mucinous layer of the tear film, which is in direct contact with the corneal epithelium. This layer interacts closely with the glycocalyx of the corneal epithelial cells to enable hydrophilic spreading of the tear film with each eyelid blink. Two-thirds of the eye's total refractive power is provided by the air-tear film contact and the cornea underneath it. Additionally, the tear film provides

immunological and growth elements that are essential for the survival, growth, and repair of epithelial cells (DelMonte & Kim, 2011). The basal layer, which is made up of a single cell layer of columnar epithelium, is the deepest cellular layer of the corneal epithelium. The only corneal epithelial cells that can undergo mitosis are these ones.

The corneal stroma represents 90% of the corneal thickness and it is formed by cross-linked collagen fibers arranged in lamellar layers and by a rich aqueous matrix. The normally transparent cornea contains 80% ±2% water. To achieve their distinctive and small diameter, stromal collagen fibrils are made of type I collagen in a heterodimeric combination with type V collagen. Specialized proteoglycans with keratan sulfate or chondroitin sulfate/dermatan sulfate side chains surround these complexes, helping to control their structural characteristics and hydration. The primary stromal cell type, keratocytes, is responsible for maintaining the ECM environment. They can produce glycosaminoglycans, collagen, and matrix metalloproteases (MMPs), all of which are essential for preserving stromal homeostasis (Zachary, 2017).

The stroma lacks blood vessels: recently it has been suggested that the avascularity of the cornea is due to the expression of soluble vascular endothelial growth factor (VEGF) receptor-1 within corneal tissues. This receptor serves as a trap, binding available VEGF, preventing it from inciting vessel formation (Ambati et al., 2006). The corneal nutrition and oxygen depend on the tear film, the limbus vessels and the aqueous humor.

There are several factors that contribute to corneal transparency, besides the avascularity and the non-keratinized and non-pigmented epithelium. The stromal hydration state and its colloidal-osmotic composition optimizes the collagen fiber refraction index. In addition, the narrow diameter of the fibers and their compact arrangement ensure that the interfibrilar distance is lower than the wavelength of visible light. Lastly, also the low cell density of the stroma contributes to maintain the transparency (Zachary, 2017).

The Descemet's membrane divides the stroma to the endothelium. The fibers, which are primarily type-V collagen, are structured in a three-dimensional reticulum into which iris muscle fibrils are inserted.

The endothelium is made up of simple squamous epithelium which appears in an honeycomb-like organization; this mosaic creates the anterior chamber coating while

also covering the cornea internally. It is a semipermeable layer that allows the selective water transport: through an anionic pump bicarbonate and chloride are actively transported to preserve the corneal hydration level (Zachary, 2017).

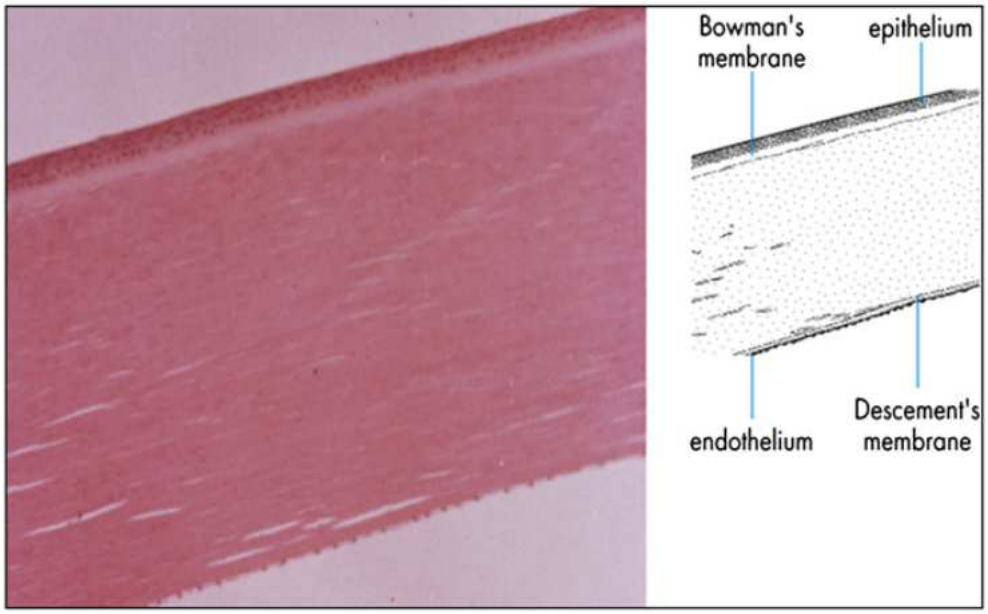

Figure 3. Microscopy of the cornea (DelMonte & Kim, 2011)

THE VASCULAR TUNIC (UVEA)

The uvea is composed by a connective tissue layer that includes pigmented cells, elastic fibers, several vessels and nervous plexuses. The ciliary body and the iris form the anterior uvea, while the choroid forms the posterior uvea.

The **ciliary body** is positioned at the lens level, where it runs from the base of the iris to the junction with the choroid and retina. It is attached to the lens by the zonular ligaments (zonules). The ciliary body defines the posterior chamber and it is adherent to the sclera. Externally this region is covered by a two-layer simple epithelium: the pigmented epithelium and the non-photosensitive area of the retina. Anteriorly the ciliary body presents several ciliary folds that include connective tissue and capillaries. These folds support the aqueous humor formation through both filtration and active transport mediated processes such as the carbonic anhydrase pathway. Elastic fibers,

pigmented cells vessels, and the ciliary muscle are all found within the ciliary body's connective stroma. The ciliary muscle provides accommodation by changing the lens position or shape, and its contraction improves aqueous humor drainage (Zachary, 2017).

The **iris** is settled between the anterior chamber and the posterior chamber, it partially covers the lens and with its free margin defines the pupil. The anterior surface consists of an irregular and intermittent epithelium with invaginations and folds. This epithelium includes pigmented cells, flat single fibroblasts and stromal connective fibers. The iris stroma is formed by bundles of arch-shaped collagen fibers that follow the iris modifications during miosis and mydriasis. In addition, the collagen fibers stabilize the vascular network surrounding the capillaries and avoiding damages to the microcirculation during contractions. There are two smooth muscles within the iris, the pupil constrictor muscle and the pupil dilator muscle, which control the size of the pupil and therefore light penetration.
The color of the iris is due to the pigmented cells that protect the retina from direct light rays and obligate them to enter only through the pupil. A layer of neuroepithelium called posterior iris epithelium covers the posterior side of the iris and is continuous with its counterpart in the ciliary body. In horses and ruminants, the posterior iris epithelium forms a nodular structure named respectively corpora nigra and granula iridica. The pectinate ligament, which runs from the anterior base of the iris to the inner peripheral cornea at the Descemet's membrane's terminal, defines the iridocorneal angle anteriorly. The iridocorneal angle also includes a network of trabeculae termed ciliary cleft and corneoscleral trabecular network that allow drainage of aqueous humor (Zachary, 2017).

The **choroid** lies between the sclera and the retina. It is rich in blood vessels and consists of pigmented fibrocytes, elastic fibers nets and round basophil cells. From outer to inner there are four layers: suprachoroid, choroidal stroma, choriocapillaris and Bruch's membrane. The suprachoroid provides transition between the choroid and sclera and consists of pigmented connective cells.

The choroidal stroma is the thicker layer and includes melanocytes and numerous blood vessels that supply the retina. These vessels pass through the choriocapillaris where they create the choroid internal capillary net, a packed reticular blood system that vascularize rods and cones.

The Bruch's membrane separates the retina to the choriocapillaris through a thick elastic core layer.

In domestic species, except the pig, the inner region of the choroidal stroma includes the tapetum lucidum. This structure is a specialized layer that serves to reflect light that has previously passed through the retina, further stimulating the photoreceptor cells and increasing vision in low light (Zachary, 2017).

THE INNER TUNIC (RETINA)

The retina includes a non-photosensitive region and a photosensitive region. The light sensitive one is divided into a pigmented external epithelium and a nervous internal layer. The pigmented epithelium consists of single wall cuboidal cells and it is located between the choroidal Bruch's membrane and the photoreceptors. These cells have several functions: cones and rods nutrition, metabolism products transport, melanin synthesis and rhodopsin renewal.

The nervous region includes three layers of neurons (ganglion cell layer, inner nuclear layer, and outer nuclear layer) separated by cell-free layers formed by the intermingling of the axons and dendrites of those neurons. Histologically ten layers are identifiable. Ganglion cells, bipolar cells, horizontal cells, amacrine cells, and photoreceptors are the five types of neurons present in the retina (rods and cones). Müller glial cells are non-neuronal cells found in the retina (Zachary, 2017).

The optic nerve is formed by the axons, which are positioned parallel to the retinal surface. The lamina cribrosa, a set of perforations located within the sclera near the posterior pole of the globe, is where the axons leave the globe. To retain transparency, the axons within the nerve fiber layer are not myelinated. The axons in the majority of animals myelinate when they leave the body at or near the level of the lamina cribrosa.

The retina in domestic species receives two blood supplies. The inner retina is fed by blood vessels, whereas the choroidal vasculature supplies the outer retina, specifically

the photoreceptors. Between species, there are significant differences in the location of blood vessels in the retina. The majority of the retina of domestic ruminants, pigs, and carnivores is covered in blood vessels (holangiotic pattern). Only the region immediately around the optic disc is vascularized in horses; the rest of the retina has a paurangiotic pattern, which increases reliance on choroidal supply (Zachary, 2017).

THE DIOPTRIC MEANS

Into the interior space of the eyeball other structures are identifiable: the lens, the anterior and the posterior chambers containing the aqueous humor and the vitreous chamber which is constituted by the vitreous.

The **lens**'s role is to focus and refract light onto the retina: it is a biconvex structure located between the iris and the vitreous. It is maintained in place in part by the presence and pressure of the vitreous and suspended by the zonular ligaments created by the ciliary epithelium. The lens epithelium, which is made up of a single layer of cuboidal epithelial cells just inside the anterior lens capsule, is the only type of cell that form the lens. Because the lens lacks blood vessels, it depends on aqueous humor to carry nutrients and remove waste from cells. Since the lens's purpose is to refractively focus light that has already traveled through the cornea onto the retina, the lens must therefore continue to be transparent. The precise orientation of the lens fibers, the lack of cytoplasmic organelles, the presence of specific intracellular crystalline proteins, and the maintenance of a dehydrated state are all factors that affect the transparency of the lens (Zachary, 2017).

The **anterior chamber** and the **posterior chamber** contain the aqueous humor, which is a transparent liquid that resembles plasma but contains less proteins. It is responsible for nutrition and removal of waste product of the lens. It is created by fibrocytes and capillaries from the ciliary processes and is moved via the pupil of the anterior chamber of the eye to the posterior chamber by epithelial cells. The drainage of this fluid is carried out by the trabecular network in the iridocorneal angle (Zachary, 2017).

The **vitreous chamber** contains the vitreous, which is a transparent, elastic hydrogel. Its main functions are supporting the lens and retina, aiding to keep them in their proper locations and offering protection from trauma. The vitreous makes up about 80% of the globe's volume and is a modified extracellular space rather than a cavity. It is made up almost entirely (99%) of water. Collagen, hyaluronic acid, and broadly distributed cells known as hyalocytes make up the majority of the remaining 1%. The hyalocytes are the source of fibroblasts in healing responses and are hypothesized to have secretory and phagocytic activities (Zachary, 2017).

THE ACCESSORY ORGANS

The bony orbit, the eyelids and the conjunctiva shield all of these structures and layers from outside influences and from the spread of illnesses from neighboring tissues. Together, they form a physical barrier.

The **bony orbit**, depending on the species, results from the fusing of five to seven bones and protects the globe. Except in carnivores and pigs, where the orbital ligament creates the dorsal roof, it forms a full shell. Along with the globe, the orbit also houses the zygomatic salivary gland, lacrimal glands, extra ocular muscles and fat. Numerous foramens, through which blood vessels and nerves enter or exit the globe, are present on the posterior surface (Zachary, 2017).

The **eyelids** are movable folds of skin that move across the cornea's surface on the tear film to distribute the protective fluid and clear away surface debris. The upper eyelid has more rows of larger modified hairs than the lower one, in which they are occasionally absent. These rows of hairs define the eyelid boundaries. The Meibomian glands, modified sebaceous glands located on the margin, are crucial for producing the tear film's superficial lipid layer, which helps to evenly distribute the aqueous component across the cornea's surface and prevents evaporation (Zachary, 2017).

The **conjunctiva** is a mucous membrane consisting of a stratified squamous nonkeratinizing epithelium that also contains goblet cells (except for the bulbar part), melanocytes, dendritic cells, and leukocytes. Both substantia propria of the conjunctivas is made up of diffuse lymphoid tissue and loose connective tissue with vessels.

The third eyelid, also referred to as the nictitating membrane, is formed by undergoing an extra specialization of the ventral conjunctiva. Between the inferior eyelid and the anterior cornea, it protrudes from the ventral-medial canthus of the eye and is supported by a T-shaped plate of cartilage that is encircled by accessory lacrimal glands (Zachary, 2017).

The **lacrimal apparatus** is formed by lacrimal glands and ducts. The lacrimal gland is a flat structure between the globe and the dorsal lateral wall of the bony orbit; there are also the third eyelid associated glands and other accessory glands. The lacrimal film is created by these structures and is made up of three layers, the outermost of which is lipidic (created by the Meibomian glands) and aids in spreading tears across the surface of the eye. The lacrimal glands create the intermediate layer, which is primarily made of water and vital to the cornea's nutrition and humidity. The conjunctiva generates the innermost layer, which is mucinous and connects the tear film to the cornea. Through the lacrimal points, tears enter the lacrimal channels. They then reach the lacrimal sack and continue in the nasolacrimal duct. The glands are seromucous in dogs and ungulates and serous in the cat (Zachary, 2017).

1.2 PORCINE CORNEA

Since the shape of the pig eye is comparable to that of the human eye, it is frequently employed as an ex vivo animal model in research on vision sciences. Due to the distribution of the retinal layers being comparable to that of the human retina, the swine eye has been utilized in neuroretinal investigations and it is also a verified animal model of glaucoma. Additionally, it has served as a model for investigations on aberrometry, corneal transplantation, and cataract surgery.

The pig eye's horizontal and vertical corneal diameters are 14.23 mm and 12.69 mm, respectively. In an ex vivo model, the ultrasonic pachymetry ranges from 1013±10 μm to 666 μm (with a range of 534 m to 797 m) in a living mammal. The 80 μm thickness of the corneal epithelium can change by 25 μm and is not constant. Descemet's membrane with the endothelium has a thickness of around 30 μm, whereas the stromal thickness is 900 μm. The pig cornea has a water content of 71.93±0.47% and a transparency of 54.77±0.47%. All the variations may result from the varying ages of the slain animals or the type of pig employed. Additionally, if measurements are collected a long time after animal killing in ex vivo models, corneal pachymetry may rise as a result of corneal edema (Sanchez et al., 2011).

Porcine cornea lacks the Bowman's layer: although this, the porcine cornea is about twice as thick as the human cornea. Bowman's layer was seen in pig corneas in earlier research, but it was absent in subsequent histological examinations (Sanchez et al., 2011).

Parameter	Porcine eye	Human eye
Corneal steepest meridian	7.85 mm	7.65 mm
Corneal flattest meridian	8.28 mm	7.79 mm
Corneal astigmatism	0.43 mm	0.14 mm
Central corneal pachymetry	1009 μm	523 μm
Peripheral corneal thickness	1340 μm	564 μm
Anterior chamber depth	1.77 mm	3.11 mm
Anterior chamber angle	28.8°	38.1°
Shortest corneal diameter	12.69 mm	11.71 mm
Longest corneal diameter	14.88 mm	12.00 mm
Endothelial cell density	3250 cell/mm^2	2496.9 – 4049.5 cell/mm^2

Table 1. Comparison of mean porcine eye parameters obtained and estimated average human eye parameters according to the scientific literature (Menduni et al., 2018) *.*

Cat and dog corneal epitheliums were found to be the thinnest. In comparison to carnivores, the epithelium of the horse cornea was two to three times thicker. Horse epithelium has 12–15 cell rows compared to carnivore epithelium's six–nine cell rows, which coincided with the thicknesses seen. The bovine epithelium has 11–15 rows of cells. There were 8–12 rows of squamous cells in the corneal epithelium of the goat and pig. Except for cats, all surviving species in the stratum basale had cells with a columnar form. Pigs have pencil-shaped stratum basale nuclei in contrast to carnivores and herbivores' spherical nuclei. The thickness of the Descemet membrane layer revealed clear species-specific variances, with the horse, cow, and dog having the thickest dimensions. While the Descemet membrane in cats and goats was similar in thickness, the one in pigs was the thinnest (Nautscher et al., 2016).

1.3 CORNEAL RESPONSE TO INJURY AND WOUND HEALING

Although the cornea reacts to damage in a variety of ways, the majority of disorders cause a few basic processes that may be also observed in combination.

A. Epithelial necrosis

Acute trauma, severe desiccation, chemical burns, and less frequently viral illnesses are the usual causes of epithelial necrosis. Minor wounds may merely result in erosions, whereas more serious wounds will result in full thickness epithelium loss (corneal ulcers). Following corneal ulceration there is an immediate osmotic absorption of water from the tear film in the anterior stroma, which causes focal superficial stromal edema. The region will quickly become infiltrated by neutrophils from the tear film, shielding the cornea from opportunistic infection and supplying growth factors for a successful healing process. Small, simple lesions with little stromal involvement will recover through epithelial sliding and growth (Zachary, 2017).

B. Stromal necrosis

Injury to the cornea that penetrates the epithelium will also result in stromal necrosis, which is clinically known as keratomalacia. This can occur in sterile wounds as well as fast developing ulcers that are infected with bacteria or fungi. Large numbers of neutrophils will migrate from the limbus and tear film, and they will release lytic enzymes that contribute to stromal damage and lead to neutrophil-induced suppurative keratomalacia. These ulcers, also known as melting ulcers, will develop quickly over a short period of time. In these circumstances, fibrotic repair will be necessary for corneal healing (Zachary, 2017).

The Descemet's membrane will be exposed in the most extreme cases of full-thickness stromal necrosis. A descemetocele can develop when Descemet's membrane protrudes anteriorly into the hole left by the loss of the stroma and epithelium above it. This often results in rupture of Descemet's membrane (perforating ulcer), leakage of aqueous humor from the anterior chamber, and possibly iris prolapse in the absence of prompt medical attention (Zachary, 2017).

C. Corneal edema

Also known as stromal edema, is characterized by the buildup of extra fluid and changes in the glycosaminoglycan composition of the stroma, which cause the lamellae to separate and the transparency to deteriorate. Numerous factors can lead to stromal edema, which can develop after damage to the epithelium, stroma itself, or endothelium.

Any lesion that interrupts the corneal epithelium might result in stromal edema due to the osmotic absorption of tear film fluid. Edema may accompany inflammation or leukocyte infiltration that occurs in the stroma and originates from the surface, conjunctiva, or anterior chamber. It also frequently develops from the stroma becoming neovascularized as a result of blood vessel formation at the limbus. Any damage to the corneal endothelium may result in edema through the absorption of fluid from the aqueous humor or from a diminished capacity to react to edema as a result of epithelial or stromal injury. Inflammation inside the eye, glaucoma, and contact between the lens and corneal endothelium from anterior lens luxation are typical causes of endothelial damage (Zachary, 2017).

D. Corneal neovascularization

Since the stroma is avascular in the normal state, stromal neovascularization is always seen as a pathologic reaction. Wide-ranging factors, including as trauma (both accidental and surgical), inflammation, infection, degenerative diseases, and others, can result in corneal neovascularization. Vascular endothelial growth factor (VEGF) is often the main mediator of corneal neovascularization. After the starting event, there is a latency period during which VEGF levels will rise. About 24 hours pass during the latent phase. After then, the limbal blood vessels enlarge. Multifocal enzymatic digestion of the limbal vessels' basement membrane and endothelial cell proliferation are required for vascular sprouting to take place.

If the initial cause is eliminated or regulated, corneal neovascularization can be stopped. On the other hand, the framework of corneal neovascularization may continue for a long time after the triggering factor has been eliminated and blood flow has stopped, with the formation of "ghost vessels". In the lack of fresh vessel creation and

with only a slight stimulation, these remaining vessel walls may quickly become engorged with blood (Zachary, 2017).

E. Corneal degenerations and depositions

The buildup or deposition of extra material within the cornea can result from a range of genetic and acquired diseases. In veterinary medicine, the majority of cases illustrate the deposition of lipids or minerals (Zachary, 2017).

F. Corneal inflammation

In acute keratitis neutrophils are typically the main leukocyte. Lymphocytes and plasma cells will infiltrate the stroma as a result of almost any chronic corneal damage.

The non-specific chronic keratitis with epidermalization (cutaneous metaplasia) is an adaptive reaction to a minor but enduring corneal damage. The goal is to retain corneal integrity and prevent ultimate rupture because of chronic damage, however these modifications invariably result in loss of corneal transparency. Tear film irregularities and mechanical irritation are the most frequent causes of mild chronic irritation. Nonspecific chronic keratitis causes hyperplasia with the production of melanosis and keratinization as epithelial alterations. Because the corneal epithelium develops characteristics associated with the skin's epidermis, the combination of these changes is known as corneal epidermalization or cutaneous metaplasia. Melanin buildup inside the corneal basal cells and centripetal migration of limbal melanocytes cause corneal melanosis. Significant pigmentary incontinence, the leaking of melanin from the epithelial basal cells, may also cause superficial stromal melanosis as a result of pigment buildup in macrophages and fibroblasts. The superficial neovascularization and fibrosis that characterize nonspecific chronic keratitis are the main stromal alterations. Inflammatory cells, most frequently lymphocytes and plasma cells, may infiltrate the tissue (Zachary, 2017).

If the underlying cause can be treated, certain lesions of nonspecific chronic keratitis may be curable, although there may be a persistent loss of transparency .

CORNEAL WOUND HEALING

The cause and degree of the damage define the complex chain of events that make up the systems that control corneal wound healing. The response to corneal injury is not strictly limited to the cornea itself: the tear film, as an example, plays a crucial role in the process by supplying numerous growth hormones and proteases as well as the means for leukocyte migration and the elimination of injured cells. Also the fibrinogen needed to produce a fibrin clot that closes a full-thickness disruption and triggers the healing process is sourced posteriorly from the aqueous humor of the anterior chamber (Zachary, 2017).

When the corneal epithelium is disrupted, epithelial cells are lost. By centripetal migration of limbal stem cells to replace the basal cells, the corneal epithelium is continuously regenerated. The surface maturation process concludes with the apoptotic shedding of the superficial cells while the basal cells are mitotically active. There are four stages to the healing of corneal epithelial wounds. There is no cell migration or proliferation during the first phase, the latent phase. In the tear film, damaged cells go through apoptosis and are expelled. Over the injury site, fibronectin polymerizes to provide a transitory extracellular matrix scaffold that will aid in cell migration. This phase may last several hours. During the second phase the basal epithelial cells near the defect's edges will slide in a centripetal motion, covering the defect. The cells have the potential to slide up to 1 mm every day. Studies have revealed that the leading border of the migrating epithelial sheet is where the cells are most securely connected to the substrate, which may indicate that the leading cells are "pulling" the epithelial sheet as it migrates (DelMonte & Kim, 2011). The third stage of proliferation starts after the defect has been re-epithelialized. The resumption of mitoses and maturation will return the thickness to normal. In the fourth phase, known as attachment, hemidesmosomes are formed to strongly adhere to the basement membrane (Zachary, 2017).

Stromal healing involves more remodeling of the tissue, with keratinocytes transformation and production of matrix. Within one to two hours of the damaging

event, edema, local keratinocyte apoptosis, and neutrophil infiltration are the early symptoms of stromal damage. By eliminating the mediating cells, keratinocyte apoptosis is a crucial step that prevents a fibrotic repair. There are three stages of stromal healing: during the first phase the nearby stromal keratocytes reach the site of the damage and produce collagen and extracellular matrix. During this phase growth factors and metalloproteases (MMPs) are also secreted. It has been suggested that the loss of certain type IV collagen isoforms in the epithelial basement membrane, which results in scarring, may be caused by the overexpression of these MMPs and activated inflammatory cytokines (DelMonte & Kim, 2011). The second stage is when keratinocytes proliferate and undergo a change and become fibroblasts or myofibroblasts. Monocytes have also the ability to become fibroblasts and aid in stromal repair. The wound closes during the third phase, and myofibroblasts undergo apoptosis and necrosis. The continued presence of myofibroblasts can lead to excessive matrix formation, exuberant contraction, fibrotic healing, and loss of transparency.

The corneal endothelium healing occurs by sliding and enlarging the nearby healthy endothelial cells. In most species, indeed, the corneal endothelial cells are postmitotic and have little to no capacity for regeneration. If enough endothelial cell density (400 to 700 cells/mm^2) is still present, normal function can be recovered. Three steps are taken to resurface the affected region. The first stage is distinguished by the creation of early wound coverage by migration of neighboring endothelial cells, which creates a transient imperfect barrier with diminished pump sites and incompletely established tight junctions. In the second stage, the endothelial cells form irregular polygons, the tight connections return to normal levels, the quantity and quality of pump sites improve, the corneal thickness usually returns to normal, and transparency is regained. The final step, which might last for many months, involves modifying the endothelial cells to create more regular hexagons (DelMonte & Kim, 2011).
If Descemet's membrane is damaged, the endothelial cells could produce a new basement membrane. The Descemet's membrane may duplicate as a result of this procedure, which is frequently imperfect.

MOLECULAR MODULATION OF CORNEAL HEALING

Tumor necrosis factor (TNF-α) and interleukin 1 and 6 (IL-1 and IL-6) are the major cytokines that are released in response to epithelial damage.

IL-1 and IL-6 are produced in proportion to how badly the epithelial tissue has been damaged. Together with epithelial growth factor (EGF), IL-1 promotes wound healing. It also increases the secretion of hepatocyte growth factor (HGF) and keratinocyte growth factor (KGF) and amplifies the effects of platelet-derived growth factor (PDGF). Additionally, IL-1 increases the synthesis of collagenase and matrix metalloproteinase (MMP) by keratocytes, as well as keratocyte apoptosis and neutrophil recruitment. The integrin receptor for fibronectin is upregulated by IL-6, which therefore promotes epithelial cell migration. Through transforming growth factor (TGF-β), TNF-α affects epithelial repair, neutrophil recruitment, and keratocyte apoptosis. TNF-α and IL-1 also induce upregulation of IL-8 that encourages angiogenesis and neutrophil recruitment.

Serine proteases and MMPs are the major types of proteases that are important for modifying the stroma. The physiological equilibrium of proteases and protease inhibitors, which supports corneal maintenance and regeneration, is upset by injury to the cornea. Injury to the cornea changes the ratio in favor of remodeling and breakdown, and it also reduces the function of protease inhibitors (Zachary, 2017).

The main MMPs that have been studied are MMP-2 and MMP-9. MMP-9 is mostly found near the wound's leading edge and is generated by leukocytes and epithelial cells. Proteins in the basement membrane and collagen are broken down by MMP-9, which also affects IL-1 and stimulates TGF-β. Following wound closure, MMP-9 also breaks down the temporary fibronectin matrix. The corneal epithelium and keratocytes both generate MMP-2. It contributes to proper corneal regeneration and increases after corneal damage to affect stromal remodeling (Zachary, 2017).

1.4 CORNEAL DISORDERS

The cornea is shielded from the majority of physical and chemical harm by the eyelids' many reflex actions, the bony orbit, and the continuous flow of tear film. When the cornea or eyelids are mechanically stimulated, many responses are triggered. When triggered by contact with any solid object or vigorous airflow, the blink reflex forces the eyelids to shut. When a visual threat to the globe is perceived, the menace reaction forces the eyelids to blink. When the cornea is irritated by outside stimuli, the corneal reflex forces the eyelids to close. In reaction to corneal injuries, the globe retracts reflexively into the orbit, and the third eyelid passively slides down to cover the cornea. The tear film provides the avascular cornea with nutrition, with a mucus layer to stop the protective fluid from evaporating, with soluble antibacterial compounds, and with a flushing action to shield the cornea from pathogens and foreign objects. Conjunctival goblet cells, several auxiliary glands inside the conjunctival substantia propria, and Meibomian glands also contribute to the production of the tear film, which is formed by the lacrimal gland and the gland of the third eyelid. The outermost layer of the tear film is created by goblet cells, which also produce mucins. Ocular surface mucins operate as a bonding agent between the corneal epithelium and tear film, prevent bacterial colonization, and aid in the removal of foreign objects (Zachary, 2017).

The central corneal epithelium contains immature dendritic cells, whereas the periphery contains adult and immature dendritic cells. The ocular surface is covered with toll-like receptors (TLRs), which can immediately trigger an innate defense against the pathogen and activate adaptive immunity.

Antimicrobial peptides such lysozyme, lactoferrin, lipocalin, angiogenin, secretory phospholipase A2, secreted immunoglobulin A (IgA), complement factors, defensins, and others that prevent the invasion of pathogenic organisms are also included in the innate immune response (Zachary, 2017).

Corneal disorders can be congenital or acquired. Dermoid is the main congenital one and the lesion is made up of ectopic hair follicles and adnexal glands within the cornea, similar to the conjunctival dermoid. The ectopic tissue might be as little as a few

dispersed sebaceous glands or as large as mature hair follicles and other characteristics of healthy skin (Zachary, 2017).

Within the acquired disease the main are: corneal ulcers, indolent corneal ulcers, suppuratives keratomalacias, corneal sequestrums, corneal dystrophies and depositions and neoplasms.

Corneal ulcer

Infectious and noninfectious categories are used to categorize ulcers. The majority of infections are caused by bacteria, mostly Pseudomonas and Staphylococcus, but fungi parasites and viruses are also frequent. Chemical burns, autoimmune, neurotrophic, toxic, and allergic keratitis, as well as keratitis related to entropion, blepharitis, and a variety of other disorders are all examples of noninfectious ulcers.

Bacterial keratitis often presents as an extremely painful, injected eye that is frequently accompanied by copious weeping and discharge. It is normal to see stromal invasion with an area of overlaying epithelial excavation, and the lesion may release mucopurulent material. The conjunctival and episcleral vessels will be hyperemic and inflamed, and the cornea and/or eyelids may be puffy. There may be a significant anterior chamber response in severe instances, frequently with pus (Weiner, 2012).

Spontaneous chronic corneal epithelial defects

Also known as nonhealing/persistent/recurrent ulcers or indolent ulcers, they mostly develop in dogs. The illness is characterized by surface ulcers that did not heal correctly even though there was no underlying reason. The stromal surface is coated with fibronectin and the basement membrane is missing or discontinuous in afflicted regions. At the ulcer edges, slug expression and other factors necessary for epithelial cell movement are absent or diminished. The lesion is identified histologically as wide flaps of epithelium that have been severed from the stroma. When the corneal epithelium separates due to a number of corneal stromal disorders, including corneal edema, a histologic lesion that resembles an indolent corneal ulcer can develop (Zachary, 2017).

Suppurative keratomalacia ("melting ulcer")

Numerous organisms generate lytic enzymes that can induce stromal necrosis/malacia, and neutrophils from the limbus and tear film can also release these enzymes. Keratomalacia can develop in sterile lesions, however ulcers that pick up bacterial or fungal contamination are more likely to develop severe suppurative keratomalacia. In the most severe instances, descemetocele and corneal perforation will develop. This often results in rupture of Descemet's membrane (perforating ulcer), leaking of aqueous humor from the anterior chamber, and perhaps iris prolapse in the absence of prompt medical attention (Zachary, 2017).

Corneal sequestrum

The specific pathophysiology of the disease is unknown, however it frequently follows chronic ulceration. The superficial stroma contains imbibition of dark pigment. As a result, the disease's prominent and fundamentally pathognomonic symptom is a highly distinctive center corneal dark brown pigmentation. There is evidence to support and refute the presence of melanin and iron/porphyrins, but the origin of the pigment is still unknown (Zachary, 2017).

Dystrophies and depositions

The endothelium, the stroma, or the epithelium may be impacted by the lesions. True dystrophies lack inflammatory or metabolic causes, are bilateral and symmetrical and are frequently breed-related. Breed, age, precise anatomic position, and macroscopic appearance are frequently distinguishing clinical aspects of these deposits that enable a diagnosis to be determined without histopathologic investigation.

Dogs are the primary carriers of corneal epithelial dystrophy. These lesions, which include dyskeratosis and necrosis of the epithelial cells as well as anomalies to the corneal epithelium's basement membrane, are unlikely to be histologically examined.

Although uncommon, corneal stromal dystrophies are composed of lipid or mineral deposits. Due to the gradual death of corneal endothelial cells, corneal endothelial dystrophy manifests in various dog breeds as bilateral, diffuse corneal edema.

The superficial appearance of the corneal stroma or the epithelium's basement membrane may both develop acquired mineral deposition (band keratopathy). Secondary mineral deposition may be brought on by hypercalcemia and corneal irritation. The corneal stroma develops milky or crystalline stromal deposits of serum lipids as a result of acquired corneal lipidosis (lipid keratopathy). Primary corneal illness or lesions in nearby tissues that might overflow in the cornea can cause it. Hyperlipidemia might be a contributing cause (Zachary, 2017).

1.5 CORNEAL BIOMECHANICS

Finding a mathematical model that represents the response of the tissue to applied external stress is one of the most crucial goals of the study of the mechanical behavior of biological materials. The models have certain accuracy limitations and are dependent on the stress (force per unit of area) conditions that are applied to the material in order to accurately explain mechanical behavior. The description of the structure's deformation (strain) when a force is applied serves as the foundation for defining the mechanical behavior of a system.

In material science, the cornea is referred to as a complex anisotropic composite with non-linear elastic and viscoelastic characteristics. It is a composite because the interaction of several materials, such as collagen and a polyanionic ground substance, determines its characteristics, and it is anisotropic because its qualities are not uniformly distributed along directions. The center to periphery, anterior to posterior, and rotational dimensions of the cornea are likewise quite diverse (Dupps & Wilson, 2006).

The crucial factors affecting the material characteristics of the corneal tissue are the ECM components, the organization of the collagen structure and the corneal hydration/osmotic pressure.

Proteoglycans (PGs) and glycosaminoglycans (GAGs) are essential for the ECM's transparency and construction. It is commonly accepted that dermatan sulfate proteoglycans control interfibrillar spacing and lamellar adhesion qualities whereas keratan sulfate proteoglycans control the diameter of collagen fibrils. GAGs are necessary to sulfate PG core proteins, although they merely electrostatically interact with collagen and barely effect nucleation or growth. A number of corneal ectatic diseases have been linked to de-glycosylated small leucine-rich repeat proteoglycan core proteins, which have been hypothesized to influence collagen fibrillogenesis. The degree of collagen fiber organization throughout the human corneal stroma is closely correlated with the quantity of acidic GAGs. Physiological changes are concomitant with variations in GAG and PG composition. The amount of oxygen that is readily available has a significant impact on the ratios of GAGs and PGs. According to research on the

cornea and cartilage, keratan sulfate (KS) rather than chondroitin sulfate (CS) is created when there is a lack of oxygen. This might explain why the posterior stroma is dominated by KS. The KS:GAG percentage can reach up to 60–70% in large animals with thick corneas, such cows, pigs, or humans, whereas it is entirely missing in tiny animals like mice. It is generally accepted that KS stabilize collagen fibrils on a short-range basis, whereas CS/DS proteoglycans support multiple fibrils up to lamellae. Consequently, the cornea may become weaker if chondroitin sulfate proteoglycan levels drop (Kling & Hafezi, 2017).

In all species, collagen fibril orientation corresponds with visual acuity and dictates corneal transparency as well as direction-dependent material qualities. The maximum visual acuity and best predicted corneal shape maintenance are found in orthogonal orientation (human), which is followed by vertical orientation (horse, cow), then circumferential orientation (pig, rabbit, mouse). According to certain theories, variations in the stromal collagen organization may be caused by species-specific eye movements. They cause the extraocular rectus muscles to contract in a certain way, evoking opposing pressures that cause the collagen fibers to align. Each corneal layer contributes to the total biomechanical resistance to a greater or lesser amount because of the various collagen orientation and density. As pure cell layers, the epithelium and endothelium do not directly affect the cornea's rigidity. However, by controlling the hydration of the cornea, these cell layers may indirectly influence its rigidity. Collagen lamellae are most tightly packed in Bowman's membrane, which is thought to be crucial for corneal stability. The layer that primarily determines the cornea's biomechanical characteristics is the stroma, which makes up the majority of the cornea. Studies that presume the cornea to be a single layer of material generally refer to the stroma.
The amount of corneal hydration affects not only how transparent the cornea is, but also how elastic it is. The more hydrated the corneal tissue, the lower the elastic modulus, which may result from a different collagen attachment to the proteoglycans and/or glycosaminoglycans based on their ionic interaction. The swelling characteristics of ocular tissue are not just caused by osmotic pressure, but also result from electrolyte exclusion caused by the amount of collagen fibrils (Kling & Hafezi, 2017).

The tensile qualities of the collagen microstructure are referred as elastic properties, which are a material's static characteristics. Viscosity is a term for dynamic (time-dependent) features that result from noncovalent configurations of the ECM, such as electrostatic interactions between GAGs and collagen and water diffusion.

Collagen fibers are primarily responsible for elastic characteristics, which define the instantaneous deformation reaction to the application of a mechanical force. The collagen fibers initially crimp when a force is applied to the ocular tissue that has not been previously strained, creating a "toe region" in the stress-strain diagram. The tissue only deforms elastically when the fibers become straight. The physiological condition is thought to be located between the end of the toe and the start of the elastic area. A larger load causes permanent plastic deformation when the elastic zone is exceeded, leading the tissue to rupture. The static elastic modulus, also known as Young's modulus, is the standard elastic parameter. It is described as the stress-strain diagram's tangent's slope. While non-linear elastic materials (like the cornea) have elastic moduli that vary with strain, linear elastic materials have an elastic modulus that is constant. Even non-linear elastic materials, nevertheless, deform linearly for extremely tiny deformations. Pigs' corneal elastic modulus measurements range from 1.5 MPa to 3 MPa (Kling & Hafezi, 2017).

The dynamic deformation response is due to the viscoelastic material characteristics. These time-dependent characteristics result from osmotic diffusion in response to the application of a mechanical load as well as molecular rearrangement. With time, viscoelastic deformation is entirely reversible. A hysteresis between the loading and unloading cycle is seen in the stress-strain curve, and its area corresponds to the energy lost during the viscous deformation (Kling & Hafezi, 2017).

BIOMECHANICAL TESTS

In vivo, ex vivo, and in vitro techniques can be used to explore the biomechanical characteristics of corneal tissue by deforming the cornea's surface and allowing the tissue to relax.

There are tests that are just mildly invasive for in vivo research to look at the mechanical characteristics of the cornea using an air puff, particularly in human medicine. A non-contact tonometer that indentates the cornea with an air puff is the Ocular Response Analyzer (ORA, Reichert Ophthalmic Instruments, Buffalo, New York, USA). Both corneal hysteresis and corneal resistance factor, or tissue elasticity, may be tested using the apparatus (Luce, 2005).

The most popular ex vivo study techniques are uniaxial tensile tests and inflation tests. Through inflation testing, one may assess the tissue's short-term nonlinear behavior and how its stiffness changes as intraocular pressure rises, while the tensile testing can assess the medium- and long-term viscoelastic response as well as the stress-strain curve. In these tests, either the intraocular pressure changes or the tissue elongates, causing the tissue to deform.

The inflation test examines the entire eyeball adjusting IOP (intra-ocular pressure) when its value rises and falls and specifically evaluate corneal thickness and radius of curvature. The usage of the complete eye globe creates a condition that is comparable to comprehend the natural behavior of the cornea, making this test one of the most appropriate ways to explore the biomechanical features of corneal tissue. Additionally, the test is minimally intrusive, the cornea's natural borders are kept, stress is induced by adjusting IOP, and analysis may be done while taking into account the tissue's orientation. Results can therefore be more effectively used in clinical practice (Lombardo et al., 2014).

For the assessment of corneal biomechanics and to gain insight into the link between the outcomes of inflation and uniaxial tests, experimental methodologies and testing protocols were developed, which were carried out sequentially on the same ex vivo swine sample. All corneas were discovered to have a bilinear behavior during inflation

testing, which is explained by the presence of collagen fibrils. When the samples were stretched, the fibers aligned their axes in the direction of the applied force, causing a noticeable shift in stiffness (Boschetti et al., 2012).

One of the fundamental techniques for assessing a material's key mechanical characteristics is the uniaxial tensile test. Standard or specially created, this testing apparatus is typically used for in vitro or ex vivo studies. The test involves the stretching a certain tissue, in this case a strip of corneal tissue, as previously mentioned.
Clamps are used to fix specimens on the apparatus; it is crucial that there is not slippage or damage to the sample during the test otherwise the test's parameters won't be administered uniformly to the tissue. Because of this, test-specific clamps are created, or adhesive is employed to ensure a firm grasp on the specimen. Additionally, to prevent dehydration, which might affect the mechanical behavior, samples must be continually hydrated with physiological solutions.
The orientation, loading parameters, length, width, and thickness of each sample, as well as the time before and after the test, are all documented in order to create the stress-strain curve that defines the tissue. The curve supports the material's viscoelasticity and nonlinear behavior in the instance of ocular tissue. When ex vivo and in vitro operations are carried out, the strain is evaluated either by employing a camera that records the movements of markers placed on the surface of the tissue or by measuring the displacement of the clamps that secure the samples. Using load-displacement data and the assumption that stress and strain distributions are constant across all samples, mechanical parameters are then determined. The stress-strain and stress-relaxation curves may be drawn using those parameters.

Here, we provide a brief explanation of the tensile stress-strain behavior for skin, an organ made primarily of connective tissues. This behavior is typical of many (collagenous) soft connective tissues. The three-dimensional network of fibers appears to have preferred routes parallel to the surface for the connective tissue regions of the skin. Some fiber orientations do, however, also include components that are out of plane in order to avoid out-of-plane shearing (Holzapfel et al., 2005).

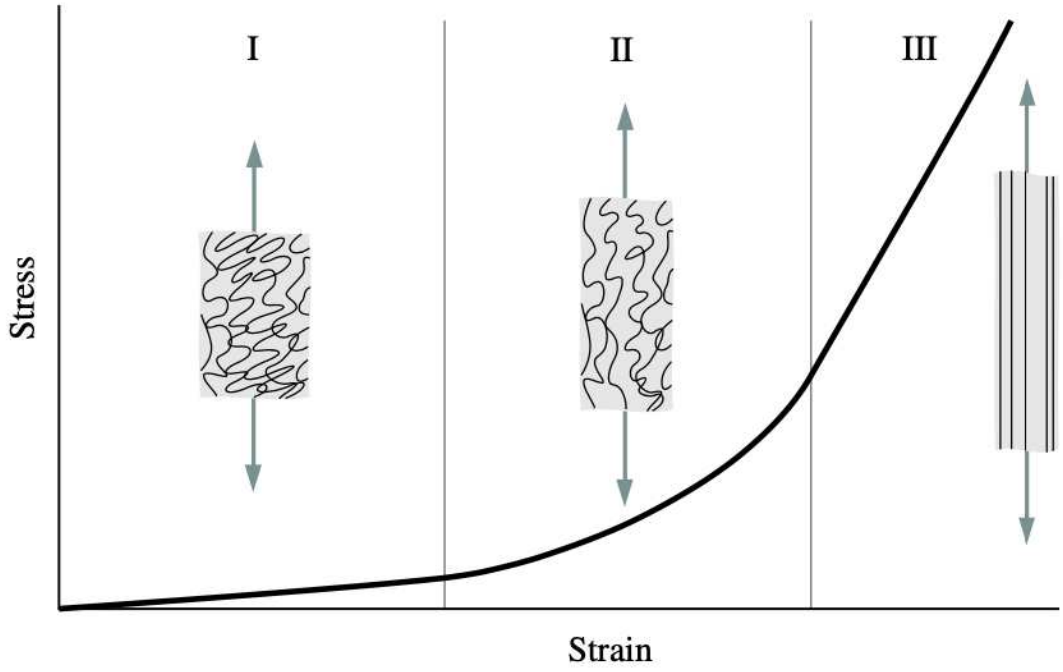

Figure 4. Schematic diagram of a typical (tensile) stress-strain curve for skin showing the associated collagen fiber morphology (Holzapfel et al., 2005).

Three phases, I, II, and III, may be used to study the deformation behavior of skin:
Stage I. Collagen fibers, which are braided into rhombic-shaped patterns, are relaxed and look wavy and crimped in the absence of load. Skin that has not been stretched behaves roughly isotropically. To obtain significant deformations of the individual collagen fibers without the need for stretching the fibers, initial low stress is necessary. In phase I, the elastin fibers are primarily in charge of the stretching process, and the tissue acts like an extremely flexible (isotropic) rubber sheet. The elastic modulus in phase I is low, and the stress-strain relationship is roughly linear.
Stage II. Collagen fibers typically align with the direction of the load and bear burdens when the load is increased. The crimped collagen fibers interact with the moist matrix as they increasingly lengthen. The crimp angle in collagen fibrils causes a series of uncrimpings as a result of deformation.
Stage III. At high tensile loads the crimp patterns vanish and the collagen fibers straighten out. The direction in which the load is applied is where they are most closely

aligned. Collagen fibers that have been straightened firmly resist the load, and with increasing pressures, the tissue stiffens. The stress-strain relationship returns to being linear. After the third step, the fibers achieve their maximum tensile strength and start to break (Holzapfel et al., 2005).

It is necessary to measure the sample's dimensions and determine stress and strain from load and displacement in order to directly compare various materials since loading responses must be normalized against sample geometry.
Strain is calculated as

$$\varepsilon_e = \frac{\Delta L}{L_0}$$

where ΔL is the displacement and L_0 the initial length.
Stress can be calculated as

$$\sigma_e = \frac{P}{A_0}$$

where P is the applied load and A_0 the initial cross-sectional area of the sample normal to the loading direction (Khlystov et al., 2013).
When dealing with biological tissues, the stress-strain curve is typically analyzed using an exponential formula to learn more about the tissue's viscoelastic nature:

$$\sigma(\varepsilon) = \frac{k}{\alpha}\, e^{(\alpha\varepsilon - 1)}$$

where σ stands for stress, ε for strain, k for the initial stiffness of the tissue in the absence of strain, and α for the stiffening of the tissue during the deformation process (Natali et al., 2016).

In creep testing, the stress is changed to assess the variations in the tissue's response, whereas stress-relaxation and hysteresis tests assess the tissue's behavior under various strain conditions. During stress-relaxation testing, the tissue is quickly stretched while the displacement is held constant for a period of time. Initially at its maximum, the response force, the load required to keep the tissue in its distorted state, decreases during the course of the period toward an asymptotic or equilibrium value.
It is likely that during this period, the material's microscopic structures exhibit some relative sliding, which results in a slight apparent stiffness of the tissue. This is seen in the curve's declining slope and the lowering value of load required to keep the tissue in its deformed state. The stress-relaxation curve for corneal tissue has a similar pattern of behavior, supporting the viscoelasticity of this substance. Collagen fibers reorganize themselves as an external tensile tension is applied, which results in this response.

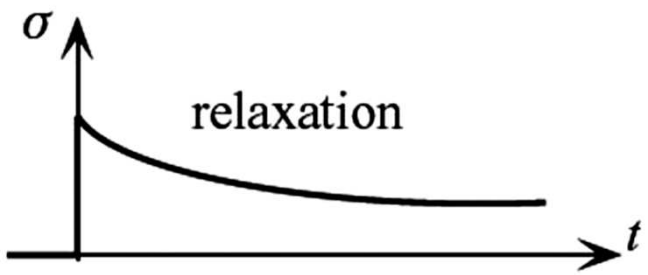

Figure 5. Schematic diagram of a typical (tensile) stress-relaxation curve in a viscoelastic material

The samples' nonlinear behavior is confirmed by uniaxial testing for anisotropy and viscoelasticity, however these tests cannot be regarded as an accurate representation of the mechanical behavior due to inherent methodological errors.
Actually, there are some drawbacks to uniaxial tensile tests: samples are taken from curved surfaces, lamellae are cut, and there are variations in corneal thickness throughout the specimens' length. Additionally, a number of factors, including the specimens' age, species, preservation method, hydration liquid, testing procedure, endothelium and epithelium presence, and degree of strain, might influence the

mechanical characteristics (Boschetti et al., 2012). Another difficulty is the preconditioning effects brought on by strip extensiometry techniques, which might change the tissue's biomechanical characteristics: in particular, the corneal tissue results stiffer during uniaxial tests than in inflation tests. Due to these factors, it is challenging to compare various research, and the outcomes might differ significantly from those of inflation tests, almost by an order of size (Kling & Hafezi, 2017).

2. THE PLASMA

2.1 THE PHYSICS OF PLASMA

Along with gases, liquids, and solids, plasmas are frequently referred to as the fourth state of matter, however this designation provides nothing to explain their primary physical characteristics. In reality, depending on its density and temperature, a plasma can display behavior typical of all three of the more recognizable states. Plasma can be simply defined as a quasi-neutral gas of charged particles that exhibits collective behavior. Even though the particles that make up a plasma are made up of free electrons and ions, their total charge densities cancel each other out at equilibrium, which is what is meant by the term "quasi-neutrality." The second characteristic, "collective behavior" means that small disruptions in equilibrium can have a significant impact on distant parts of the plasma. Indeed, a net charge imbalance will quickly produce an electrostatic field since long-lived microscopic fluctuations are often suppressed by macroscopic fields (Gibbon, 2014).

In the cosmos, 99% of the material that can be seen, including stars, the interstellar medium, and material jets from various astronomical objects, is in a state of plasma. Closer to us, the ionosphere that shields life on Earth from solar radiation is also an example. Street lights, industrial torches, lightning discharges and fusion devices (devices made to contain, ignite, and eventually extract energy from fuel) all use terrestrial plasmas (Gibbon, 2014).

This particular type of ionized gas often contains electrons, positively charged ions and neutrals (atoms, molecules, radicals). Although the electron temperatures in the resulting plasma may reach many tens of thousands of Kelvins, the ions and neutral gas are typically described as being "warmer" than the electrons. However, because of their relatively low mass, electrons are unable to efficiently transmit much of their thermal energy as heat to the surrounding walls or the heavier plasma components (Wiesemann, 2013)

Dielectric barrier discharge (DBD) and nonequilibrium atmospheric pressure plasma jets (N-APPJ) are the primary devices utilized in plasma medicine research.

Non-equilibrium atmospheric plasma jets produce plasma plumes that dissipate into the surrounding atmosphere and away from the electrodes' enclosure. This makes it possible to send the plasma to a distant target from the plasma generating location. Pulsed direct current, radiofrequency and microwave power, among other power driving techniques, have all been employed (Laroussi et al., 2017). In fact, ionization, the process that produces plasmas, can take place in a number of different ways, including when rapid particles collide with atoms, when electromagnetic radiation causes photoionization, and when electrical breakdown occurs in powerful electric fields (Gibbon, 2014). Noble gases like helium and argon have been employed as operating gases. These background gases may contain additions of air or oxygen. Stable plasma plumes with lengths up to several centimeters have frequently been produced, depending on the amount of power used, the kind of gas used, and the flow velocity (Laroussi et al., 2017).

2.2 PLASMA MEDICINE

The term "plasma medicine" describes the therapeutic use of actual plasma to or inside the human (or animal) body. Since the 2000, it has been driven mostly by physicists and has evolved into a multidisciplinary research area that includes biological sciences and medicine. The use of cold atmospheric-pressure plasmas (CAP), or plasmas that produce temperatures no greater than 40°C at the target location of therapy, is the main emphasis of plasma medicine in its restricted definition.
Although there are other variations, the majority of devices utilize either dielectric barrier discharges in air (DBD) or nonequilibrium atmospheric pressure plasma jets (N-APPJ) with rare gas (He, Ne, or Ar) (Graves, 2014).

Recent biological uses of plasma technology include sterilization, wound healing, cancer therapy, tissue or cellular removal, dentistry treatment and polymer material preparation and they are made possible by the technology's distinctive chemical and physical features (Laroussi et al., 2017).
The reactive chemical species, in particular the reactive oxygen and nitrogen species (RONS) produced in the plasma, which are similar to those naturally created by cells, are the most plausible "active agent" behind CAP biomedicine. These species include hydroxyl, OH, atomic oxygen, O, singlet delta oxygen, $O_2(^1\Delta)$, superoxide, O_2, hydrogen peroxide, H_2O_2, and nitric oxide, NO.

Numerous studies have demonstrated that CAPs are highly efficient against gram-negative and gram-positive bacteria, bacteria that form biofilms, spores, viruses, and fungus. Gram-negative bacteria are far more resistant than gram-positive bacteria. It's conceivable that CAPs puncture the membrane a few number of times and inflict irreparable harm on membrane constituents, causing cell death without changing the microorganism's outward appearance. This could be connected to a series of physical and physiological cascaded processes brought on by CAP impact and leading to ultimate slow death. (Kong et al., 2009). Plasma has been demonstrated to be effective at killing MRSA and other bacteria that are resistant to antibiotics: no instances of microorganisms developing a resistance to plasma exposure have been recorded up to

this point. As antibiotic-resistant strains proliferate, major health issues are becoming more prevalent: patients with weakened immune systems experience a significant rate of mortality from nosocomial infections (Laroussi et al., 2017). There are virtually no surviving bacteria (detectable as single colony forming units) where the plasma was administered, showing a 99.9999% decrease in the bacterial burden. These findings imply that major microbial pollutants for hospital acquired infections can be safely deactivated by CAPs (Kong et al., 2009).

Initially, oxidative stress from reactive species like oxygen and other sorts of radicals was believed to be only harmful, and substances known as antioxidants were supposed to be helpful in reducing their amount. Until recently, it was thought that free radicals, an inevitable byproduct of metabolism, were the main source of the cumulative damage that results in aging. It is now recognized that this is a too-simplistic point of view and that RONS play an important role in both pathology and normal physiology. For example, white blood cells like neutrophils and macrophages use a process called phagocytosis to locate and destroy invasive bacteria and the production and use of free radicals is a crucial aspect of how these cells work (Graves, 2014). More recent studies have confirmed this dual nature of RONS and their importance in maintaining regular cellular processes. On the one hand, elevated free radicals levels destroy proteins, DNA, membranes, cellular organelles, they have been linked to ageing, cancer, and neurological illnesses. On the other hand, cells have developed specific ways to control intracellular RONS levels, including antioxidant enzymes, creating a perfect homeostasis. In fact, the innate immune system during local inflammation carries out mechanisms to prevent causing severe harm to host tissue and limitate the damages. (Brun et al., 2014).

It has been demonstrated that the use of CAP can aid in the healing of persistent wounds that are resistant to other traditional treatments, such as diabetic ulcers. This can be achieved because plasma prevents the infection by eliminating a significant portion of the germs that are invading the wound and then promotes fibroblast proliferation and angiogenesis (Laroussi et al., 2017). The strength and distinguishing quality of plasma over established and traditional wound care methods is in fact the direct combination

of wound antisepsis with a stimulating influence on tissue regeneration (von Woedtke et al., 2020). For a very long time, it was thought that the major cause of faster healing was due to the antibacterial qualities of gas plasma. However, research on human patients and animals suggests the presence of some pathways unrelated to microbicide activity. This does not call into doubt the crucial part that infection plays in impaired wound healing, particularly in immunocompromised individuals and with types of bacteria that are resistant to antibiotics but identify that the presence of bacteria is not necessarily the cause of poor wound healing (Bekeschus et al., 2021).

The promising results might be explained by a number of pathways that are involved. Plasma jets are abundant in NO, which is known to relax the arteries and so improve blood flow. The inherent thermal energy of plasma, which is at or slightly above body temperature (37–40 °C), may even increase this by warming the treated target, which is known to stimulate endogenous NO generation and increase blood flow. Increased microcirculation improves the movement of nutrients, freshly formed leukocytes, and ultimately oxygen to combat hypoxia, one of the major factors in wound ulceration. As seen in various animal models after gas plasma treatment, which constantly improved vascularization and tissue oxygenation, hypoxia is also repaired by increased angiogenesis. The antioxidant nuclear transcription factor Nrf2, which was recently discovered as a useful target for pharmacological activation and wound healing promotion, was shown to be strongly stimulated in vitro and in vivo, according to the data (Bekeschus et al., 2021).

In another study, it was shown that non-thermal atmospheric pressure plasma ionizing helium gas combined with air produces active chemical species that regulate the activation of two populations of cells that resemble fibroblasts by causing intracellular ROS. Because ROS stimulate intracellular signaling pathways at low to moderate concentrations, soluble factors involved in cell growth and proliferation are produced (Brun et al., 2014).

Table 2 shows some results that were obtained through the last ten years.

Wound size/ location	**Plasma (gas)**	**Main findings in the gas plasma exposure group**	**References**
17×17mm skin removal (dorsum)	NO generator (Air)	Improved angiogenesis, wound healing, granulation, and shortened inflammation in both aseptic and infected wounds	(Shekhter et al., 2005)
6 mm punch (dorsum)	Jet ($He/O_2/N_2$)	Improved epithelization and neovascularization, decreased microbial burden of natural wound flora	(Yu et al., 2011)
8 mm punch (dorsum)	SteriPlas (Ar)	Accelerated wound closure, increased macrophage and neutrophil infiltration, increased MCP-1 and IL-6, more collagen type I	(Arndt et al., 2013)
10x15 mm skin removal (dorsum)	Jet (He)	Accelerated wound closure with intermediate but not low or long gas plasma treatment times	(Jacofsky et al., 2014)
2 mm punch (dorsum)	Jet (Ar)	Accelerated wound healing and re-epithelization	(Nasruddin et al., 2014)
2nd ° burn (dorsum)	Get (Ar/N2)	Increased healing rates, angiogenesis, blood flow, epithelization, wound contraction, and secondary ROS/RNS in wound tissue	(Ngo Thi et al., 2014)
5 mm punch (dorsum)	Jet (Ar, Ar/Air)	Accelerated wound closure, better in Ar/Air over Ar, more IL-6 mRNA in Ar/Air treated wounds	(H. Y. Kim et al., 2015)
4 mm punch (dorsum)	Jet (Ar)	Accelerated wound healing and increased myofibroblasts, especially in watered (humidified) wounds	(Nasruddin et al., 2015)
4 mm punch (dorsum)	Jet (Ar)	Accelerated healing with short and intermediate but not long exposure times	(Xu et al., 2015)
2 mm punch (dorsum)	Jet (He)	Accelerated wound closure in both non-diabetic and diabetic rats, more acute inflammation and neovascularization	(Fathollah et al., 2016)
1.5 mm punch (ear)	Jet (He)	Increased angiogenesis and vascularization early after gas plasma exposure	(D. W. Kim et al., 2016)
3x20 mm laser (dorsum)	Jet (Ar/N_2)	Improved wound healing with 3x over 1x exposure, increased blood flow and RNS release into tissue, increased wound strength and laminin, decreased MMP3	(Shao et al., 2016)
6 mm punch (dorsum)	SteriPlas (Ar)	Increased angiogenesis and FGF-2 generation	(Arndt et al., 2018)
8 mm punch (dorsum)	Jet (He)	Accelerated wound closure, mRNA expression changes (increased IL-	(Kubinova et al., 2017)

		6, Nos2, and Ptgs2; decreased Nfκb and Sod1), effects only at day 7 but not at days 3 and 10	
4 mm punch (dorsum)	Jet (Ar)	Accelerated wound healing and re-epithelization	(Nasruddin et al., 2017)
2x2 mm skin removal (ear)	kINPen jet (Ar)	Accelerated wound healing and angiogenesis	(Schmidt et al., 2017)
6 mm punch (dorsum)	kINPen jet (Ar)	Accelerated wound closure and re-epithelization, less fibrosis and more acute inflammation	(Breathnach et al., 2018)
10 mm pressure ulcers (dorsum)	Jet (He)	Accelerated wound closure, increased angiogenesis and re-epithelization as well as inflammation, higher force resistance and elastic stiffness	(Chatraie et al., 2018)
8 mm punch (dorsum)	Jet (Ar)	Accelerated wound closure, improved re-epithelization and fewer neutrophils and T cells in diabetic wounds at late stages, increased SOD and catalase as well as GPx in treated tissues	(Cheng et al., 2018)
6 mm punch (dorsum)	Jet (He)	Accelerated wound healing across several exposure durations	(Shahbazi Rad et al., 2018)
17×17mm skin removal (dorsum)	NO generator (Air)	Accelerated wound healing, decreased long-term inflammation, improved collagen I/collagen III ratio	(Shekhter et al., 2019)
4 mm punch (dorsum)	Jet (Ar)	Lack of beneficial effect of combination with hydrocolloid dressings and medical honey	(Wahyuningtyas et al., 2018)
4 mm punch (dorsum)	Jet (Ar)	Long exposure of direct contact-style jet treatment heated the tissue (>50 ◦C) and was highly detrimental for wound healing, longer distances promoted wound healing and epithelization	(Darmawati et al., 2019)
4 mm punch (dorsum)	Jet (Ar/Air)	Accelerated healing with dual-frequency over single- frequency and 2 over 1, 3, and 4 treatment cycles	(Lee et al., 2019)
2x2 mm skin removal (ear)	kINPen jet (Ar)	Accelerated wound healing and angiogenesis as well as re-epithelization, increased collagen fibers, keratin production, Nrf2 response, p53 activation, macrophage infiltration, inflammation, and granulation	(Schmidt et al., 2019)
13x13 mm skin removal (dorsum)	Jet (He)	Accelerated wound healing, angiogenesis, epithelization, and wound contraction; collagen	(Zhang et al., 2019)

		unchanged; TNFα and IL-1β but not IL-10 increased	
17 mm punch (dorsum)	Jet (He, He/Ar)	Accelerated wound healing and granulation tissue formation, He/Ar performed better than He gas plasma, short gas plasma treatment times performed best	(Lou et al., 2020)
40 x 40 mm (dorsum)	Jet (He)	Accelerated wound healing and increased angiogenesis	(Martines et al., 2020)
6 mm punch (dorsum)	Jet (He, He/O2)	Accelerated wound healing and highest VEGF and bFGF with He/0.1% O_2 over He and He/1% O_2	(Pan et al., 2020)
6 mm punch (dorsum)	DBD, Jet (He, Ar)	Improved wound healing with DBD but better wound healing with Ar and He gas plasma jet treatment	(Shahbazi Rad & Abbasi Davani, 2020)
2nd ° burn (dorsum)	Jet (Ar)	Increased early leukocyte influx, MPO release, free thiols, and angiogenesis	(Souza et al., 2020)
10x10 mm skin removal (dorsum)	Jet (He)	Accelerated wound healing; less scar formation, TGF-β/pSmad2/3/αSMA positive cells, and collagen deposition	(Wang et al., 2020)
2x2 mm skin removal (ear)	kINPen jet (Ar)	Changes in matrix remodeling and focal adhesion complex, elevated microcirculation	(Schmidt, Liebelt, et al., 2021)
2x2 mm skin removal (ear)	kINPen jet (Ar)	Increased wound tissue oxygenation in superficial and deep layers as well as increased tissue hemoglobin index, increased tissue water index at late time points	(Schmidt, Niesner, et al., 2021)

Table 2. Animal studies on gas plasma-stimulated wound healing (Bekeschus et al., 2021).

The issue of selectivity arises because it is simple to kill any type of cell, however, is not that easy to limit harm to healthy tissue while eliminating infectious pathogens. As previously mentioned, the chemical similarities between the types of free radicals found in plasma and those that are known to affect how the innate immune system responds raise the possibility that RONS produced by CAP are somehow responsible for the reported results. The reactive species do not distinguish between the genetic source of their chemical targets, and this is the most prominent example of non-specificity. Physiologically the multicellular organism (animal or plant) may locally sacrifice some of its own cells at the location of an apparent damage and infection that, if left unchecked, might spread and destroy the entire organism. But as was said before, if this behavior isn't stopped promptly, the host will sustain unacceptable damage. For this reason, we would hypothesize that CAP treatments should be spatially targeted and relatively brief treatments at known areas of infections or tumors, similar to how the innate immune system normally functions (Graves, 2014).

According to studies, treating a polymicrobial illness locally with nonthermal plasma is highly advantageous. Bacteria are sensitive to low levels of RONS, but cellular organelles can shield eukaryotic cells from reactive species overload. This impact, nevertheless, is dose-dependent (Brun et al., 2015). In general, it has been shown that the effects are stronger and can alter in nature if the plasma is operated at greater delivered power, for longer periods of time, and at places closer to the treated tissue. Mammalian cells developing in cell culture, for instance, have a tendency to proliferate at "low" CAP dosages; nevertheless, at higher levels, they will suffer apoptosis (controlled cell death), and at even higher doses, necrosis (uncontrolled cell death) is seen. Similar remarks apply to how plasma exposure affects cellular DNA and other toxicity indicators (Graves, 2014).

If oxidative reactions aren't properly counterbalanced, they can damage cells' ability to function, whereas groups of ineffectively repaired oxidative DNA lesions can cause mutations and degenerative conditions. Prokaryotic and eukaryotic cells react to CAP in different ways, and this difference is most likely caused by the haploid situation, as well as changes in cell structure and DNA repair processes. In reality, DNA mutations

can induce bacterial mortality because of the rapidity of transcription and protein synthesis and are instantly apparent in the phenotypic of haploid cells when they affect critical genes (Rosani et al., 2015).

The gas flow, distance from the plasma source, and exposure period all affect how cold plasma affects eukaryotic cells and tissues. In a study, it was found that corneal tissues exposed to CAP for two minutes had temporary and mild oxidative damage. The overall variations in gene expression point to a protective or stimulatory response rather than a flaw in how cells function (Rosani et al., 2015).

Numerous gas plasma devices have been examined for any possible genotoxic side effects. After repeated gas plasma therapy of wounds, no tumor growth was shown in mice after one year, the equivalent of 60 years in human terms. Additionally, the treated wounds had no aberrant skin growths such hypertrophic scar development. Hyperspectral imaging and confocal laser scanning microscopy analysis of gas plasma-treated wounds in human patients at one and five years after treatment also revealed no aberrant healing responses (Bekeschus et al., 2021).

To produce a complete and comprehensive image, however, we require more effort and thorough research. Some of the needed researches are: accurate measurements of the relevant species' fluxes and concentrations in both gaseous and liquid phases; research into the function of the plasma-generated electric field, which can create holes in the cell membrane; clarification of the plasma-triggered biochemical pathways through which death in cancer cells can occur; further research should be done on how plasma affects macromolecules like DNA and proteins; any potential long-term cytotoxic effects of plasma on healthy cells should be identified; any potential genotoxic effects, especially on healthy cells, should be investigated because they could have serious repercussions (such as mutations); determining what additional impacts plasma, such as altered blood flow or oxygen levels, may have on tissues and cancers; determining how much plasma exposure affects the immune system (Laroussi et al., 2017).

2.3 APPLICATIONS IN OPHTALMOLOGY

Ophthalmology is a possible therapeutic field of application of plasma that has strangely received little investigation despite the results being quite encouraging. Here, potential uses are concentrated on treating corneal ulcerations as well as infections. It has been consistently shown in both in vitro and in vivo research that the treatment impact on the eye's surface may inactivate bacteria without causing any damage to the cornea (von Woedtke et al., 2020).

A medical condition of great concern is ulcerative keratitis, which can be brought on by harmful microorganisms (bacteria, fungus, amoebae, and viruses), ocular trauma, or chemical exposure. Clinical consequences might be severe, requiring penetrating keratoplasty, corneal transplants, enucleation, and partial or full vision loss. To minimize the likelihood and severity of ocular abnormalities that are a result of ulcerative infectious keratitis instances, there is an urgent need for treatment techniques that are successful in killing the invading bacteria while also minimizing ulceration and inflammation (Saleem et al., 2019).

It has been demonstrated for the first time that a CAP device has the potential to have a significant clinical influence on the successful management of keratitis caused by *Pseudomonas aeruginosa*. The results were encouraging despite the inability to do tissue histology, immunohistochemistry, or research into the molecular pathways, as well as to include comparison groups of animals that were given conventional antibiotics of choice. Both the prevalence of corneal ulceration and the degree of swelling (edema) were significantly decreased by an average of 76% and 67%, respectively, compared to untreated (Saleem et al., 2019).

The following images demonstrate how Pseudomonas keratitis in rabbit eyes causes rapid disease progression that eventually leads to the development of moderate to large mucopurulent corneal ulcers (red arrows in the figures 6a-6b) and edema. However, if treated with iCAP, ulcer formation is significantly decreased or completely eliminated, and edema is significantly lowered.

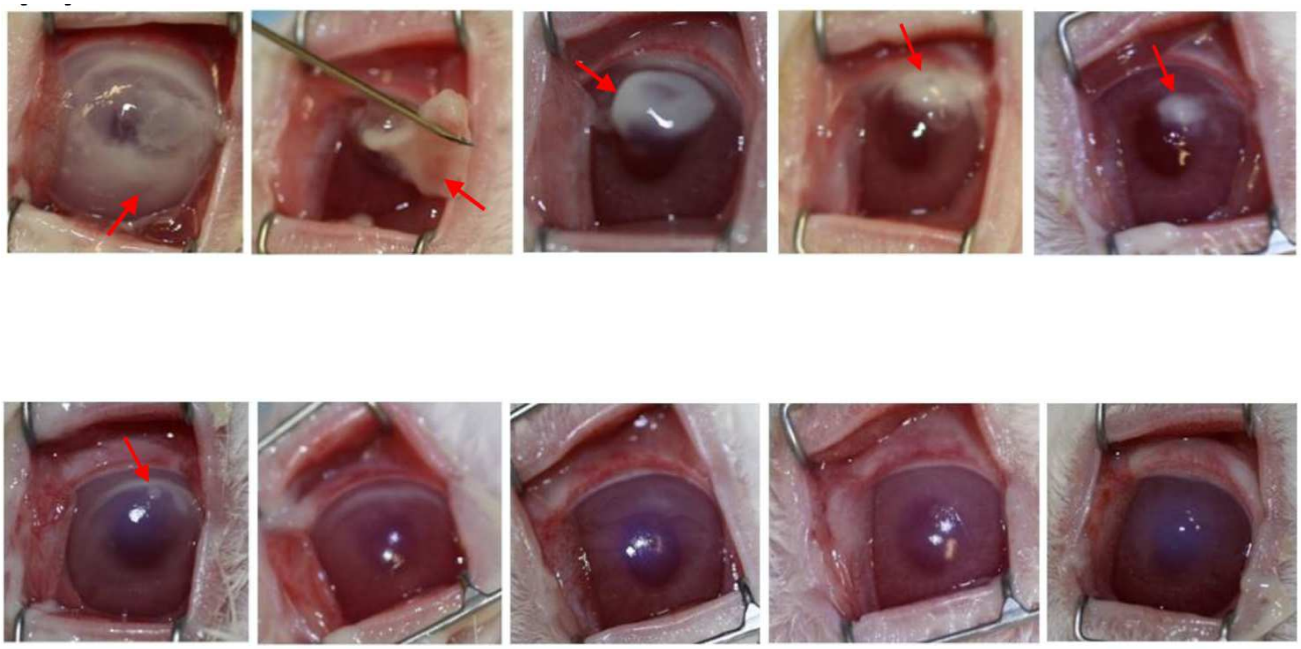

Figures 6a-6b. Lesions left untreated on top row and treated with plasma on lower row (Saleem et al., 2019).

Another study proved that 2 minutes of plasma therapy on human corneas ex vivo greatly reduced bacterial colony numbers without changing the microscopic corneal structure. Analysis of DNA fragmentation demonstrated that the quantity of apoptotic nuclei was similar to that seen in control tissues and did not show any appreciable apoptotic effects in corneal tissues. Conjunctival fibroblasts and keratocytes both kept their usual morphologies, according to cell morphology observations made using reversed optical microscopy. Furthermore, the same helium gas that produced CAP was applied for an hour to conjunctival fibroblasts without having a discernible effect on cell viability, while drastically lowering the number of CFU/ml of bacterial and fungal germs.

In conjunctival fibroblasts and keratocytes, flow cytometry revealed a distinctive hypodiploid peak 2 hours post-treatment, which is a sign of dead cells. At 24 hours after treatment, however, when the cells displayed a typical distribution of cell cycle phases, dead cells were no longer visible.

ROS levels were three times greater in corneal cells than in cells not exposed to CAP after 30 seconds. Under these experimental conditions, substantial concentrations of radicals created by a brief exposure killed a variety of bacteria, whereas the much smaller, transient burst of reactive species produced by exposed ocular cells had no effect on the survival of corneal cells and tissues.

Oxidized bases like 8-oxodeoxyguanosine (8-OHdG) can enable DNA strand breaks and create pro-mutagenic lesions with the destiny of the cell ultimately depending on a balance between physiological adaptations and irreversible modifications towards cell death, senescence, and degenerative processes. Regardless of the endogenous or external origin, base oxidation of DNA, RNA, and similar precursors is frequently viewed as a sign of genetic damage. In the DNA of the CAP-treated cells, it was detected a brief buildup of 8-OHdG. After 24 hours, after the intracellular ROS burst had subsided, the 8-oxodeoxyguanosine quantities were back to normal, showing that a 2-minute treatment did not affect the survival of ocular cells in vitro (Brun et al., 2012).

3. AIM OF THE THESIS

The aim of this study was the characterization of corneal mechanical behavior in healthy, injured and helium plasma treated populations.

A medical condition of great concern is represented by corneal ulcers, which can be brought on by harmful microorganisms (bacteria, fungus, amoebae, and viruses), ocular trauma, or chemical exposure. They can be simple or complicated, and in the worst-case scenario even collagenolytic. Those are complicated ulcers where collagen, the main component of the stroma, is digested by collagenase enzymes: numerous organisms generate lytic enzymes, and neutrophils from the limbus and tear film can also release them.
There is an urgent need for treatment techniques that are successful in killing the invading bacteria while also minimizing ulceration and inflammation and stimulating wound healing processes. The use of cold atmospheric-pressure plasma (CAP), or plasma that produce temperatures no greater than 40°C at the target location of therapy, has been demonstrated effective in aiding wound healing thanks to the direct combination of wound antisepsis and a stimulating influence on tissue regeneration. It has been consistently shown in both in vitro and in vivo research that the treatment impact on the eye's surface does not cause any damage to the cornea.

73 porcine corneas were collected and the samples were divided into two main populations: corneas that were considered healthy before slaughtering (H, healthy) and corneas that were injured with alkaline solution after enucleation to create an experimental ulcer (L, lesioned). Within the two main population the samples were tested in two different conditions: fresh, a few hours after enucleation (F, fresh), and cultured for seven days in a specific medium (C, cultured). Furthermore, another condition was considered: every population underwent or not the helium plasma treatment for 2 minutes (P2) and for 4 minutes (P4). As a result, we obtained ten different populations.

To study stress-strain behavior and ultimately determine the change in stiffness that can be observed during the healing of a corneal ulcer, all of the samples were subjected to stress-relaxation uniaxial tensile tests.

The research team intends to examine the samples in each population histopathologically and biomolecularly as part of a wider investigation, of which this thesis is a part. The outcomes will also be compared to those of previous investigations into other corneal ulcer treatments.

4. MATERIALS AND METHODS

Ten groups of specimens were created in order to prepare corneas in various ways and then compare the outcomes, as shown in Table 3.

Group	Denomination	Number of samples
Lesioned, cultured, treated for 2 minutes	LCP2	9
Lesioned, cultured, treated for 4 minutes	LCP4	6
Lesioned, fresh, treated for 2 minutes	LFP2	6
Lesioned, fresh, treated for 4 minutes	LFP4	6
Healthy, cultured, treated for 2 minutes	HCP2	6
Healthy, cultured, treated for 4 minutes	HCP4	6
Healthy, fresh, treated for 2 minutes	HFP2	7
Healthy, fresh, treated for 4 minutes	HFP4	6
Healthy, fresh, no treatment	HFN	8
Lesioned, fresh, no treatment	LFN	5
Healthy, cultured, no treatment	HCN	3
Lesioned, cultured, no treatment	LCN	5

Table 3. Groups of specimens

Data from earlier studies were utilized for the final four groups: the healthy fresh untreated and lesioned fresh untreated corneas (Fontanella et al., 2021). These studies' methods and all of their materials are identical to those used in this study, included the research team.

4.1 SAMPLES SELECTION AND COLLECTION

Because they resemble human corneas, porcine corneas were used for this research. Numerous studies have utilized this animal model because of its biological affinity and comparable biomechanical behavior, allowing us to compare our findings when appropriate. In fact, it is acknowledged that the porcine cornea is a suitable model for the human cornea in terms of mechanical properties, despite differences in corneal thickness and stiffness: the average porcine cornea is 1.6 thicker than the human one and it characterized by an higher elasticity. Although the viscoelastic creep is greater in humans than in swine corneas, they both demonstrate comparable stress-strain behavior under short- and long-term loading and respond similarly to prolonged loading (Kling & Hafezi, 2017).

Ex vivo eyes were used to collect corneas for this investigation: this decision was made because to the ability to get several samples from a local slaughterhouse and the fact that this procedure ensures the examination of the tissue's key biomechanical features. The globes utilized in this research were obtained from a local abattoir where swine are slaughtered on a regular basis; as a result, all eye-donor animals were determined to be healthy during the pre-mortem examination. All eyes were taken from animals that were similar in age and overall health, individual differences were viewed as unimportant to the study. The lack of any eye defect either from a pathological condition or from the enucleation process was the only factor that mattered for the selection.

To prevent autolytical lesions, eyes were removed from the animals within an hour of their deaths. They were then transferred to the lab in a container containing betadine, a 10% concentrated antiseptic solution, to prevent contamination. The container was chilled at 4°C.

4.2 INDUCTION OF THE LESIONS

All lesioned groups underwent the same induction of the lesion, for a total of 37 corneas. To remove the antiseptic solution used for the transfer eyeballs were first washed with sterile PBS solution 1% (phosphate-buffered saline), then they were put on the biological plant's working table above a sterile circular support to prevent slippage and contamination from the workstation during the procedure.

It was decided to employ the caustic chemical for one minute after conducting multiple tests under various settings according to a previous histological study. The corneal lesion was created by placing a little paper disk with a diameter of 0.8 cm that had been saturated with sodium iodide (NaOH) at a concentration of 1N over the eyeball for one minute before being removed, , as shown in Figure 7. The next step was rinsing the eyes with PBS solution to remove any remaining caustic soda and end its corrosive effects. The same operator made all the lesions, making them equivalent to one another.

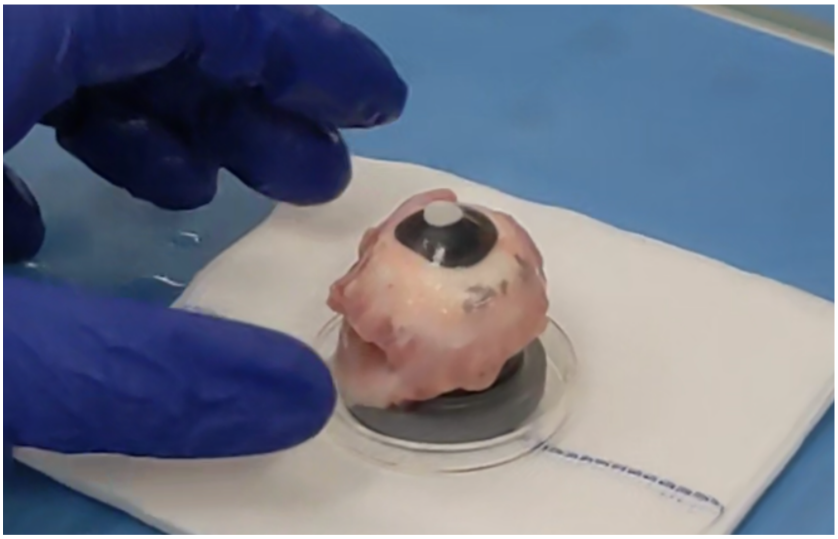

Figure 7. Creation of experimental ulcers

4.3 PLASMA TREATMENT

The plasma device comprises of two coaxial tubes: an inside tube constructed of an insulating substance and an exterior copper tube that is 80 mm long and has an outer diameter of 12 mm (polyethylene, 100 mm long, 10 mm outer diameter). A metal grid with wires that are 0.2 mm in diameter and placed 1 mm apart covers the end of each tube to seal it off. Electrical connections are made between the exterior brass grid and the external copper tube. Using a micrometric screw, the tubes may be shifted in relation to one another to change the spacing between the two grids to a value that permits breakdown but inhibits arc formation (1 mm). To completely exclude the risk of an arc forming between the electrodes and the substrate to be treated, the external electrode is grounded. When working with living tissues, this is a fundamental necessity since arcs concentrate power on a very tiny region, badly harming the substrate (Martines et al., 2013).

Helium with a purity of 99.9999% is used as the working gas and is fed into the inner tube. 1.75 litres per minute have been established as a promising value for stable plasma generation with little gas consumption. Typical gas flows fall between 0.5 and 5 litres per minute. Setting a high flow value at first, which may later be decreased to the required amount, aids with plasma startup. The prototype is powered by a radio transmitter that has a fixed power setting of 5 W and a programmable frequency. The transmitter is connected to the device using a series 100 H inductor as part of a minimal matching network. This inductor and the device's parasitic capacitance, which is thought to be around 10 pF, combine to produce a resonance at 4.8 MHz, which results in a voltage up to 900 Vpp on the plasma. The He flux affects the voltage that is produced and applied to the electrodes (Martines et al., 2013).

Regarding the reflected to transmitted power ratio, which is greater than 2, the configuration is far from ideal. The majority of the transferred power is lost on the inductor, and it is calculated that less than 1 W is really linked to the plasma itself, meaning that there hasn't been any discernible heating of the treated substrate observed (Martines et al., 2009).

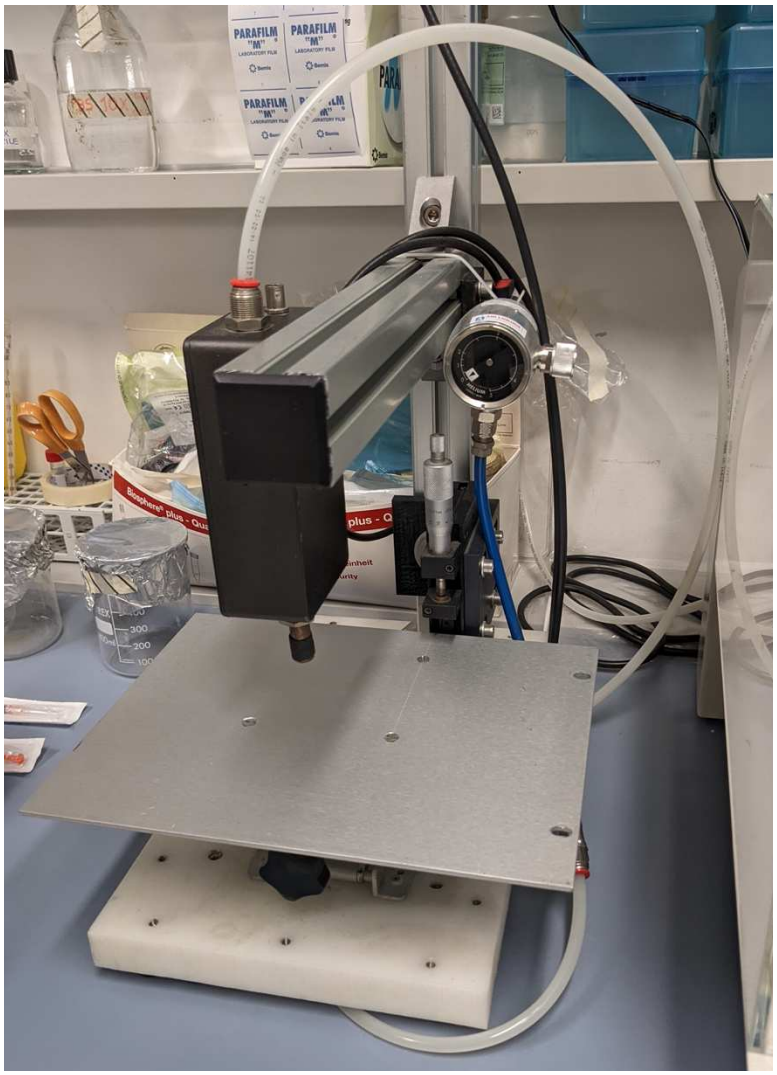

Figure 8. Helium plasma device

The globes were placed under the plasma device, still above their support.
Groups LCP2, LFP2, HCP2, and HFP2 received a two-minute treatment, whereas groups LCP4, LFP4, HCP4, and HFP4 received a four-minute treatment. Every minute, the globe was removed from the plasma source, hydrated with sterile PBS solution, and then put back in place beneath the apparatus to complete the procedure.

Figure 9. Helium plasma treatment

4.4 SAMPLES PREPARATION

The groups of corneas that were selected to undergo the culture for seven days (HCN, LCN, LCP2, LCP4, HCP2, HCP4) were removed from the eye underneath the biological plant. The operator used a scalpel to make a small incision in the sclera, which was then finished with a scissor around the eyeball to produce a circular sample. The inside side of the sample was then stripped of its crystallin lens and iris. The entire cornea was used as a sample, along with a 0,5 cm ring of sclera. Leaving this ring is useful because it preserves the limbus, a specific region in which there are some staminal cells that play a crucial role in the specimen's preservation and recovery after treatment.
The sample was hung within the medium in a 45 mL sterile falcon bottle used for the culture after a suture string was inserted in the sclera to create a loop, as shown in Figure 10. With the medium, each cornea had its own falcon.

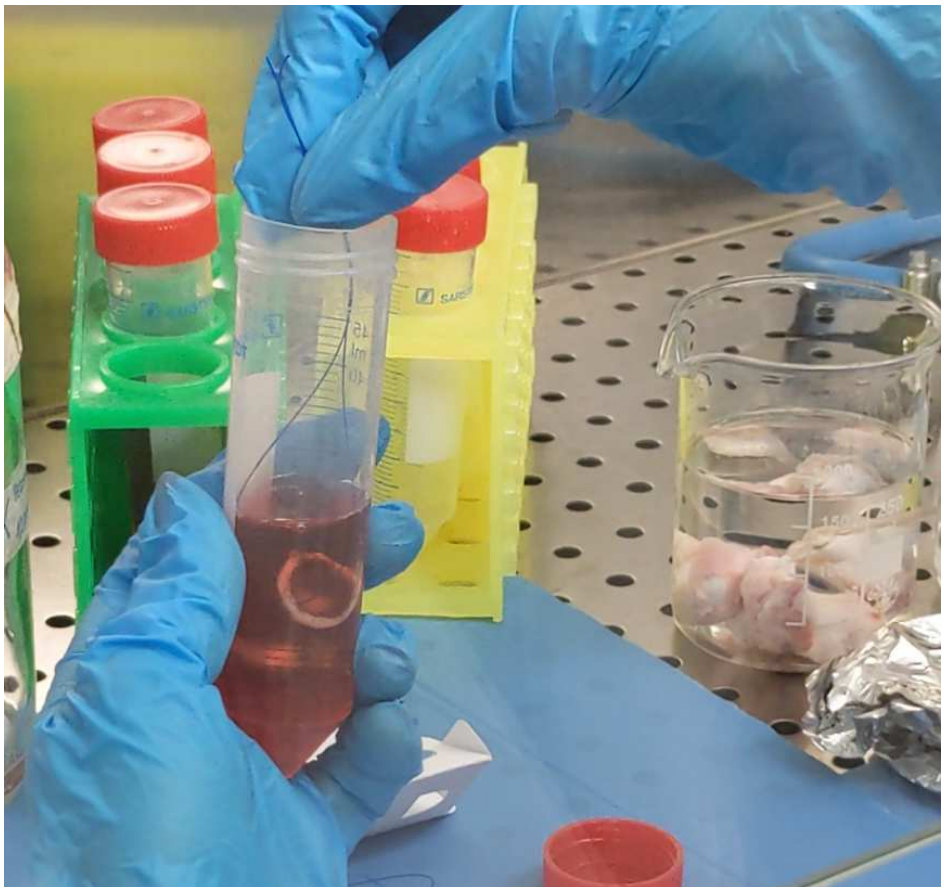

Figure 10. Cornea sample hung in a falcon with the medium

The medium that was used is CARRY-C, by Alchimia. It has a pH of 7.40 (7.20-7.60) and an osmolarity of 300 mOsm/kg (255-345) and is intended for the transportation and deturgescence of cornea. It contains antibiotic and antimycotic solution, and a color indicator that detects pH shift is also included. The culture process actually allows the growth of any microorganisms that may have been left on the surface of the cornea and a contamination will cause a change in the pH, with a consequent visible change in color.

Figures 11-12. Medium and ph-color comparison chart related to the medium

The specimens were then placed in an incubator for seven days, during which time corneas were kept there at a constant 37 °C temperature and under normal humidity and pressure conditions at 5% CO2 levels. Every day, the falcons were examined to assess the condition of the medium and the corneas; during this phase, several specimens were discarded due to contamination, and they were disqualified from the biomechanical testing. Throughout that time, the medium was never altered.

The samples were taken out of the incubator on the seventh day, removed from the falcon, and, if they were properly preserved, transported to the mechanical engineering lab to be prepared for the uniaxial tensile tests.

The mechanical engineering lab in Padova treated the eyeballs from the fresh groups; as there was no biological plant present, the eyes were kept in the transportation solution until the cornea was removed.

Fresh corneas were removed immediately, after the lesion, or after the injury and therapy. The operator used a scalpel to make a small incision in the sclera, which was then finished with a scissor around the eyeball to produce a circular sample. The inside side of the sample was then stripped of its crystallin lens and iris. The entire cornea was used as a sample, along with a 0,5 cm ring of sclera, as shown in Figure 13. The portion of the sclera is crucial for the biomechanical test, in which it serves as a very useful point of grip for the instrument.

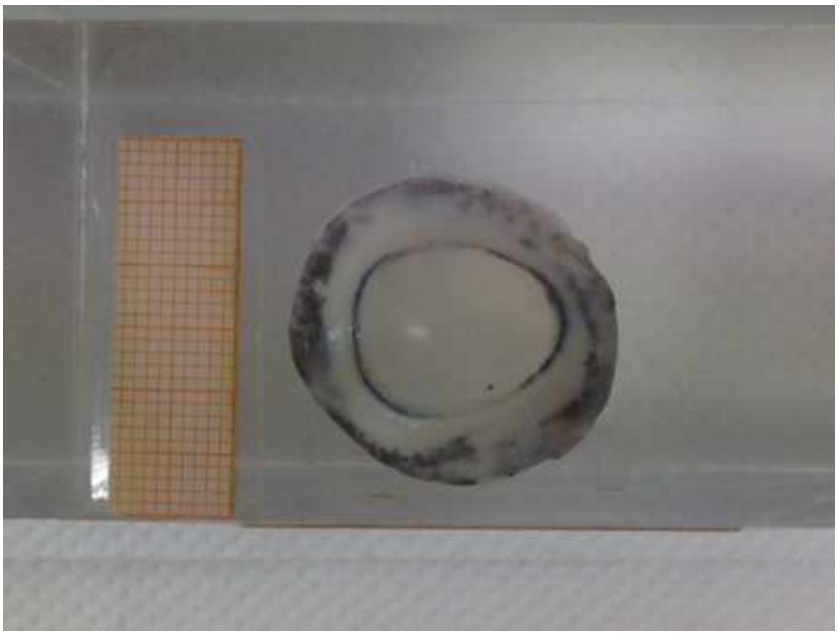

Figure 13. Cornea excised from the globe

4.5 UNIAXIAL TENSILE TESTS

Workers prepared the corneal test strips while wearing gloves, and experimental tests were done right away to prevent contamination. A rectangular sample was acquired by making two parallel incisions in the cornea and the lateral sclera with a specific device with two parallel blades, as shown in Figure 14. The samples were obtained in accordance with the cornea's medial-lateral direction: in fact, because the cornea is an anisotropic material, it is crucial to consistently maintain the same orientation to avoid getting distorted results.

The sample, which is made up of the middle longitudinal strip of each cornea, was carefully measured using graph paper images taken above a clear prism for length and depth and video camera assembly images for width. The rectangle was approximately 2,0 cm long, 0,3 cm wide, and 0,1 cm deep (Figure 15).

With order to prevent the samples from slipping during the biomechanical test, the scleral portions of the strip were glued to a support made of a rectangular piece of balsa wood wrapped in velcro on each side.

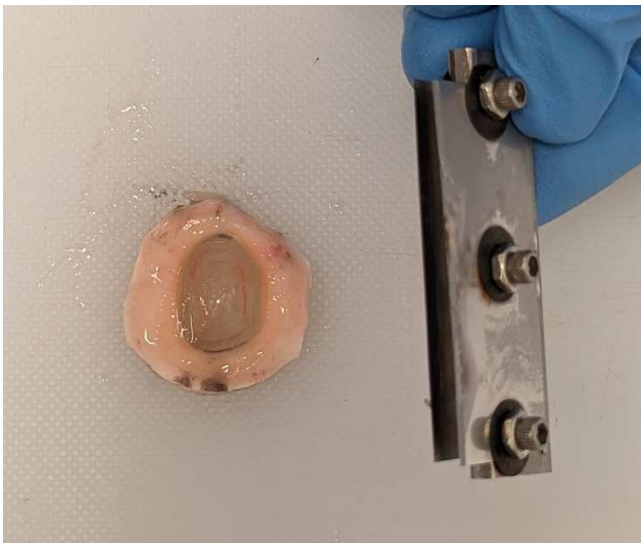

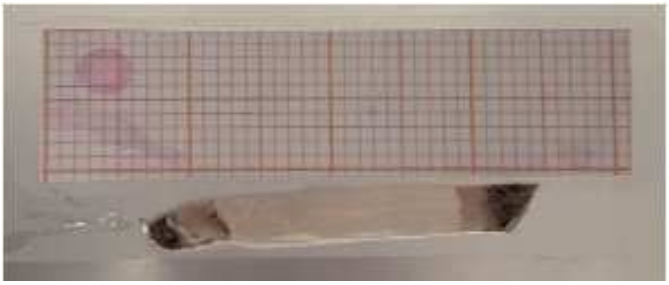

Figures 14-15. Device used for the parallel incision and the rectangular sample obtained

The uniaxial tensile test is carried out in this work using a Bose ElectroForce apparatus (Bose Corp., ElectroForce Systems Group, Eden Prairie, MN, USA).

Supports were positioned on the device's clamps to hang the cornea's central portion in the air, making possible to center the sample exactly and snap a photo for the measurement. A hydration system was built on the top surface of one of the clamps: this was important to safeguard the corneal tissue throughout the test. This apparatus consisted of a bowl of ringer lactate solution placed higher than the sample, coupled to a clamp and fluid line to control the flow of the drops hydrating the tissue.

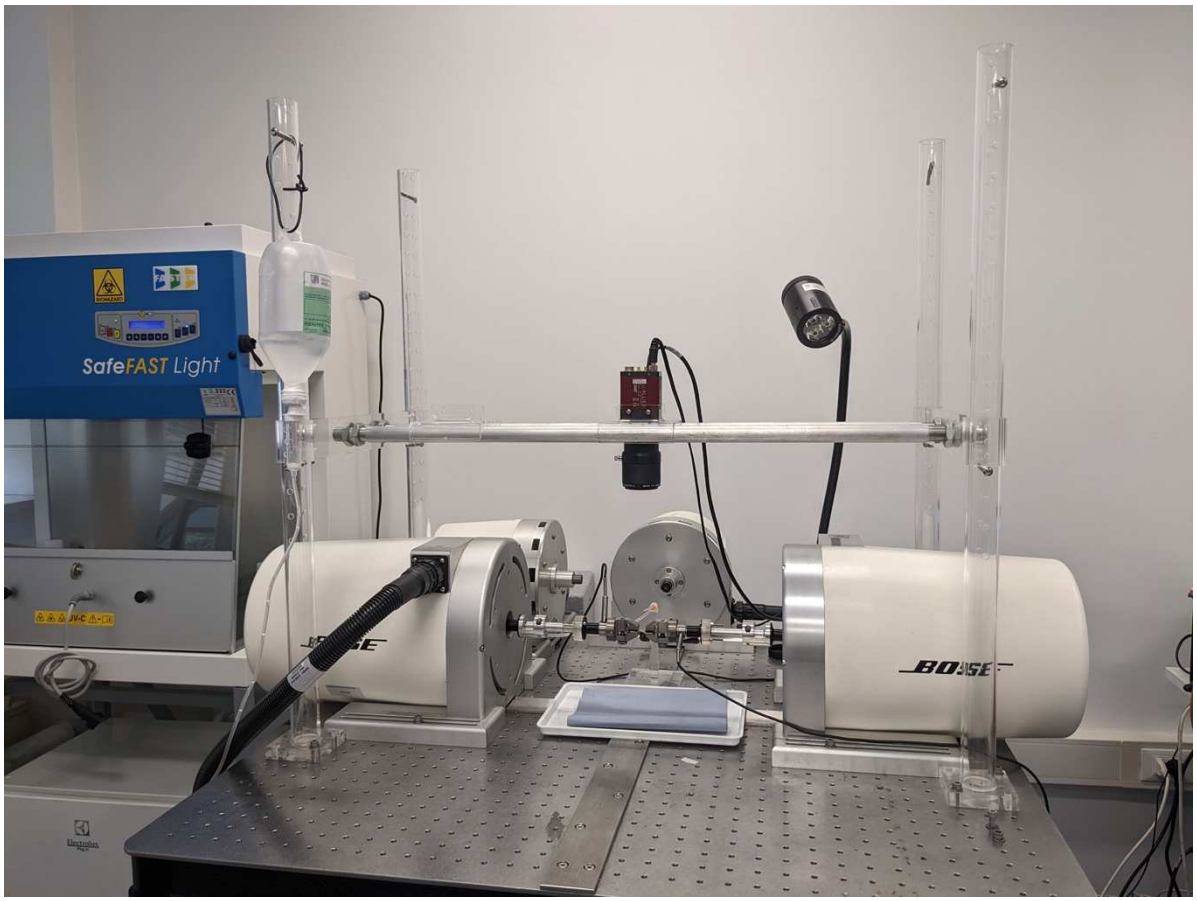

Figure 16. Bose ElectroForce apparatus

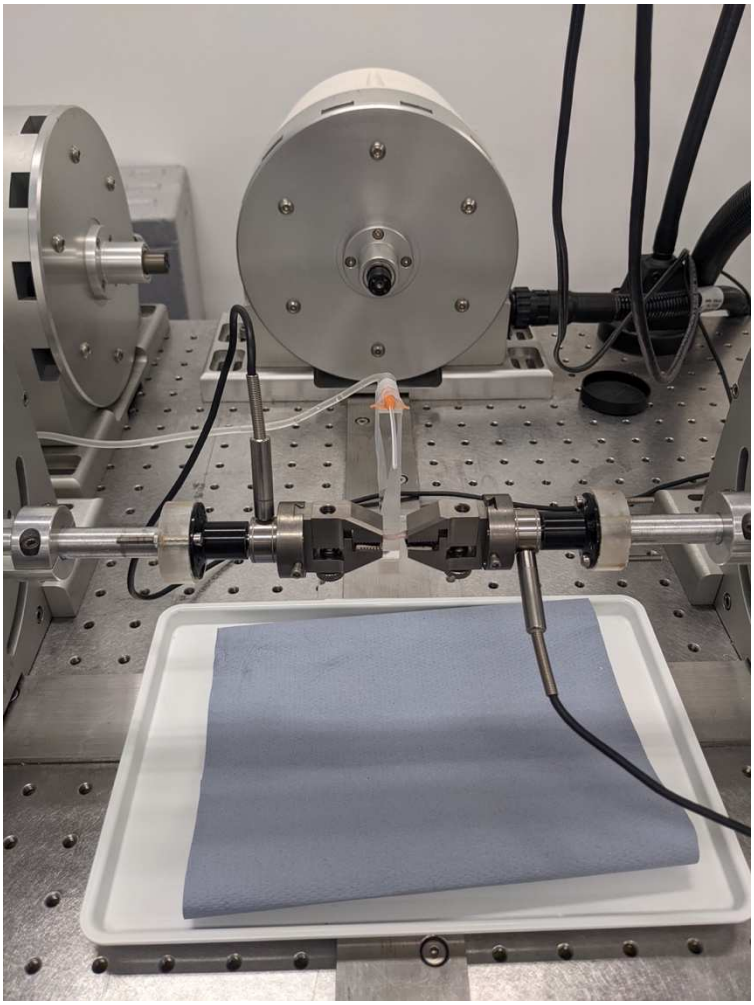

Figure 17. Detail of the hydration system

The biomechanical test began once the sample was properly positioned and hydrated. It included a preconditioning phase in which the sample underwent 10 cycles of loading and unloading with a maximum strain of 8% (0,4 mm + 0,4 mm) and a deformation speed of 0,5 mm/s.

Then, mechanical testing was performed via a multi-step procedure. Each step was composed of 8% strain at 80 mm/s strain rate, and subsequent 400 s of resting to allow the almost complete development of relaxation phenomena. The step was repeated up to 32% strain. After completing these procedures, the sample was returned to its original length at a speed of 1 mm/s.

The apparatus that deforms the samples was linked to a computer running specialized software (MATLAB, MathWorks®, and GraphPad, available at https://www.graphpad.com), which records all actions, elaborates data, and concurrently generates two diagrams.

The first graphic in Figure 18 shows how the computer compares time (x axis) and displacement (y axis): vertical increments of straining of 0.8 mm are visible in the image, while horizontal lines denote the periods (400 s) in which the value imposed by elongation is maintained. In the second diagram, time (x axis) and force (y axis) are compared: curving lines in the picture reflect the tissue's relaxation with the application of force. The test's data were ultimately expanded to create stress-strain and relaxation curves.

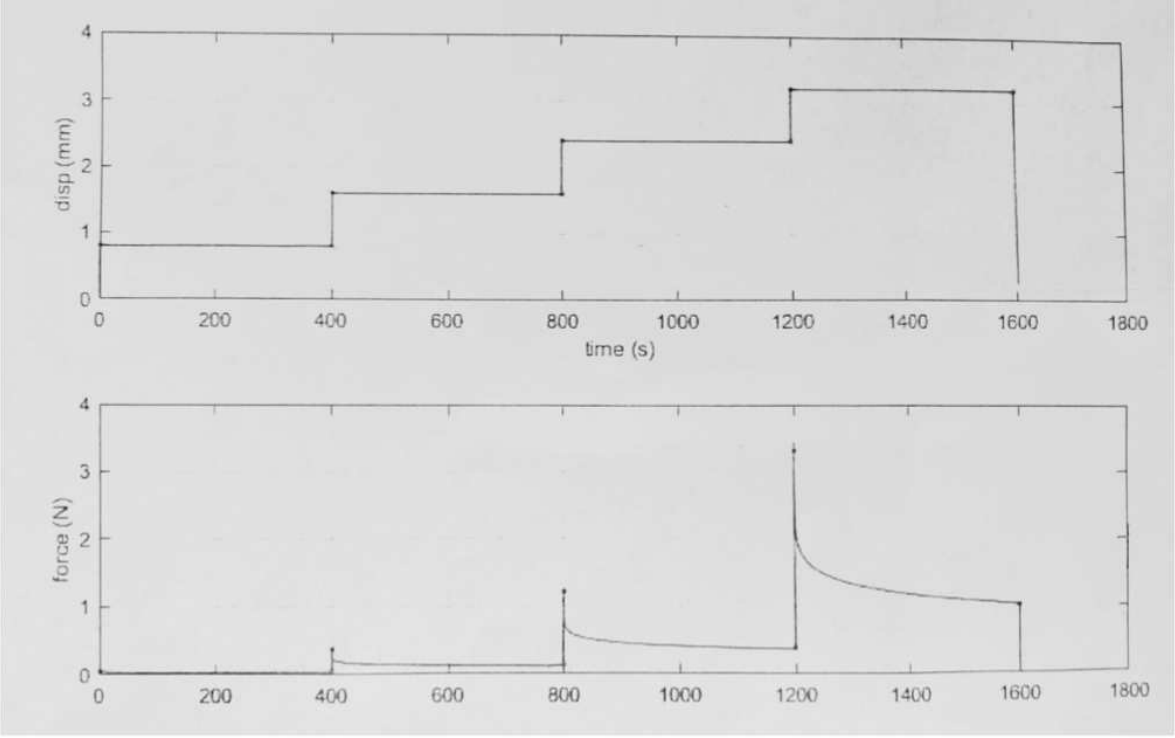

Figure 18. Diagrams obtained from uniaxial tensile tests

To calculate the values of stress and strain, these data were refined using MATLAB software (MathWorks®, https://it.mathworks.com/products/matlab.html).

Stress is computed as $\sigma_e=P/A_o$, where P is the applied load and A_o is the initial cross-sectional area of the sample normal to the loading direction.

Strain is calculated as $\varepsilon_e=\Delta L/L_o$, where L is the displacement and L_o is the starting length.

To describe the biomechanical behavior of porcine corneas, stress-strain and relaxation curves were generated using this data using Microsoft® Office Excel and Minitab® (https://www.minitab.com/en-us/).

5. RESULTS

5.1 STRESS-STRAIN CURVES

For each of the corneal samples, the program recorded the displacement (mm) and the applied force (N) during experimental testing. Graph paper photographs taken above the transparent prism and pictures taken by the video camera built within the Bose ElectroForce gadget were compared to compute the exact length, width, and thickness of the samples.

To calculate the values of stress and strain, these data were refined using MATLAB software (MathWorks®, https://it.mathworks.com/products/matlab.html).

Stress is computed as $\sigma_e=P/A_o$, where P is the applied load and A_o is the initial cross-sectional area of the sample normal to the loading direction. Strain is calculated as $\varepsilon_e=\Delta L/L_o$, where L is the displacement and L_o is the starting length.

To describe the biomechanical behavior of porcine corneas, stress-strain curves were generated using this data using Microsoft® Office Excel and Minitab® (https://www.minitab.com/en-us/).

Samples' stress-strain curves are compared in the figure. The mean values for the sample groups are shown as colored lines and the correspondent-colored area indicates the dispersion within the population. As previously stated, the cornea's nonlinear, anisotropic, and viscoelastic behavior is determined by the micro-structural composition of the tissue. The nonlinear behavior in this figure is obvious since all of the lines show a propensity to bend. A certain amount of data dispersion is also obvious, which results first from biological differences between animal donors, then from errors made during sample preparation and measurement, and, to a lesser extent, from a measurement error of the BOSE device.

Knowing that the stiffness of the tissue subjected to the mechanical test determines the slope of the individual segments of the curve, curves derived from corneas within the same population and circumstances were compared in order to substantiate the differences and similarities.

In Figure 19 appears clear that corneas treated for a longer period of time are significantly stiffer in behavior.

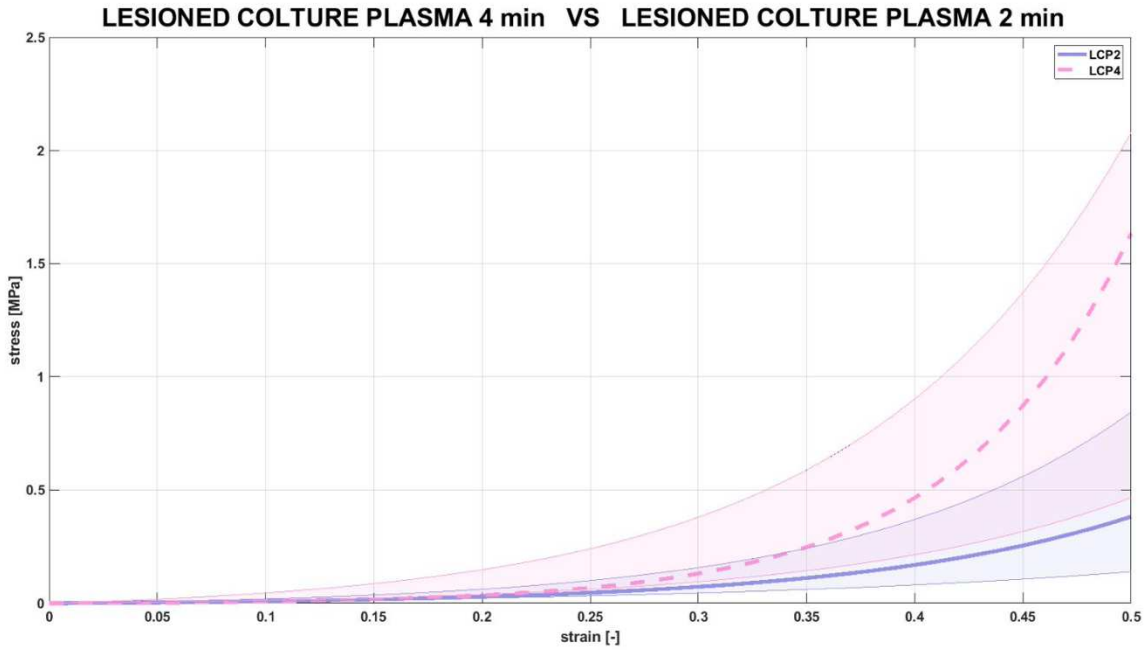

Figure 19.

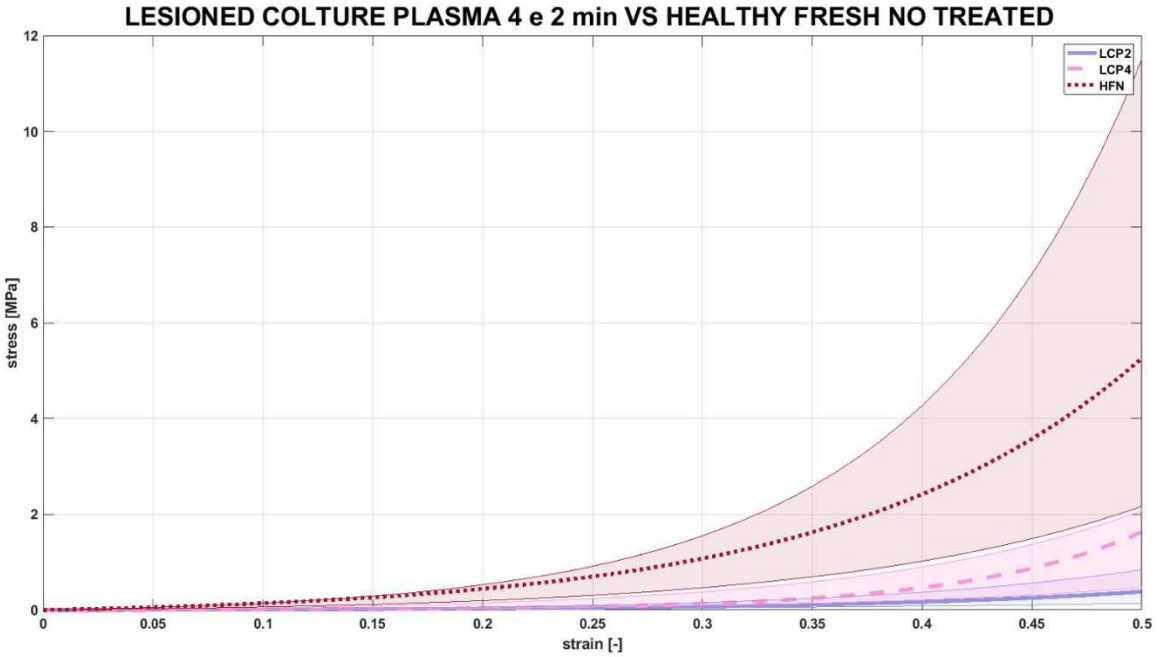

Figure 20.

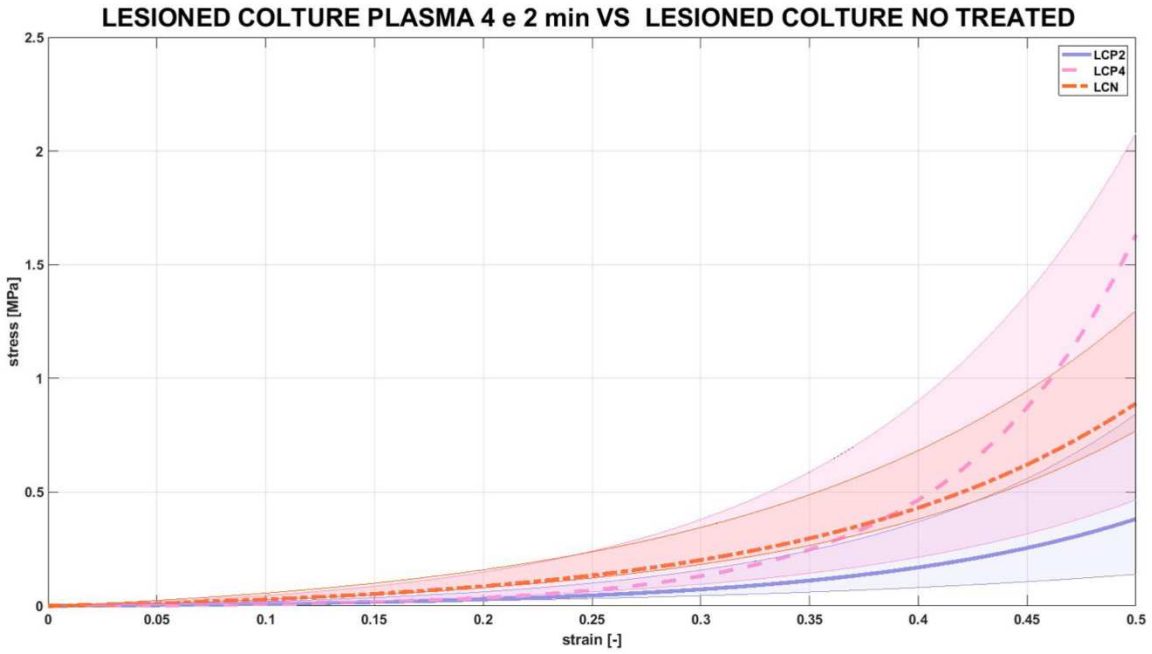

Figure 21.

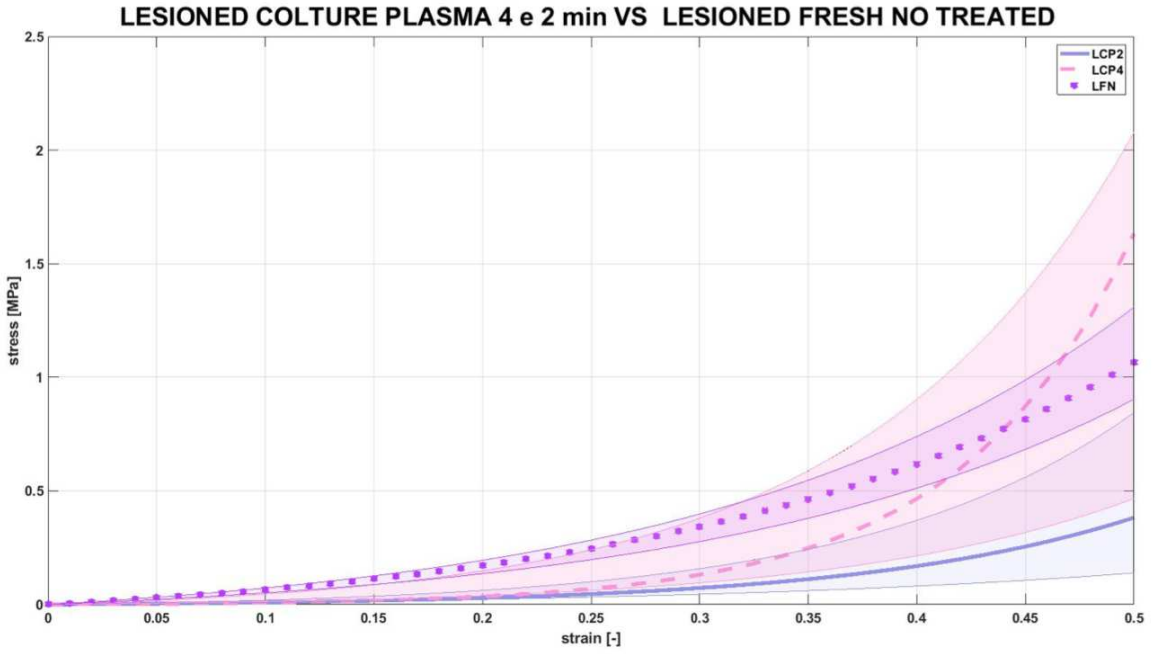

Figure 22.

Figures 20, 21 and 22 show the behavior of the lesioned cultured treated samples in comparison with our control group (HFN), with the lesioned cultured sample that did not underwent the treatment (LCN) and with the lesioned fresh sample that did not underwent the treatment (LFN).

Appears clear that healthy corneas that were evaluated shortly after enucleation in their unmodified form are the stiffest (Figure 20). Samples treated for only 2 minutes result to be less stiff than both the lesioned untreated ones (Figure 21 and 22).

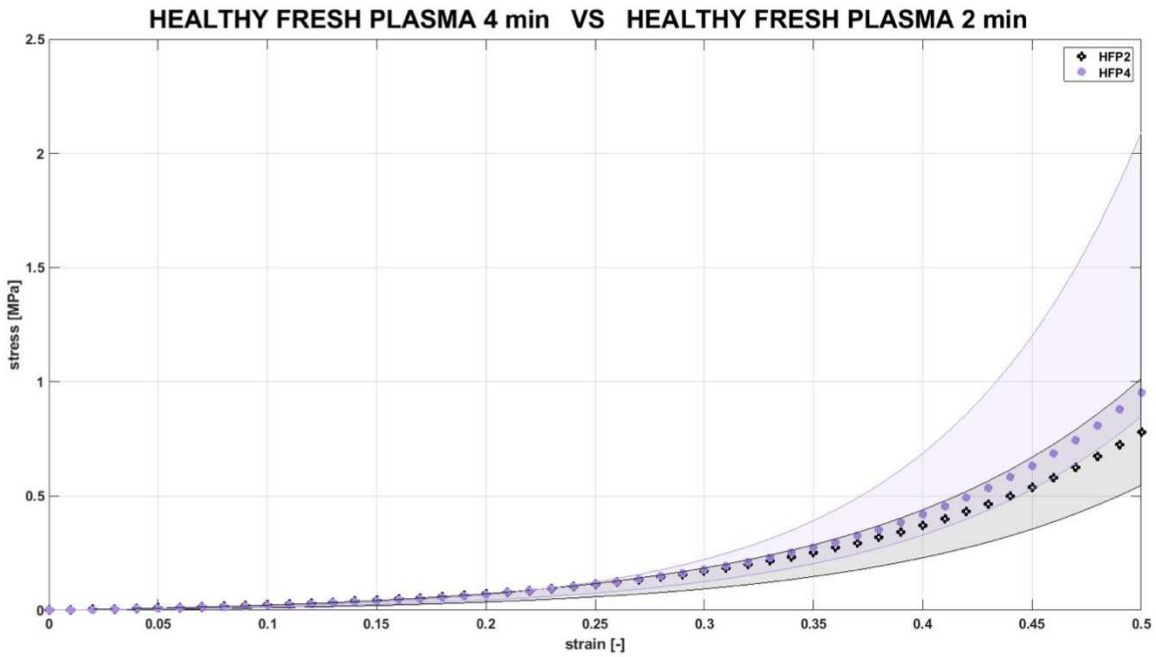

Figure 23.

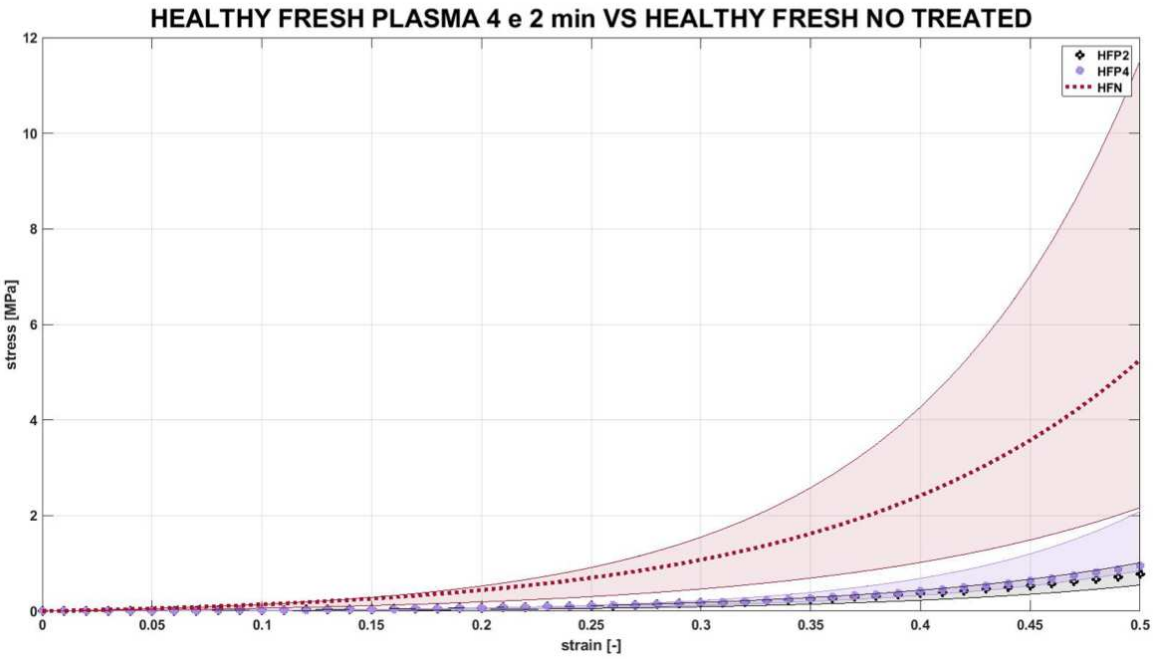

Figure 24.

As shown in Figures 23 and 24 corneas treated with helium plasma in the absence of any produced lesions had the group's lowest level of stiffness. Therefore, plasma appears to be significantly involved in reducing corneal stiffness in corneas treated in an unchanged condition a few hours after the enucleation of the eye. The lesser stiffness relative to untreated groups is an unexpected outcome.

Evaluation of the culture parameter

In Figures 25, 26, 27 and 28 by comparing fresh and cultured samples that experienced the same therapy and lesion, we can assess the impact of the culture on the results. In almost every chart, it appears clear that the loss in stiffness that occurs in the samples that underwent the culture for 7 days. The only chart where there is a discernible difference is Figure 28, where the lesioned cultured samples treated for 4 minutes are stiffer than their fresh counterparts.

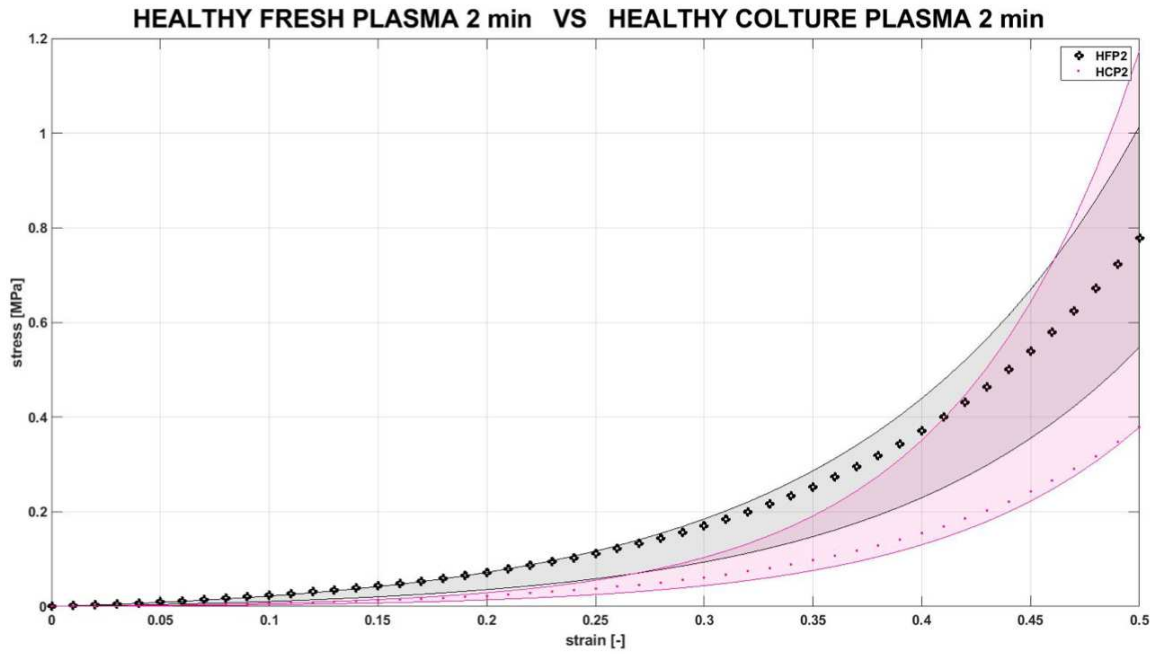

Figure 25.

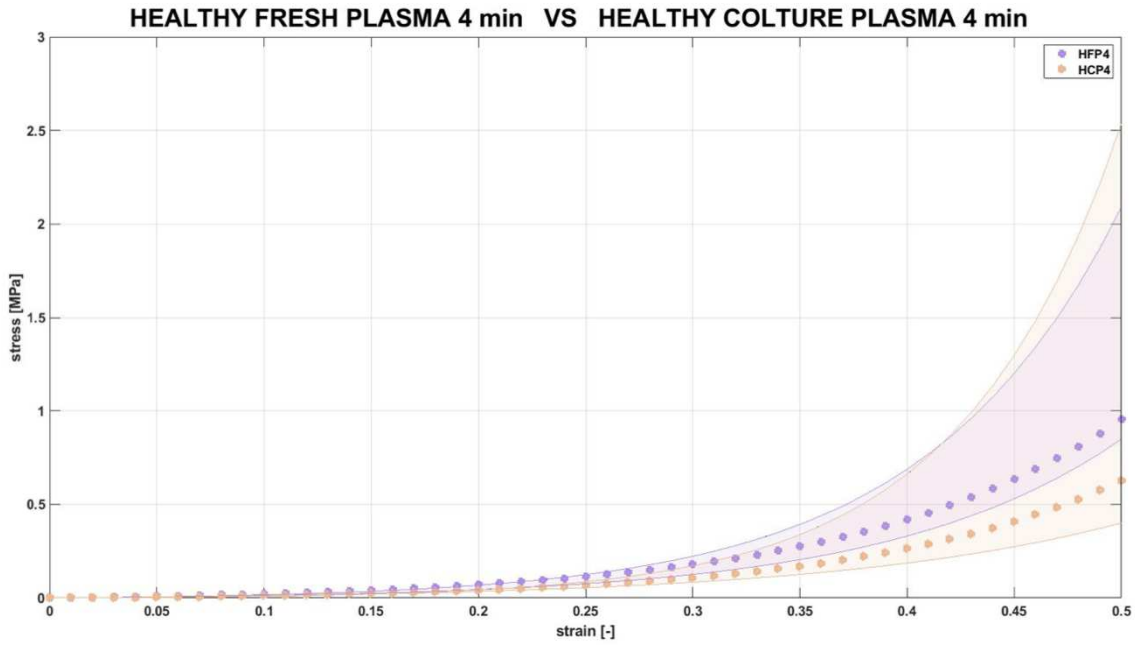

Figure 26.

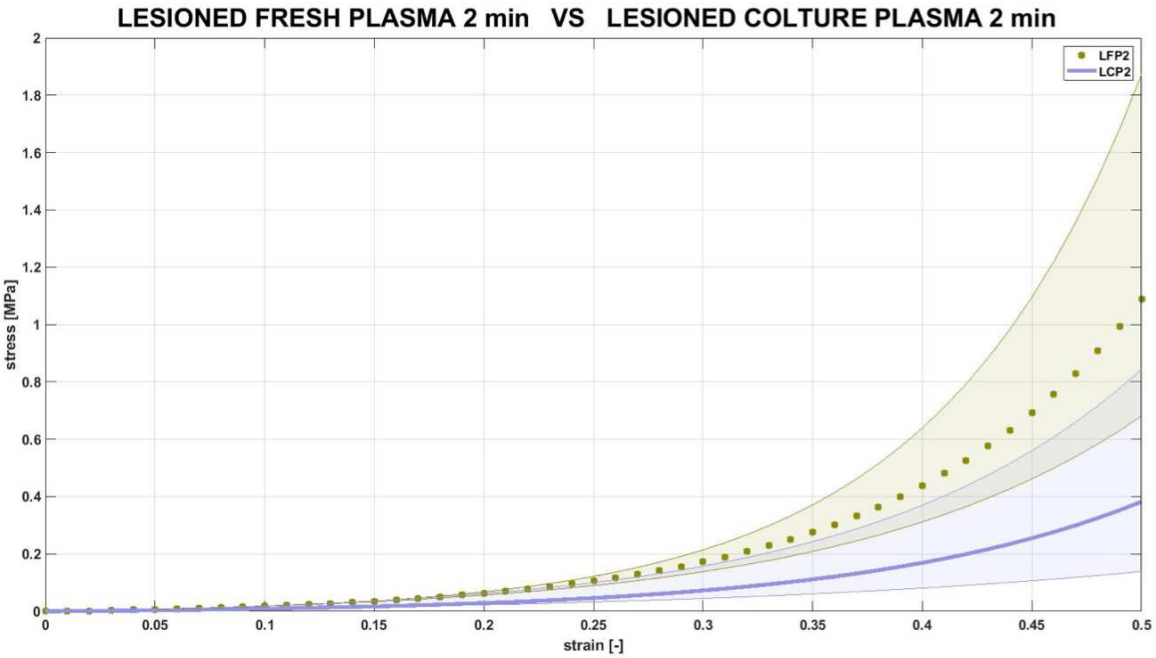

Figure 27.

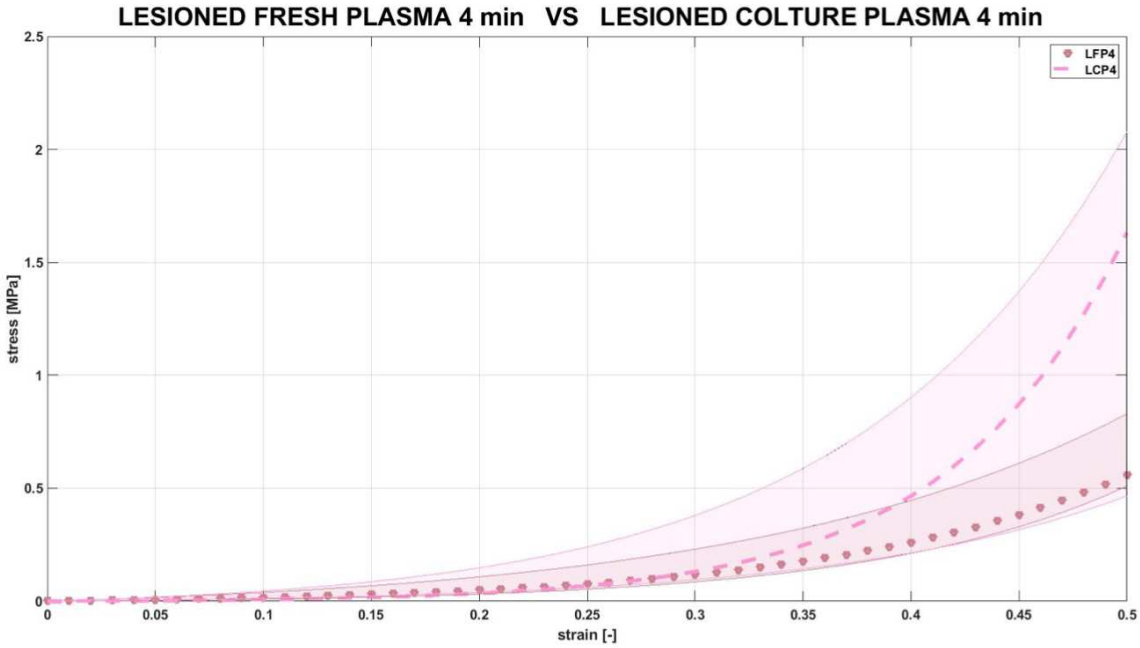

Figure 28.

Evaluation of the lesion parameter

In Figures 29, 30, 31 and 32 by comparing samples that experienced the same conservation method and treatment, we can assess the impact of the lesion on the results. Fresh samples exhibit less rigid behavior in almost every graphic. As was already mentioned, it was shown in this study that the plasma treatment used on fresh corneas reduced the stiffness of the tissue.

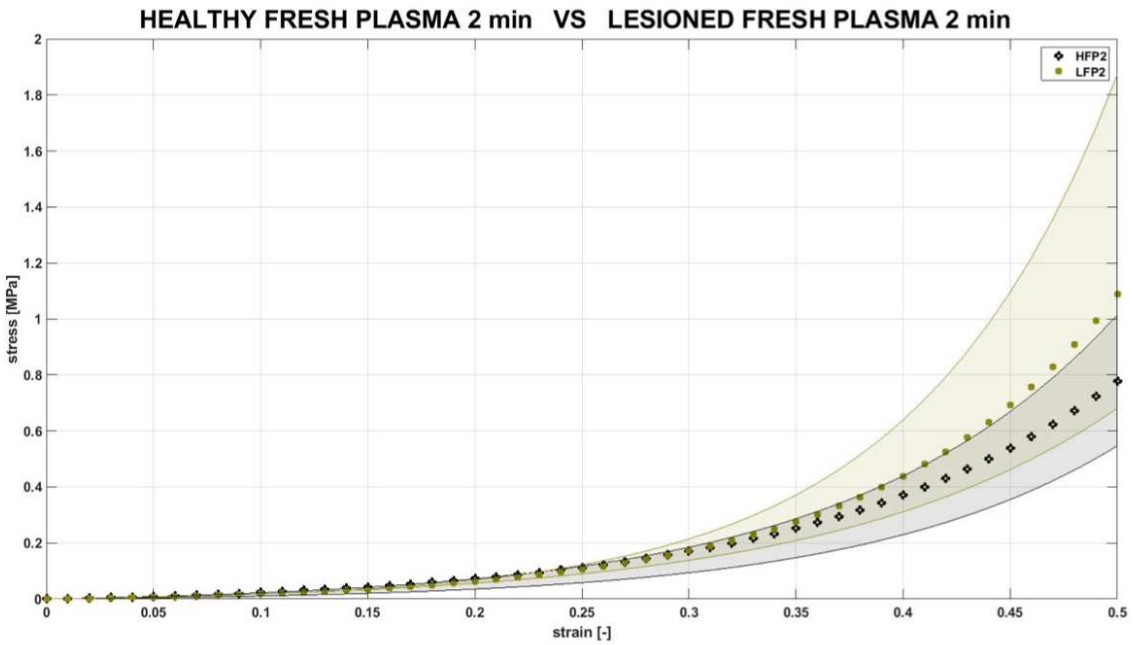

Figure 29.

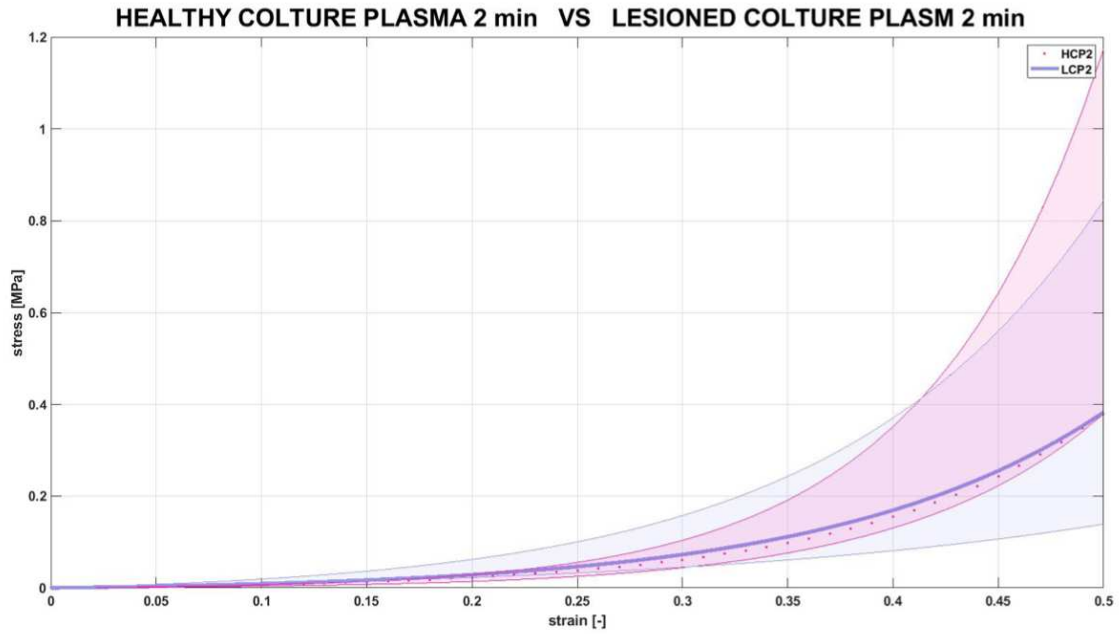

Figure 30.

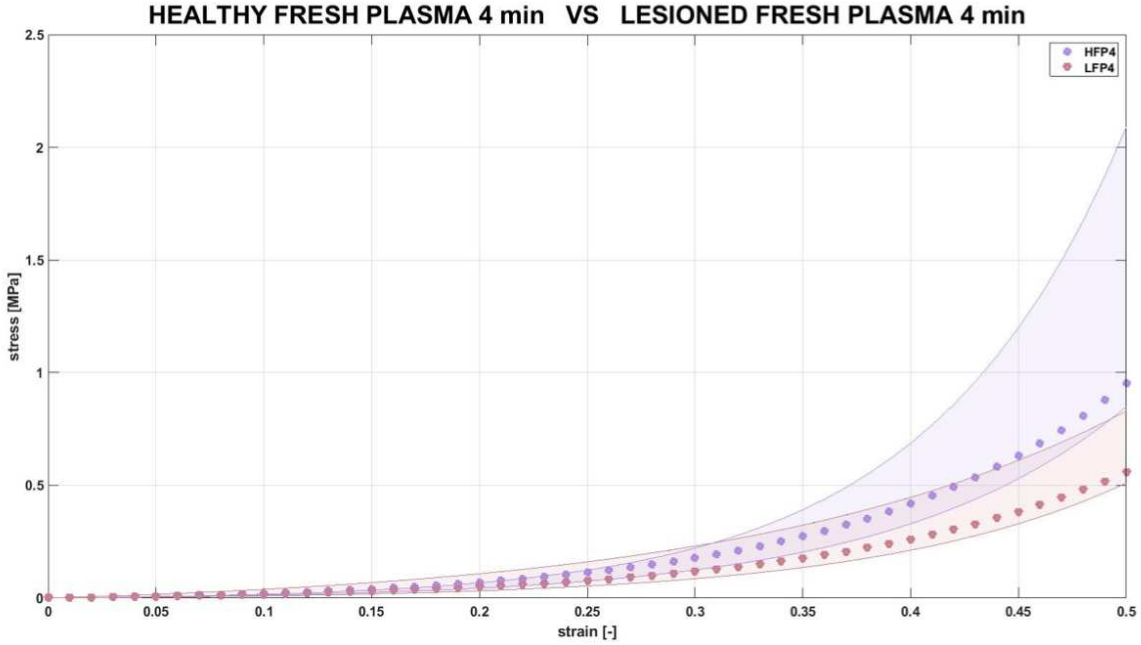

Figure 31.

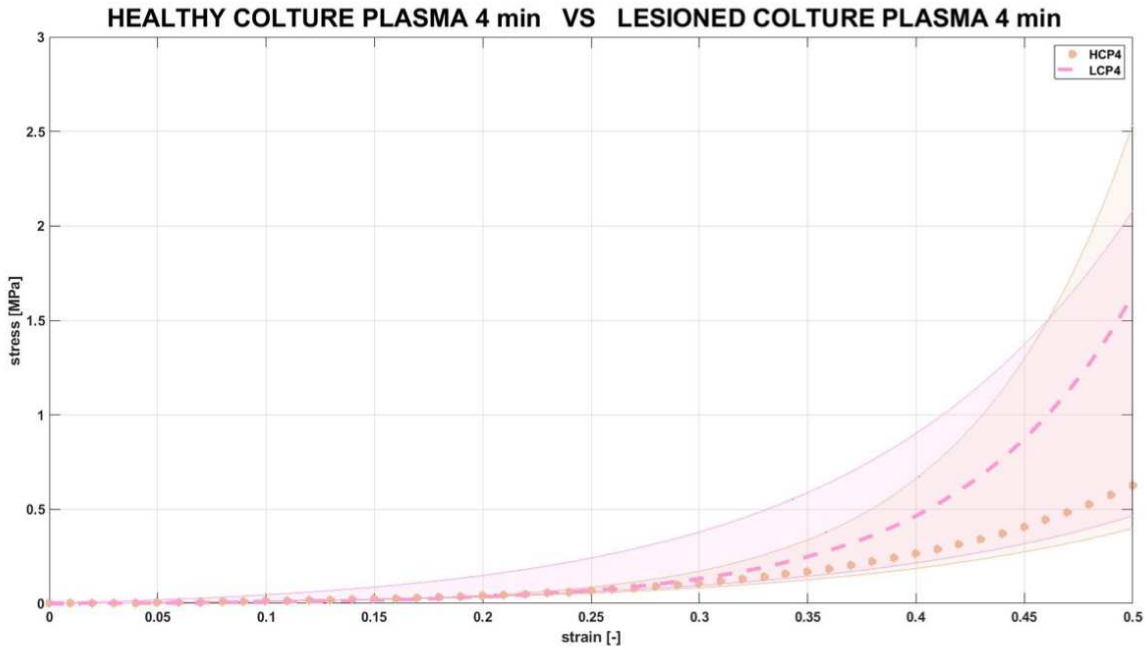
HEALTHY COLTURE PLASMA 4 min VS LESIONED COLTURE PLASMA 4 min
HCP4
LCP4
stress [MPa]
strain [-]
0
0.5
1
1.5
2
2.5
3
0
0.05
0.1
0.15
0.2
0.25
0.3
0.35
0.4
0.45
0.5

Figure 32.

5.2 STRESS-RELAXATION CURVES

Curves were generated using this data using Microsoft® Office Excel and Minitab® (https://www.minitab.com/en-us/).

Data from stress-relaxation tests were developed to show how normalized stress decreased with time. The ratio of the current stress to the peak stress at the start of the relaxation phase is known as the normalized stress: in this way it is possible to compare the curves of several samples.

By looking at the charts, it is clear that the reaction force, the load required to keep the tissue in its distorted configuration, begins at a significant magnitude and gradually declines over the course of the interval, reaching an asymptotic value. It's likely that the material's microstructures exhibit some relative sliding, which causes the tissue to seem to be somewhat more resistant. This is evident by the curve's decreasing slope and the reduced amount of stress required to keep the tissue in its distorted state. In other words, the tissue is resistive to the applied force and subsequently reorganized itself showing a decrease of stress to maintain the same strain.
In this study it was proved that ocular tissue is a viscoelastic material since this behavior is characteristic of viscoelastic materials. Additionally, it was evaluated the ability of corneal samples to relax under various situations that may have a favorable or negative impact on this behavior.

The relaxation behavior of the lesioned cultured plasma samples treated for 2 and 4 minutes are displayed in Figure 33. As shown in Figure 34, the population that underwent the treatment for 4 minutes (LCP4) is very similar to our control group (HFN), while the samples that were treated for only 2 minutes (LCP2) demonstrate a less viscoelastic behavior.
The lesioned untreated populations (fresh and cultured), as shown in Figures 35 and 36, display a significantly higher relaxation behavior.

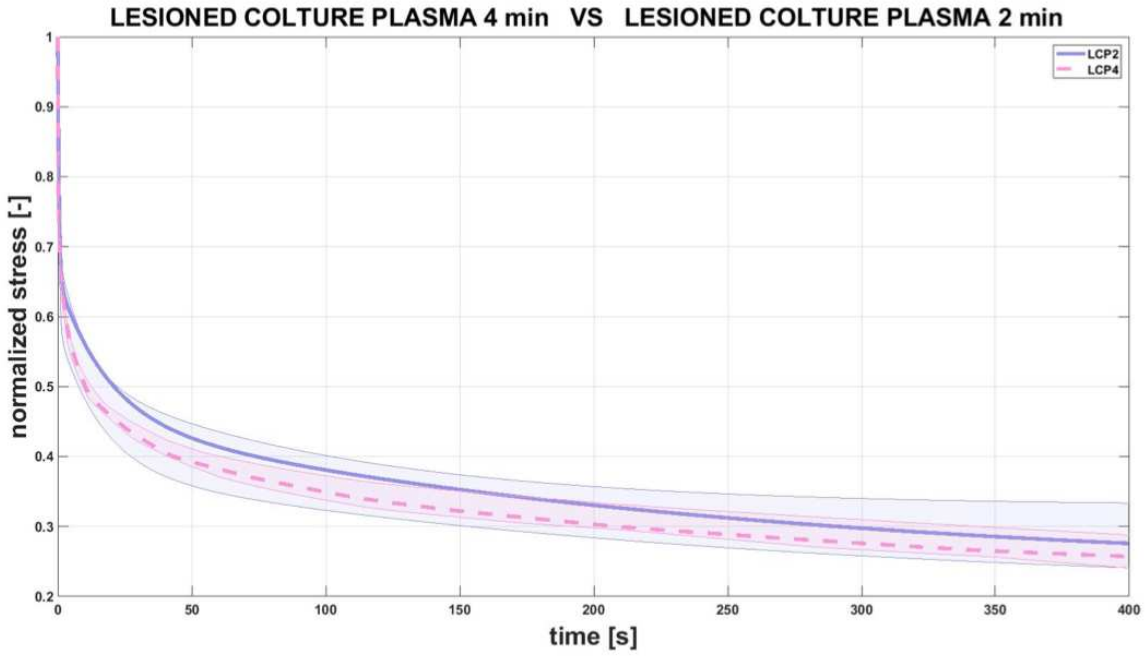

Figure 33.

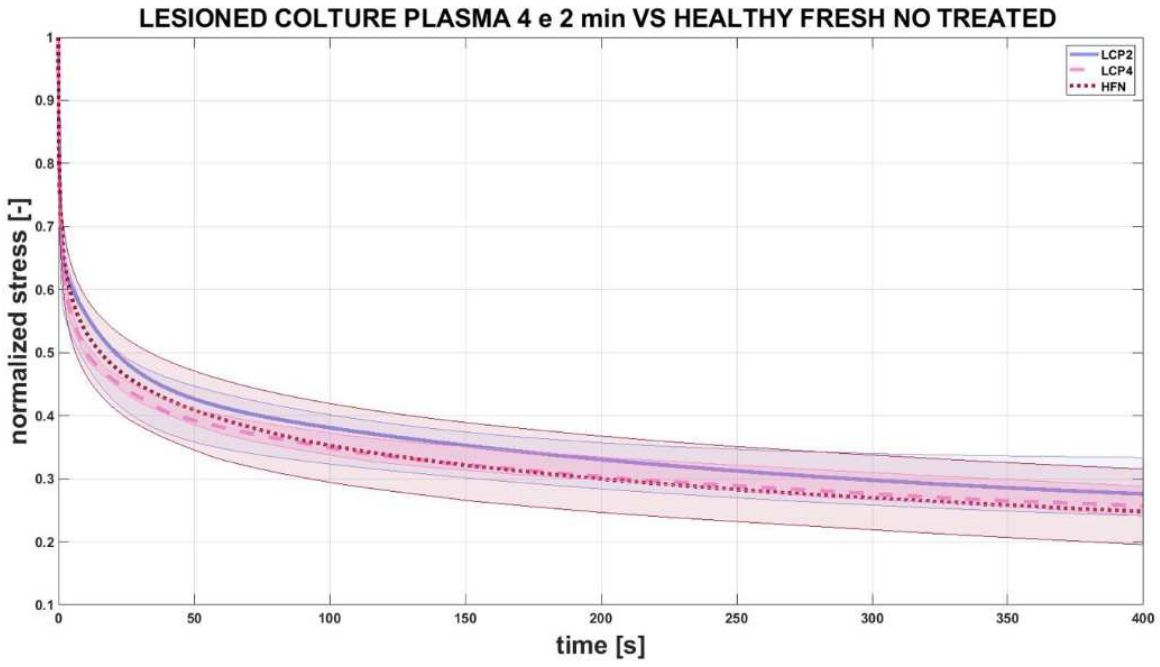

Figure 34.

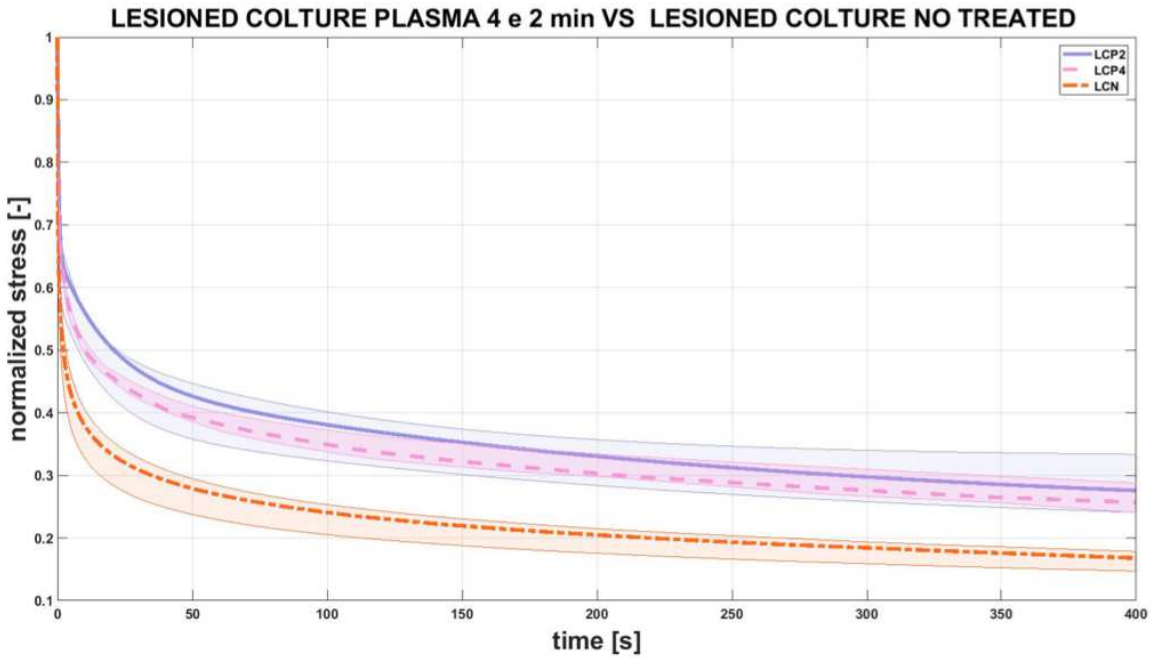

Figure 35.

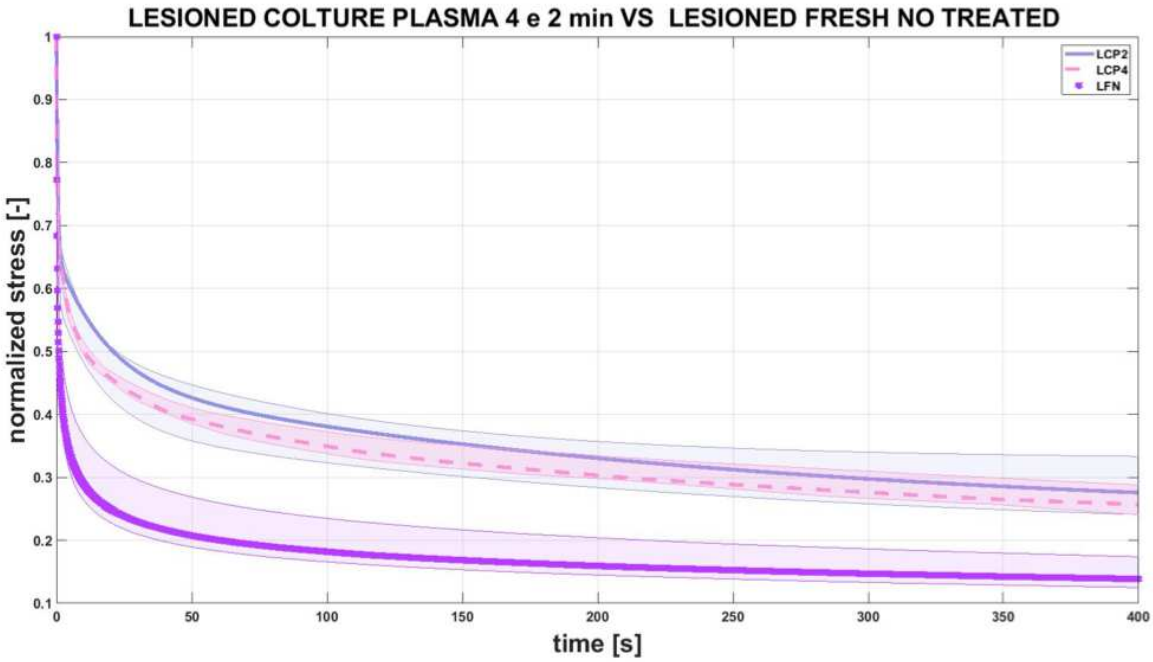

Figure 36.

Figures 37 and 38 illustrate how the behavior of healthy, fresh corneas that have not been treated (the control group) is identical to that of healthy, fresh corneas that have been treated for two minutes. Although the corneas were only treated for four minutes, the effects are extremely comparable.

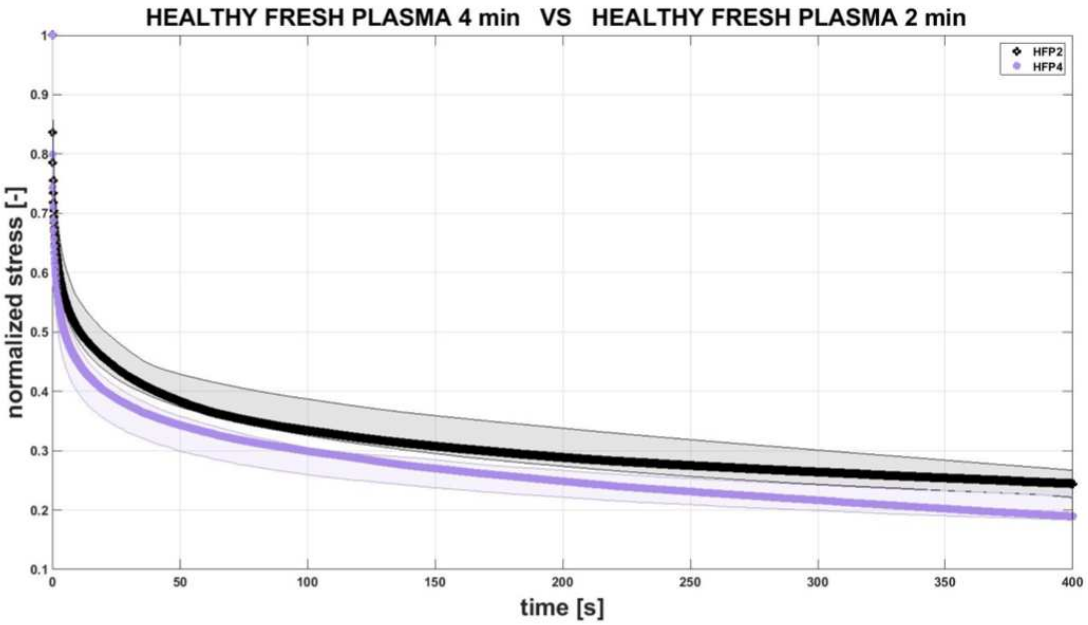

Figure 37.

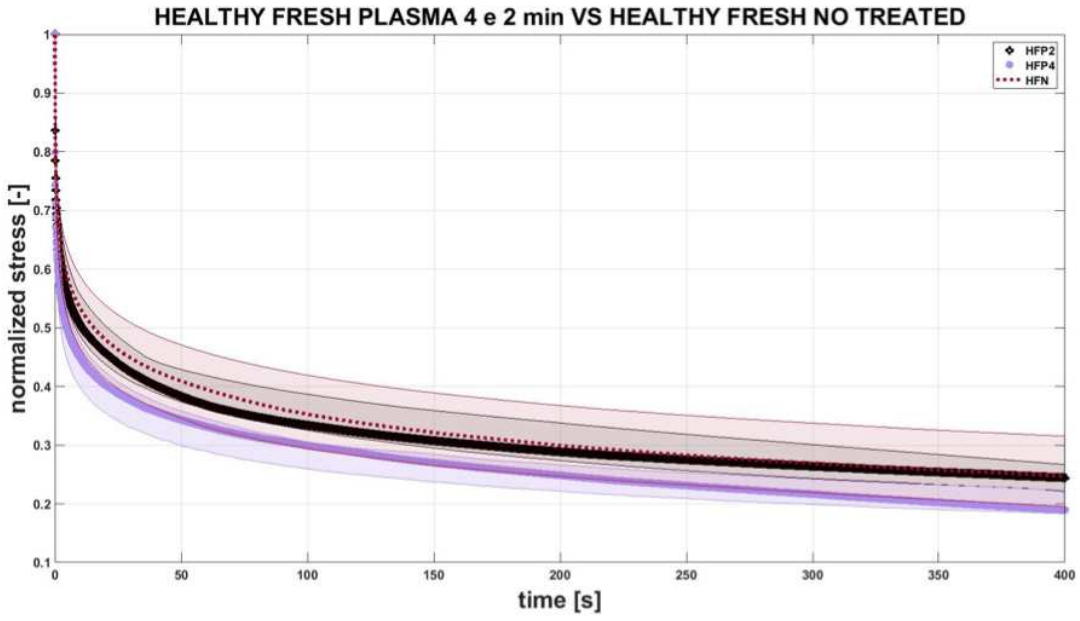

Figure 38.

Evaluation of culture parameter

As shown in Figures 39, 49, 41 and 42, the culture does not seem to affect the relaxation capacity of the samples treated for 2 minutes. Otherwise, the corneas treated for 4 minutes appear more viscoelastic than the cultured counterparts.

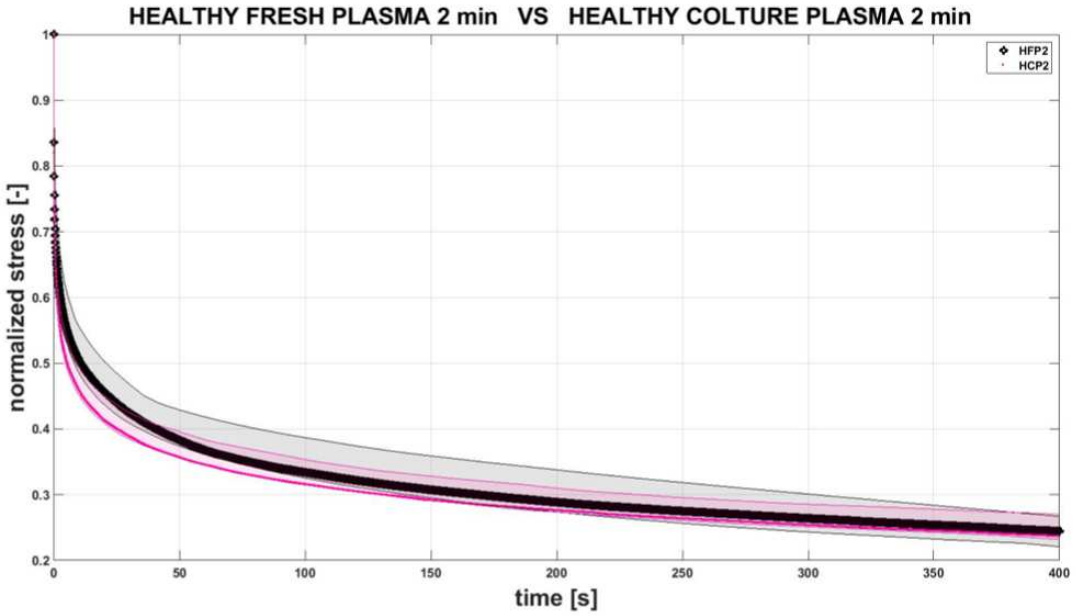

Figure 39.

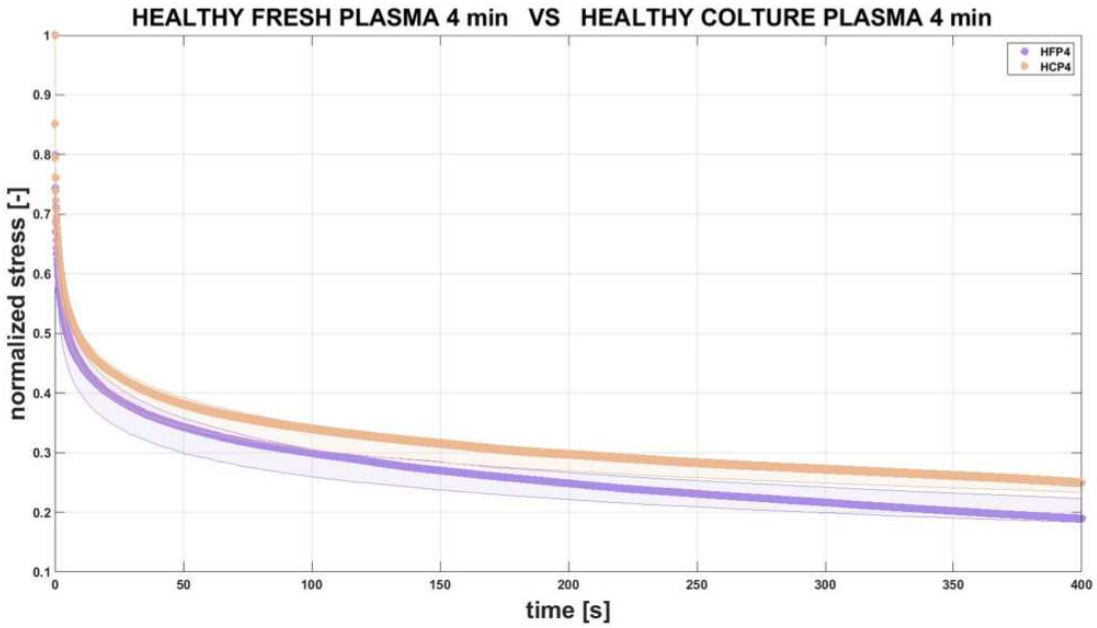

Figure 40.

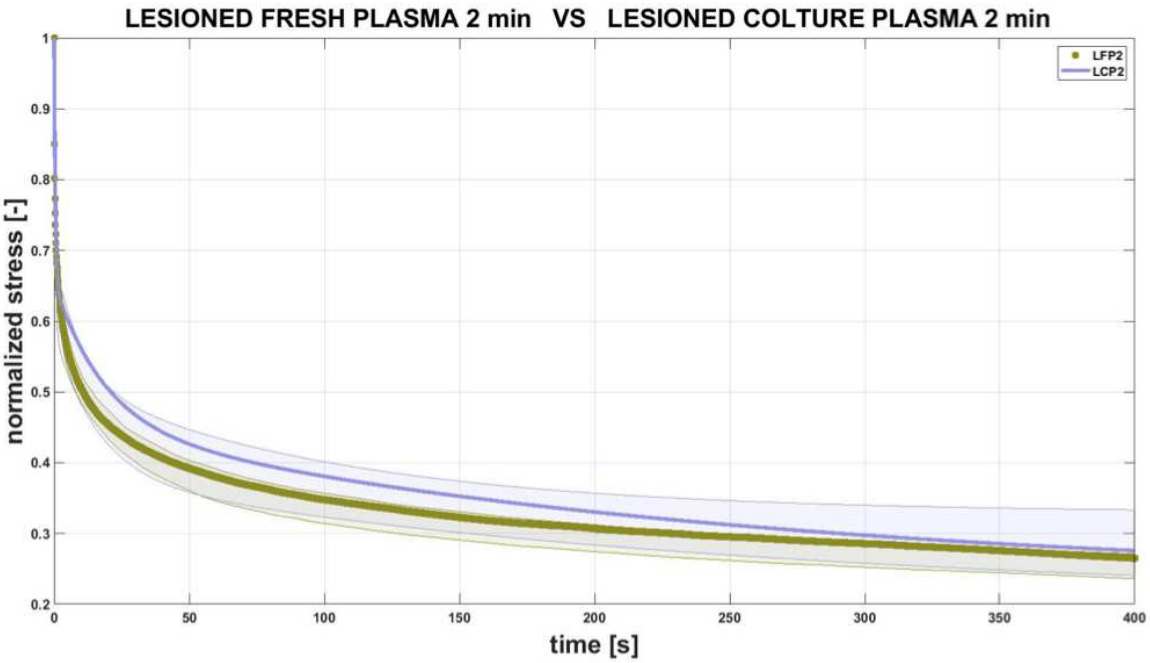

Figure 41.

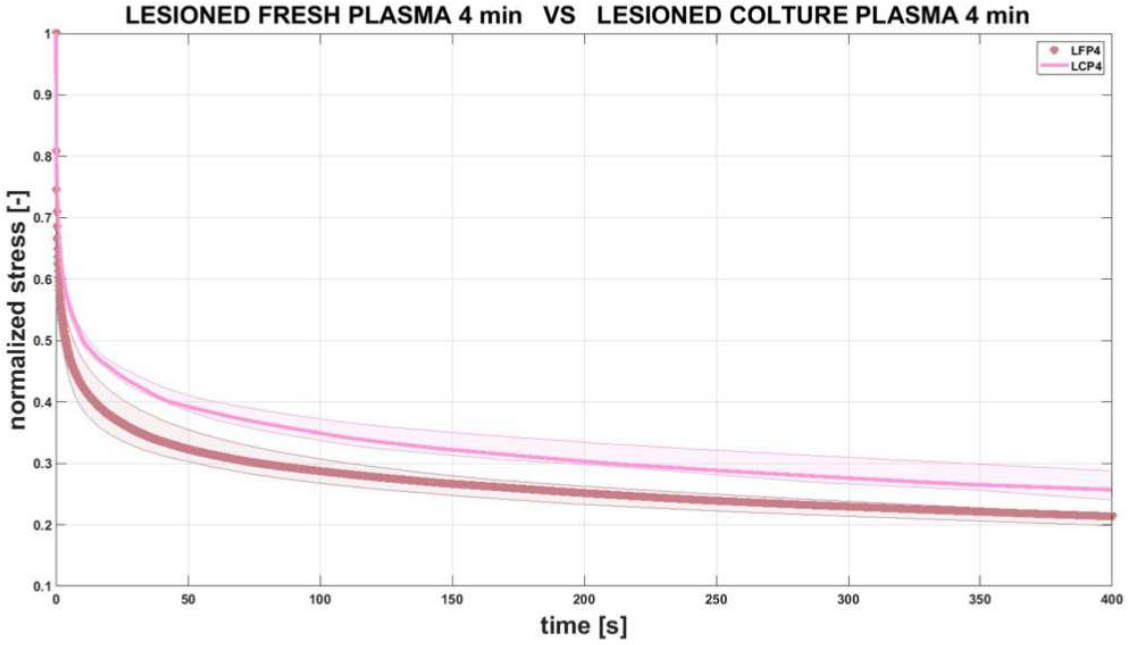

Figure 42.

Evaluation of the lesion parameter

The charts in Figures 43, 44, 45 and 46 show that healthy samples that received the treatment exhibit more relaxation than lesioned counterparts, indicating that the treatment applied on healthy samples lowers the ability to resist to a constant load. However, the results differ minimally.

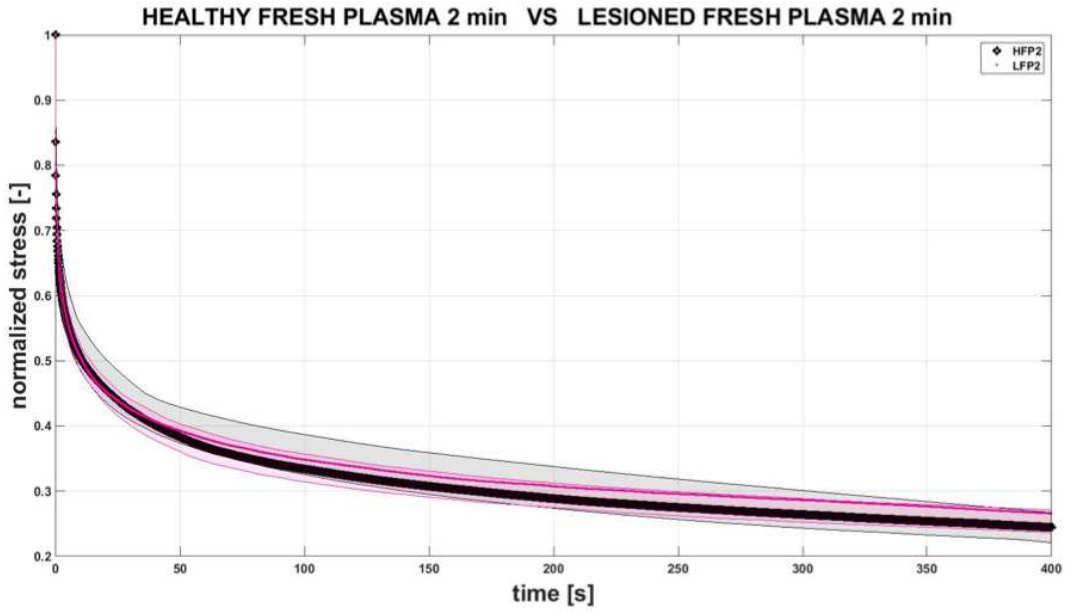

Figure 43.

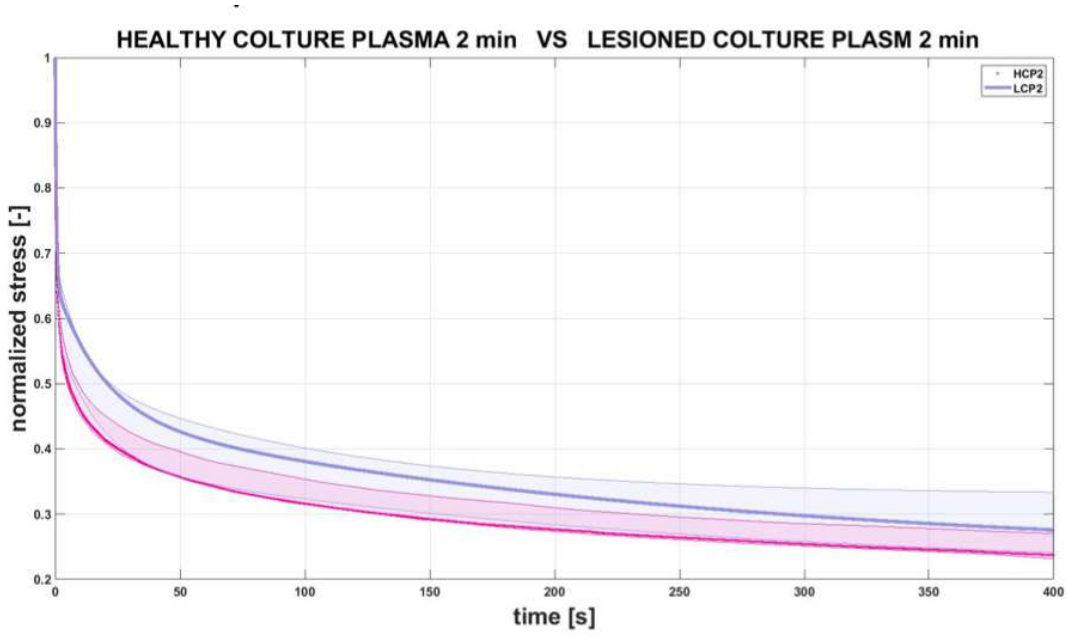

Figure 44.

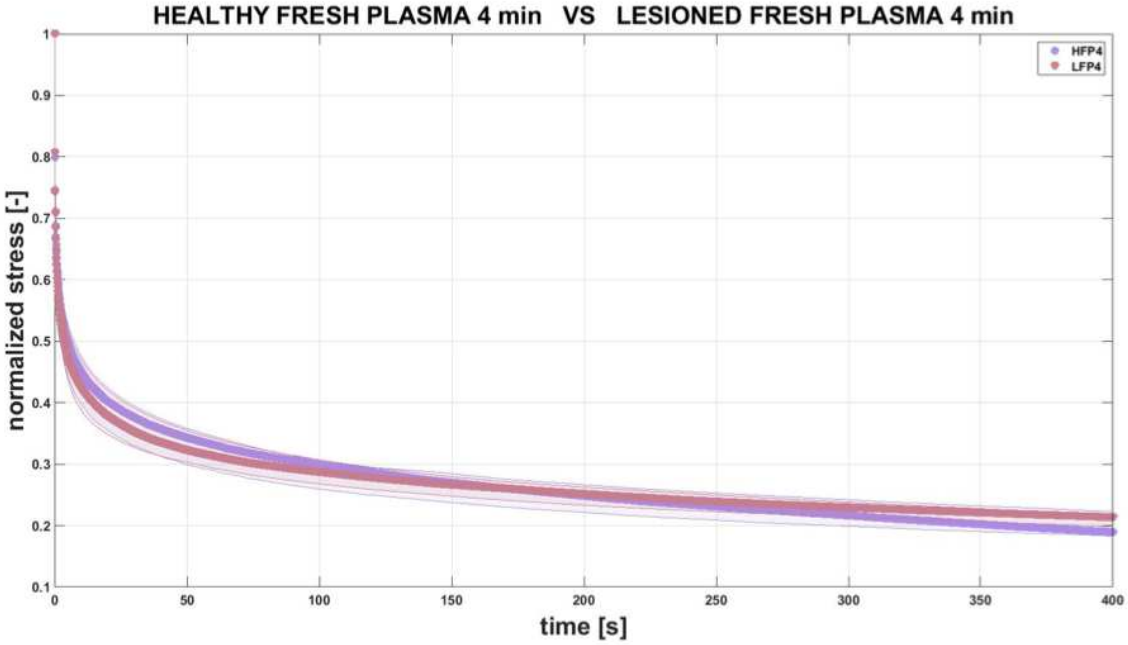

Figure 45.

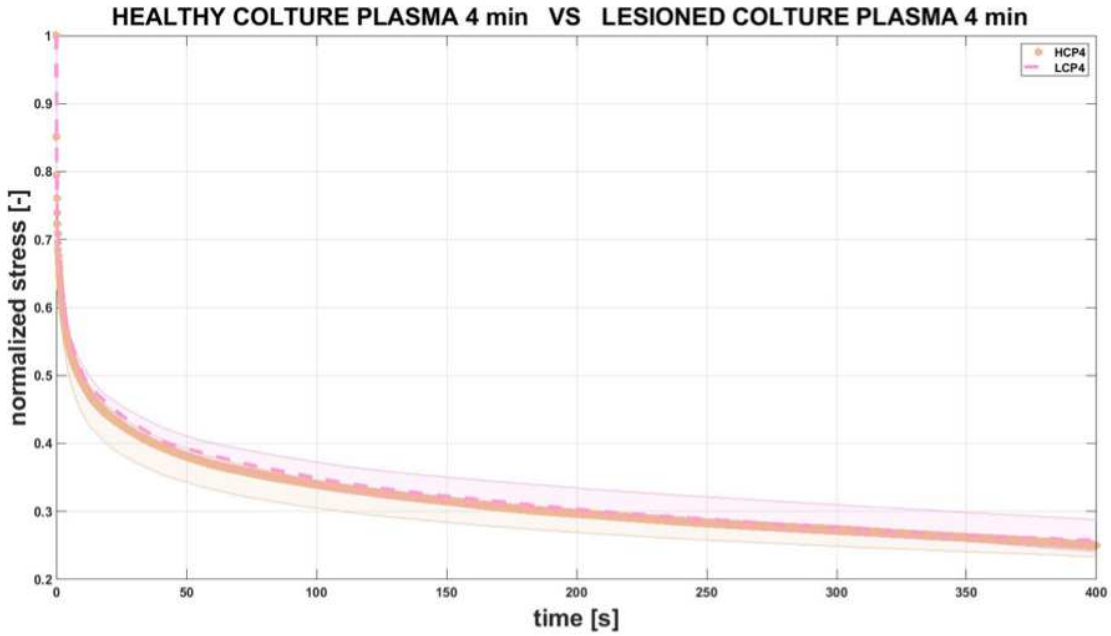

Figure 46.

6. DISCUSSION

The goal of this study is to assess and categorize how the corneal tissue responds mechanically under various conditions. We compared the mechanical behavior of healthy and lesioned, cultured and fresh and plasma treated samples.
The wider project, of which this study is just a component, presents several novelties in comparison to the existing literature: it exhibits various features that are unusually combined in other experimental protocols. To the best of our knowledge, there are no other research that investigate the mechanical behavior of damaged corneas treated with helium plasma.

The research team chose the methods used in a prior investigation to standardize the animal model and the lesion induction. It was observed that by putting a disk that has been submerged in a NaOH 1N solution for one minute, it was possible to create a lesion that resembled a corneal ulcer and assess the depth of the wounded region (Kenyon, 1989). The same procedure was employed to cause ocular tissue injury for our research as well: melting ulcers were created on the porcine corneas by applying a filter disc saturated in alkaline solution for one minute.

We proposed the organ culture for a prolonged period of time (7 days) and used a swine ex vivo model because of the similarities in mechanical behavior with other species, particularly the human one. It was examined the impact of a 7-day culture on specific sample groups as part of our study. The medium employed is CARRY-C from Alchimia, which is designed specifically for corneal tissue and ensures its preservation.
It was previously suggested to utilize organ culture to monitor the recovery of the cornea (Tanelian & Bisla, 1992). The study was focused particularly on the re-epithelialization process and showed that corneal wound healing occurs in organ culture as well, though it does that differently than in living animals and at a slower rate. In an in vivo setting, cytokines, growth factors, and proteases that play a crucial role in modifying corneal wound healing are actually carried by the corneal neo-

vascularization, which results from the injury and inflammation. All of these factors aid in the migration and proliferation of epithelial cells and play a crucial role in the remodeling of the corneal stroma (Zachary, 2017). In ex vivo models for corneal tissue, these processes are, however, rarely visible and only partially repeatable.

There are few cases in the literature where corneal organ culture is suggested for the purpose of observing the healing process. In two researches in vitro rabbit and bovine corneas were used to study the re-epithelialization procedure. In particular, the first study showed that after the epithelium or both the epithelium and the anterior stroma were removed, the cultured samples underwent re-epithelialization without the need of growth factors. Both types of injuries healed in a circularly symmetrical manner, and the wound closure rates for epithelial and subepithelial wound healing were 52±14 μm/hr and 38±7 μm/hr, respectively (complete wound closure was 51±5,5 hours and 69±4,5 hours, respectively). In vivo rates were 64±2 μm/hr for epithelial wounds and roughly 50 μm/hr for subepithelial wounds (Tanelian & Bisla, 1992). In the second experiment, it was showed that epithelial stromal damage to bovine corneas may recover quickly in organ culture. In fact, epithelial migration began after 12 hours of the injury, and by 72 hours, the wounds had fully regenerated epithelium (Carrington et al., 2006).

All of the samples underwent to stress-relaxation uniaxial tensile tests, and the curves of the groups were compared in order to understand how the external factors (injury, culture, and treatment) may affect the biomechanical behavior.

Preliminary experimental data were considered to determine the deformative levels and speed for the Bose device that was used for the biomechanical testing (Zeng et al., 2001). We evaluated the nonlinear and viscoelastic behavior of this specific material in our porcine samples using respectively stress-strain and stress-relaxation curves. We can confirm that the general biomechanical behavior of our corneal samples is linear with the one stated in the literature for corneal tissue. In fact, the charts of stress-strain and stress-relaxation tests of the untreated samples (HFN group), are comparable to the one displayed by Zeng et al (2001).

In the literature, the research groups used creep and stress-relaxation tests to evaluate the mechanical behavior of pig and human ex vivo corneas, and their findings showed that the swine samples relaxed more quickly than the human ones (Elsheikh et al., 2008). While corneal strips were kept stretched under various loads, they explained that the sustained load steadily reduced with time. In our study, we show that the same claim holds true for the other types of sample groups as well. In addition, we discover that damage, culture conditions, and helium plasma treatment have an impact on the viscoelasticity of corneal tissue.

When injured treated samples are compared to their fresh counterparts, the culture condition in particular causes a decrease in stiffness: however, the lesion's contribution is apparent when healthy untreated samples are compared with injured untreated ones, which display less tilted curves indicating inferior rigidity. In the region where the paper disk covered in alkaline solution is placed, the induction of the lesion results in the disruption of corneal structure, with disordered collagen lamellae and areas lacking tissue. Therefore, it makes sense to assume that the lesion, which was also emphasized during our stress-strain testing, is to blame for the altered mechanical behavior of the tissue.
Our corneal samples' stiffness is reduced by culture conditions in both healthy and damaged samples. This is likely due to the fact that, despite the high caliber and specificity of the culture media, the tissue probably degrades during the course of the organ culture. Although ex vivo conditions and the culture medium were utilized, it is probable that in our situation samples that were lesioned and subsequently cultured started to recover extremely slowly and as a result, exhibited a little lower relaxation capacity than fresh samples in both treated and untreated samples. The difference in tissue resistance is, however, quite small.
According to the obtained results it appears clear that a longer treatment determines a significant increase in corneal stiffness.

An unexpected outcome that we find is that corneas treated with helium plasma in the absence of any produced lesions had the group's lowest level of stiffness. Therefore, plasma appears to be significantly involved in reducing corneal stiffness in corneas

treated in an unchanged condition a few hours after the enucleation of the eye. The cause of this is unknown and deserves further investigations.

As for stress-relaxation results the lesioned untreated groups (LFN and LCN) are the samples that show the higher relaxation behavior, while the lesioned samples cultured and treated with helium plasma for 4 minutes show a viscoelasticity that is similar to the one of the control group (HFN).
A viscoelastic activity is linked to a physiological behavior, although excessive elasticity might result in a tissue's greater responsiveness to pressure changes. On the other hand, if the tissue is stiffer than normal, it is possible that the cornea will not re-adapt to the physiological shape of the eye once the normal pressure is restored, sustaining a state of buphtalmos. In fact, a healthy globe's tissue should expand as the intraocular pressure is raised and then return to normal when the normal pressure is restored.
Clinically speaking, we are unsure of the potential use of the increased stiffness and decreased relaxation behavior that we saw in our samples after they were treated with helium plasma.

To understand the natural behavior of the cornea, inflation tests are typically preferred because they use the entire eye globe, preserve natural boundaries, are minimally invasive, and respect the orientation of the tissue: the results of these tests can be more easily applied in clinical settings. On the contrary, uniaxial tensile tests have certain weaknesses since they use strips of corneal tissue, which partially disrupts the cornea's natural structure (curved surface and collagen lamellae). Because of this, results from these tests, when compared to inflation testing, only partially replicate the actual biomechanical behavior of corneal tissue. However, we used uniaxial tensile tests because they allow to compare and analyze the stiffness capacity of the corneal tissue's viscoelastic response as well as the stress-strain curve.

It's likely that it takes more consecutive days of treatment for the plasma stiffening impact to manifest: it will be intriguing to assess the mechanical behavior of corneal tissue following a prolonged therapy. For ex vivo models, time is a constraint since the tissue gradually loses vitality as the days go by.

The research group intends to also evaluate the biomechanical behavior of the cornea samples after a longer helium plasma treatment (8 minutes).

More research is required to identify a culture medium that can maintain the mechanical properties of corneal tissue following longer-term organ cultures. To better understand the in vitro healing process of porcine corneas, it would be interesting to compare histologically fresh, short-term, and long-term cultured samples as well as test the mechanical behavior of injured samples after a longer organ culture.

The cause of the increased stiffness following the helium plasma treatment is yet unknown. It may be caused by the healing process and hence beneficial in therapeutic applications, but it is unclear if there are also fibrotic processes in progress. In that situation, visual loss may occur, making the patient's therapy unsuitable.
This thesis is a portion of a larger effort, as was already indicated. The study team will eventually evaluate the negative effects of plasma therapy on corneal epithelial cells using histological and biomolecular testing.

7. CONCLUSIONS

In conclusion, we show that helium plasma therapy, the creation of lesions, and culture conditions are all related to changes in the mechanical behavior of corneal tissue, despite the cornea's nonlinear and viscoelastic behavior being confirmed.
The lesion induction and the medium for the culture decrease the stiffness and increase the capacity of the tissue to relax in the immediate and short-term periods, while the treatment, particularly the 4 minutes one, increases the stiffness and decreases the relaxation behavior. We also discovered that the therapy used on fresh healthy corneas has a negative impact on stiffness: this is an unexpected finding that requires other investigations.

Further research is required to completely understand the mechanical behavior of corneal tissue following the administration of this therapy in the future potential of clinical applications due to the relevance and value of our results. There is a chance to use helium plasma therapy for treating specific corneal disorders in both dogs and cats, as it is already done for human skin ulcers. Based on the findings given in the literature, this therapy appears to be successful and promising for veterinary ophthalmology. Cold atmospheric pressure plasma has the potential to be an effective treatment thanks to its ease of use, low cost, rapidity, and favorable outcomes are the foundation of this success and the possibility that it may eventually be used often as a synergic treatment for corneal ulcers in domestic animals.

REFERENCES

Ambati, B. K., Nozaki, M., Singh, N., Takeda, A., Jani, P. D., Suthar, T., Albuquerque, R. J. C., Richter, E., Sakurai, E., Newcomb, M. T., Kleinman, M. E., Caldwell, R. B., Lin, Q., Ogura, Y., Orecchia, A., Samuelson, D. A., Agnew, D. W., st. Leger, J., Green, W. R., Ambati, J. (2006). Corneal avascularity is due to soluble VEGF receptor-1. *Nature*, *vol. 443*, 993–997. https://doi.org/10.1038/nature05249

Arndt, S., Unger, P., Berneburg, M., Bosserhoff, A.-K., & Karrer, S. (2018). Cold atmospheric plasma (CAP) activates angiogenesis-related molecules in skin keratinocytes, fibroblasts and endothelial cells and improves wound angiogenesis in an autocrine and paracrine mode. *Journal of Dermatological Science*, *vol. 89*, 181–190. https://doi.org/10.1016/j.jdermsci.2017.11.008

Arndt, S., Unger, P., Wacker, E., Shimizu, T., Heinlin, J., Li, Y.-F., Thomas, H. M., Morfill, G. E., Zimmermann, J. L., Bosserhoff, A.-K., & Karrer, S. (2013). Cold atmospheric plasma (CAP) changes gene expression of key molecules of the wound healing machinery and improves wound healing in vitro and in vivo. *PLoS ONE*, *vol. 8*. https://doi.org/10.1371/journal.pone.0079325

Bekeschus, S., von Woedtke, T., Emmert, S., & Schmidt, A. (2021). Medical gas plasma-stimulated wound healing: Evidence and mechanisms: Mechanisms of gas plasma-assisted wound healing. *Redox Biology*, *vol. 46.* https://doi.org/10.1016/j.redox.2021.102116

Boschetti, F., Triacca, V., Spinelli, L., & Pandolfi, A. (2012). Mechanical characterization of porcine corneas. *Journal of Biomechanical Engineering*, *vol. 134*. https://doi.org/10.1115/1.4006089

Breathnach, R., McDonnell, K. A., Chebbi, A., Callanan, J. J., & Dowling, D. P. (2018). Evaluation of the effectiveness of kINPen Med plasma jet and bioactive agent therapy in a rat model of wound healing. *Biointerphases*, *vol. 13*. https://doi.org/10.1116/1.5046489

Brun, P., Brun, P., Vono, M., Venier, P., Tarricone, E., Deligianni, V., Martines, E., Zuin, M., Spagnolo, S., Cavazzana, R., Cardin, R., Castagliuolo, I., la Gloria Valerio, A., & Leonardi, A. (2012). Disinfection of ocular cells and tissues by atmospheric-pressure cold plasma. *PLoS ONE*, *vol. 7*. https://doi.org/10.1371/journal.pone.0033245

Brun, P., Pathak, S., Castagliuolo, I., Palù, G., Brun, P., Zuin, M., Cavazzana, R., & Martines, E. (2014). Helium generated cold plasma finely regulates activation of human fibroblast-like primary cells. *PLoS ONE*, *vol. 9*. https://doi.org/10.1371/journal.pone.0104397

Brun, P., Russo, V., Tarricone, E., Corrao, S., Deligianni, V., Leonardi, A., Cavazzana, R., Zuin, M., & Martines, E. (2015). Using helium-generated cold plasma to control infection and healing. In *Plasma Medicine, vol. 5.* https://doi.org/10.1615/PlasmaMed.2016015761

Carrington, L. M., Albon, J., Anderson, I., Kamma, C., & Boulton, M. (2006). Differential regulation of key stages in early corneal wound healing by TGF-β isoforms and their inhibitors. *Investigative Ophthalmology and Visual Science*, *vol. 47*, 1886–1894. https://doi.org/10.1167/iovs.05-0635

Chatraie, M., Torkaman, G., Khani, M., Salehi, H., & Shokri, B. (2018). In vivo study of non-invasive effects of non-thermal plasma in pressure ulcer treatment. *Scientific Reports*, *vol. 8*. https://doi.org/10.1038/s41598-018-24049-z

Cheng, K. Y., Lin, Z. H., Cheng, Y. P., Chiu, H. Y., Yeh, N. L., Wu, T. K., & Wu, J. S. (2018). Wound healing in streptozotocin-induced diabetic rats using atmospheric-pressure argon plasma Jet. *Scientific Reports*, *vol. 8*. https://doi.org/10.1038/s41598-018-30597-1

Darmawati, S., Rohmani, A., Nurani, L. H., Prastiyanto, M. E., Dewi, S. S., Salsabila, N., Wahyuningtyas, E. S., Murdiya, F., Sikumbang, I. M., Rohmah, R. N., Fatimah, Y. A., Widiyanto, A., Ishijima, T., Sugama, J., Nakatani, T., & Nasruddin, N. (2019). When plasma jet is effective for chronic wound bacteria inactivation, is it also effective for wound healing? *Clinical Plasma Medicine*, *vol. 14*. https://doi.org/10.1016/j.cpme.2019.100085

DelMonte, D. W., & Kim, T. (2011). Anatomy and physiology of the cornea. *Journal of Cataract and Refractive Surgery*, *vol. 37*, 588–598. https://doi.org/10.1016/j.jcrs.2010.12.037

Dupps, W. J., & Wilson, S. E. (2006). Biomechanics and wound healing in the cornea. In *Experimental Eye Research, vol. 83,* 709–720. https://doi.org/10.1016/j.exer.2006.03.015

Elsheikh, A., Alhasso, D., & Rama, P. (2008). Biomechanical properties of human and porcine corneas. *Experimental Eye Research, vol. 86*, 783–790. https://doi.org/10.1016/j.exer.2008.02.006

Evans, & de Lahunta. (2012). Miller's anatomy of the dog (4th Edition). Elsevier.

Fathollah, S., Mirpour, S., Mansouri, P., Dehpour, A. R., Ghoranneviss, M., Rahimi, N., Safaie Naraghi, Z., Chalangari, R., & Chalangari, K. M. (2016). Investigation on the effects of the atmospheric pressure plasma on wound healing in diabetic rats. *Scientific Reports, vol.6*. https://doi.org/10.1038/srep19144

Fontanella, C. G., Carniel, E. L., Corain, L., Peruffo, A., Iacopetti, I., Pavan, P. G., Todros, S., & Perazzi, A. (2021). Mechanical behaviour of healthy versus alkali-lesioned corneas by a porcine organ culture model. *BMC Veterinary Research, vol. 17*. https://doi.org/10.1186/s12917-021-03050-1

Gibbon, P. (2014). Introduction to plasma physics. *CAS-CERN Accelerator School: Plasma Wake Acceleration 2014, Proceedings*, 51–65. https://doi.org/10.5170/CERN-2016-001.51

Graves, D. B. (2014). Low temperature plasma biomedicine: A tutorial review. *Physics of Plasmas, vol. 21*. https://doi.org/10.1063/1.4892534

Holzapfel A., Sommer G., Gasser C.T., Regitnig P (2005). Determination of layer-specific mechanical properties of human coronary arteries with nonatherosclerotic intimal thickening and related constitutive modeling. *American Journal of physiology, vol. 289*, 2048-2058. https://doi.org/10.1152/ajpheart.00934.2004

Jacofsky, M. C., Lubahn, C., McDonnell, C., Seepersad, Y., Fridman, G., Fridman, A. A., & Dobrynin, D. (2014). Spatially resolved optical emission spectroscopy of a helium plasma jet and its effects on wound healing rate in a diabetic murine model. *Plasma Medicine, vol. 4,* 177–191. https://doi.org/10.1615/PlasmaMed.2015012190

Kenyon, K. R. (1989). Standard models of corneal injury using alkali-immersed filter disks. *Massachusetts Eye and Ear Infirmary*. https://www.researchgate.net/publication/20679480

Khlystov, N., Lizardo, D., Matsushita, K., & Zheng, J. (2013). *Uniaxial Tension and Compression Testing of Materials*.

Kim, D. W., Park, T. J., Jang, S. J., You, S. J., & Oh, W. Y. (2016). Plasma treatment effect on angiogenesis in wound healing process evaluated *in vivo* using angiographic optical coherence tomography. *Applied Physics Letters, vol. 109*. https://doi.org/10.1063/1.4967375

Kim, H. Y., Kang, S. K., Park, S. M., Jung, H. Y., Choi, B. H., Sim, J. Y., & Lee, J. K. (2015). Characterization and effects of Ar/Air microwave plasma on wound healing. *Plasma Processes and Polymers, vol. 12*, 1423–1434. https://doi.org/10.1002/ppap.201500017

Kling, S., & Hafezi, F. (2017). Corneal biomechanics – a review. *Ophthalmic and Physiological Optics, vol. 37,* 240–252. Blackwell Publishing Ltd. https://doi.org/10.1111/opo.12345

Kong, M. G., Kroesen, G., Morfill, G., Nosenko, T., Shimizu, T., van Dijk, J., & Zimmermann, J. L. (2009). Plasma medicine: An introductory review. *New Journal of Physics, vol. 11.* https://doi.org/10.1088/1367-2630/11/11/115012

Kubinova, S., Zaviskova, K., Uherkova, L., Zablotskii, V., Churpita, O., Lunov, O., & Dejneka, A. (2017). Non-thermal air plasma promotes the healing of acute skin wounds in rats. *Scientific Reports, vol. 7*. https://doi.org/10.1038/srep45183

Laroussi, M., Lu, X., & Keidar, M. (2017). Perspective: The physics, diagnostics, and applications of atmospheric pressure low temperature plasma sources used in plasma medicine. *Journal of Applied Physics, vol. 122*. https://doi.org/10.1063/1.4993710

Lee, J., Kim, W. S., Bae, K. B., Yun, G., & Lee, J. K. (2019). Variation of Physical Parameters and Anomalous Healing Observation in Plasma Wound Healing. *IEEE Transactions on Plasma Science, vol. 47*, 4833–4839. https://doi.org/10.1109/TPS.2019.2923750

Lombardo, G., Serrao, S., Rosati, M., & Lombardo, M. (2014). Analysis of the viscoelastic properties of the human cornea using scheimpflug imaging in inflation experiment of eye globes. *PLoS ONE, vol. 9*. https://doi.org/10.1371/journal.pone.0112169

Lou, B.-S., Hsieh, J.-H., Chen, C.-M., Hou, C.-W., Wu, H.-Y., Chou, P.-Y., Lai, C.-H., & Lee, J.-W. (2020). Helium/Argon-generated cold atmospheric plasma facilitates cutaneous wound healing. *Frontiers in Bioengineering and Biotechnology*, *vol. 8*. https://doi.org/10.3389/fbioe.2020.00683

Luce, D. A. (2005). Determining in vivo biomechanical properties of the cornea with an ocular response analyzer. *Journal of Cataract and Refractive Surgery, vol. 31*, 156–162. https://doi.org/10.1016/j.jcrs.2004.10.044

Martines, E., Brun, P., Brun, P., Cavazzana, R., Deligianni, V., Leonardi, A., Tarricone, E., & Zuin, M. (2013). Towards a plasma treatment of corneal infections. *Clinical Plasma Medicine, vol. 1*, 17–24. https://doi.org/10.1016/j.cpme.2013.10.001

Martines, E., Brun, P., Cavazzana, R., Cordaro, L., Zuin, M., Martinello, T., Gomiero, C., Perazzi, A., Melotti, L., Maccatrozzo, L., Patruno, M., & Iacopetti, I. (2020). Wound healing improvement in large animals using an indirect helium plasma treatment. *Clinical Plasma Medicine*, vol. *17–18*. https://doi.org/10.1016/j.cpme.2020.100095

Martines, E., Zuin, M., Cavazzana, R., Gazza, E., Serianni, G., Spagnolo, S., Spolaore, M., Leonardi, A., Deligianni, V., Brun, P., Aragona, M., Castagliuolo, I., & Brun, P. (2009). A novel plasma source for sterilization of living tissues. *New Journal of Physics, vol. 11*. https://doi.org/10.1088/1367-2630/11/11/115014

Menduni, F., Davies, L. N., Madrid-Costa, D., Fratini, A., & Wolffsohn, J. S. (2018). Characterisation of the porcine eyeball as an in-vitro model for dry eye. *Contact Lens and Anterior Eye, vol. 41*, 13–17. https://doi.org/10.1016/j.clae.2017.09.003

Nasruddin, Nakajima, Y., Mukai, K., Komatsu, E., Rahayu, H. S. E., Nur, M., Ishijima, T., Enomoto, H., Uesugi, Y., Sugama, J., & Nakatani, T. (2015). A simple technique to improve contractile effect of cold plasma jet on acute mouse wound by dropping water. *Plasma Processes and Polymers*, *vol. 12,* 1128–1138. https://doi.org/10.1002/ppap.201400236

Nasruddin, Nakajima, Y., Mukai, K., Rahayu, H. S. E., Nur, M., Ishijima, T., Enomoto, H., Uesugi, Y., Sugama, J., & Nakatani, T. (2014). Cold plasma on full-thickness cutaneous wound accelerates healing through promoting inflammation, re-epithelialization and wound contraction. *Clinical Plasma Medicine*, vol. *2*, 28–35. https://doi.org/10.1016/j.cpme.2014.01.001

Nasruddin, Putri, I. K., Kamal, S., Esti Rahayu, H. S., Lutfiyati, H., Pribadi, P., Kusuma, T. M., Muhlisin, Z., Nur, M., Nurani, L. H., Santosa, B., Ishijima, T., & Nakatani, T. (2017). Evaluation the effectiveness of combinative treatment of cold plasma jet, Indonesian honey, and micro-well dressing to accelerate wound healing. *Clinical Plasma Medicine, vol. 5–6*. https://doi.org/10.1016/j.cpme.2017.03.001

Natali, A. N., Carniel, E. L., Frigo, A., Pavan, P. G., Todros, S., Pachera, P., Fontanella, C. G., Rubini, A., Cavicchioli, L., Avital, Y., & de Benedictis, G. M. (2016). Experimental investigation of the biomechanics of urethral tissues and structures. *Experimental Physiology, vol. 101*, 641–656. https://doi.org/10.1113/EP085476

Nautscher, N., Bauer, A., Steffl, M., & Amselgruber, W. M. (2016). Comparative morphological evaluation of domestic animal cornea. *Veterinary Ophthalmology, vol. 19*, 297–304. https://doi.org/10.1111/vop.12298

Ngo Thi, M.-H., Shao, P.-L., Liao, J.-D., Lin, C.-C. K., & Yip, H.-K. (2014). Enhancement of angiogenesis and epithelialization processes in mice with burn wounds through ROS/RNS signals generated by non-thermal N_2/Ar micro-plasma. *Plasma Processes and Polymers, vol. 11*, 1076–1088. https://doi.org/10.1002/ppap.201400072

Pan, S., Zhang, S., & Chen, H. (2020). Low temperature plasma promotes the healing of chronic wounds in diabetic mice. *Journal of Physics D: Applied Physics, vol. 53*. https://doi.org/10.1088/1361-6463/ab7514

Rosani, U., Tarricone, E., Venier, P., Deligianni, V., Zuin, M., Martines, E., Leonardi, A., & Brun, P. (2015). Atmospheric-pressure cold plasma induces transcriptional changes in ex vivo human corneas. *PLoS ONE, vol. 10*. https://doi.org/10.1371/journal.pone.0133173

Saleem, W., Benton, A. H., Marquart, M. E., Wang, S., Saleem, W., Vigil, R., Huang, B., & Sharma, A. C. (2019). Innovative cold atmospheric plasma (iCAP) decreases mucopurulent corneal ulcer formation and edema and reduces bacterial load in Pseudomonaskeratitis. *Clinical Plasma Medicine, vol. 16*. https://doi.org/10.1016/j.cpme.2019.100093

Sanchez, I., Martin, R., Ussa, F., & Fernandez-Bueno, I. (2011). The parameters of the porcine eyeball. *Graefe's Archive for Clinical and Experimental Ophthalmology, vol.* 249, 475–482. https://doi.org/10.1007/s00417-011-1617-9

Schmidt, A., Bekeschus, S., Wende, K., Vollmar, B., & von Woedtke, T. (2017). A cold plasma jet accelerates wound healing in a murine model of full-thickness skin wounds. *Experimental Dermatology, vol. 26*, 156–162. https://doi.org/10.1111/exd.13156

Schmidt, A., Liebelt, G., Nießner, F., von Woedtke, T., & Bekeschus, S. (2021). Gas plasma-spurred wound healing is accompanied by regulation of focal adhesion, matrix remodeling, and tissue oxygenation. *Redox Biology, vol. 38*. https://doi.org/10.1016/j.redox.2020.101809

Schmidt, A., Niesner, F., von Woedtke, T., & Bekeschus, S. (2021). Hyperspectral imaging of wounds reveals augmented tissue oxygenation following cold physical plasma treatment in vivo. *IEEE Transactions on Radiation and Plasma Medical Sciences, vol. 5*, 412–419. https://doi.org/10.1109/TRPMS.2020.3009913

Schmidt, A., von Woedtke, T., Vollmar, B., Hasse, S., & Bekeschus, S. (2019). Nrf2 signaling and inflammation are key events in physical plasma-spurred wound healing. *Theranostics, vol.9*, 1066–1084. https://doi.org/10.7150/thno.29754

Shahbazi Rad, Z., & Abbasi Davani, F. (2020). Measurements of the electrical parameters and wound area for investigation on the effect of different non-thermal atmospheric pressure plasma sources on wound healing time. *Measurement, vol. 155*. https://doi.org/10.1016/j.measurement.2020.107545

Shahbazi Rad, Z., Abbasi Davani, F., & Etaati, G. (2018). Determination of proper treatment time for in vivo blood coagulation and wound healing application by non-thermal helium plasma jet. *Australasian Physical & Engineering Sciences in Medicine, vol.41*, 905–917. https://doi.org/10.1007/s13246-018-0686-z

Shao, P.-L., Liao, J.-D., Wong, T.-W., Wang, Y.-C., Leu, S., & Yip, H.-K. (2016). Enhancement of wound healing by non-thermal N_2/Ar micro-plasma exposure in mice with fractional-CO_2-laser-induced wounds. *PLOS ONE, vol. 11*. https://doi.org/10.1371/journal.pone.0156699

Shekhter, A. B., Pekshev, A. v., Vagapov, A. B., Telpukhov, V. I., Panyushkin, P. v., Rudenko, T. G., Fayzullin, A. L., Sharapov, N. A., & Vanin, A. F. (2019). Physicochemical parameters of NO-containing gas flow affect wound healing therapy. An experimental study. *European Journal of Pharmaceutical Sciences, vol. 128*, 193–201. https://doi.org/10.1016/j.ejps.2018.11.034

Shekhter, A. B., Serezhenkov, V. A., Rudenko, T. G., Pekshev, A. v., & Vanin, A. F. (2005). Beneficial effect of gaseous nitric oxide on the healing of skin wounds. *Nitric Oxide, vol.12*, 210–219. https://doi.org/10.1016/j.niox.2005.03.004

Souza, L. B. de, Silva, J. I. de S., Bagne, L., Pereira, A. T., Oliveira, M. A. de, Lopes, B. B., Amaral, M. E. C. do, de Aro, A. A., Esquisatto, M. A. M., Santos, G. M. T. dos, & Andrade, T. A. M. de. (2020). Argon atmospheric plasma treatment promotes burn healing by stimulating inflammation and controlling the redox state. *Inflammation, vol.43*, 2357–2371. https://doi.org/10.1007/s10753-020-01305-x

Tanelian, D. L., & Bisla, K. (1992). A new in vitro corneal preparation to study epithelial wound healing. *Investigative Ophthalmology & Visual Science, vol.* 33.

von Woedtke, T., Emmert, S., Metelmann, H. R., Rupf, S., & Weltmann, K. D. (2020). Perspectives on cold atmospheric plasma (CAP) applications in medicine. *Physics of Plasmas, vol.* 27. https://doi.org/10.1063/5.0008093

Wahyuningtyas, E. S., Iswara, A., Sari, Y., Kamal, S., Santosa, B., Ishijima, T., Nakatani, T., Putri, I. K., & Nasruddin, N. (2018). Comparative study on Manuka and Indonesian honeys to support the application of plasma jet during proliferative phase on wound healing. *Clinical Plasma Medicine, vol. 12*, 1–9. https://doi.org/10.1016/j.cpme.2018.08.001

Wang, X.-F., Fang, Q.-Q., Jia, B., Hu, Y.-Y., Wang, Z.-C., Yan, K., Yin, S.-Y., Liu, Z., & Tan, W.-Q. (2020). Potential effect of non-thermal plasma for the inhibition of scar formation: a preliminary report. *Scientific Reports, vol.10*. https://doi.org/10.1038/s41598-020-57703-6

Weiner, G. (2012). Confronting corneal ulcers - Pinpointing etiology is crucial for treatment decision making. *Eye Net Magazine*.

Wiesemann, K. (2013). A Short Introduction to Plasma Physics. *CERN Yellow Report CERN 007,* 82-122. https://doi.org/10.5170/CERN--2013--007.85

Xu, G., Shi, X., Cai, J., Chen, S., Li, P., Yao, C., Chang, Z., & Zhang, G. (2015). Dual effects of atmospheric pressure plasma jet on skin wound healing of mice. *Wound Repair and Regeneration, vol. 23*, 878–884. https://doi.org/10.1111/wrr.12364

Yu, Y., Tan, M., Chen, H., Wu, Z., Xu, L., Li, J., Cao, J., Yang, Y., Xiao, X., Lian, X., Lu, X., & Tu, Y. (2011). Non-thermal plasma suppresses bacterial colonization on skin wound and promotes wound healing in mice. *Journal of Huazhong University of Science and Technology [Medical Sciences*], vol. *31*, 390–394. https://doi.org/10.1007/s11596-011-0387-2

Zachary, J. (2017). *Pathologic basis of veterinary disease* (6th Edition). Elsevier.

Zeng, Y., Yang, J., Huang, K., Lee, Z., & Lee, X. (2001). A comparison of biomechanical properties between human and porcine cornea. *Journal of Biomechanics, vol. 34*. https://doi.org/10.1016/S0021-9290(00)00219-0

Zhang, J.-P., Guo, L., Chen, Q.-L., Zhang, K.-Y., Wang, T., An, G.-Z., Zhang, X.-F., Li, H.-P., & Ding, G.-R. (2019). Effects and mechanisms of cold atmospheric plasma on skin wound healing of rats. *Contributions to Plasma Physics, vol. 59*, 92–101. https://doi.org/10.1002/ctpp.201800025